25

VALIDATION OF NUMERICAL PREDICTION OF BONE INGROWTH INTO CEMENTLESS IMPLANTS

W. Galgut, BSc(Eng)(Ind)
October, 1998

Supervisors: Prof C. L. Vaughan
Dr G. R. Starke

Submitted in partial fulfilment of the requirements for a Masters degree in Biomedical Engineering

---

Department of Biomedical Engineering
University of Cape Town
Rondebosch
7700
South Africa

ABSTRACT

Total joint replacement was pioneered by John Charnley in the late 1950's, and has since revolutionised the management of arthritis sufferers. By 1991, an estimated 5 million people had undergone hip replacements. Although relatively successful, the cemented components had some problems, and this led to the development of cementless implants. These implants depend on the ingrowth of bone into a porous coating, to produce a durable method of implant fixation which the normal bone turnover process will maintain.

One of the problems with cementless implants is that the type and extent of tissue ingrowth into the porous coating is unpredictable. Movement of the implant relative to the surrounding bone may result in the formation of an interfacial fibrous tissue layer. Hence, numerical modelling has been used to predict tissue ingrowth into such implants. Numerical simulation has the advantage that comprehensive data can be extracted relatively quickly. The finite element method is a powerful tool that has become the preferred method of analysis, and takes into account critical factors such as implant design, bone properties, and loading conditions. However, these models have not been tested extensively. Little attention has been given to comparing numerical models with the actual findings of retrieval studies or radiological imaging studies. This study thus evaluates the potential of one such numerical model.

Most numerical models analyse the stress patterns of a particular state of bone ingrowth (i.e. a static case). This model considered the development of the ingrowing material - a dynamic analysis of tissue changes over a period of time. A 2-dimensional, plane stress finite element model was used to predict the ingrowth of bone into the porous coating of the femoral stem of a hip implant. A side plate was incorporated to mimic 3-dimensional characteristics.

The evaluation was achieved by comparing the predictions of the numerical model with plane X-ray images of seven patients with Zimmer Anatomic cementless hip implants. The X-rays were scanned at a high resolution, so as to be able to "magnify" the regions to be examined. Several algorithms were developed to analyse the images, and provide a quantitative

assessment of the X-ray images. The algorithms were designed to identify regions of bony and fibrous tissue. This involved the identification of the interface between the implant and the surrounding bone, and the extraction of the grayscale values of the X-rays at this interface. Thereafter, various radiographic signs that indicate the presence of fibrous tissue or bony tissue were identified, and these were used to enhance the original grayscale plot. The resulting graph was then modified slightly so as to make its presentation comparable with the numerical model. Plane X-rays proved to be suitable for the task of identifying tissue types.

These data were then compared with the predictions of the numerical model. A qualitative correlation was used, as this was deemed to be most appropriate. Several authors in the literature also found a quantitative approach to have limitations. Some agreement between the experimental findings and the numerical simulation was found to exist, although this was limited. The agreement was judged to be less than the "reasonable agreement" that several studies in the literature concluded. The correlation is better described by "some agreement". Nevertheless, the finite element method was assessed as being a tool with great potential, and modifications to the present model may provide more reliable results.

A time study was also undertaken, whereby the tissue density was evaluated at various periods after the operation. The study provided insight into the evolution of the implant-bone interface after surgery, and correlated well with the literature. The phases of repair and remodelling were evident, and it was assessed as being a valuable contribution to this work. The time study may prove to be a more useful method than those used in assessing the "static" images, and could even provide a prognostic tool in assessing implant stability over time.

ACKNOWLEDGEMENTS

I would like to express my gratitude to the following people for their assistance with this work:

Professor Johan Walters, for his time and enthusiasm in the assessment of the X-ray images.

My supervisors, Professor Kit Vaughan and Greg Starke, for their continual encouragement and assistance.

Gillan Bowie, for her time and effort in the taking of the X-rays.

Professor Trevor Sewell and Miranda Waldron, for their assistance with the scanning of the X-ray images.

DECLARATION

I, Warren Galgut, declare that the work contained in this thesis is essentially my own work and that no part thereof has been submitted for a degree at any academic institution.

Signed by candidate

signature removed

Warren Galgut

October 1998

TABLE OF CONTENTS

Chapter 1 INTRODUCTION

The ability to replace diseased and damaged joints with prosthetic implants has resulted in millions of people having restored function of joints, as well as significant relief from pain. Indeed, the ultimate goal of total joint replacement (TJR) may be defined as being the long-term restoration of pain-free function of joints. With this in mind, "success" becomes a difficult term to define, and varies somewhat between studies, as several point-scoring systems are used to evaluate success. In all cases, however, success refers to acceptable function and pain levels over the specified time span, and may be interpreted as "clinical survivorship". Total joint replacement has achieved success rates well above most other surgical procedures, with rates of between 80% and 95%, depending on such factors as implant design, implant material, surgical technique, activity levels and age of the patient. Although highly successful, problems do exist, and must be addressed if joint replacement is to remain a feasible solution.

Osteoarthritis and rheumatoid arthritis are the most common diseases resulting in joint replacement, with trauma being another relatively common reason. Both diseases are crippling in terms of joint function and excruciating pain levels, and joint replacement almost always goes a long way to alleviating these problems.

Total joint replacement was pioneered by John Charnley in the late 1950's, and has since revolutionised the management of arthritis sufferers. By 1991, an estimated 5 million people had undergone total hip arthroplasty (THA) (Harris, 1991). Charnley's hip implant consisted of a very smooth steel femoral head, articulating with a high-density polyethylene acetabular cup, to form a ball-and-socket joint. The head size and combination of materials led to the replacement becoming known as "low friction arthroplasty". Today stainless steel, cobalt-chromium, or titanium are commonly used for both the femoral component and backing of the acetabular component. It is interesting that today, almost four decades later, the principles used by Charnley are largely unchanged, with only some refinements having been made.

THA requires implantation of femoral and acetabular components. The femoral component consists of a stem, which is implanted into the medullary canal of the proximal femur, and at the top, a femoral head for articulation with the acetabular component. The medullary canal of the femur is broached so as to accommodate the stem, and the natural acetabulum is reamed, to allow implantation of the artificial acetabular cup. The acetabular component has a high-density polyethylene cup within a metal backing, so as to provide sufficient rigidity. The basic design is shown in Figure 1.1.

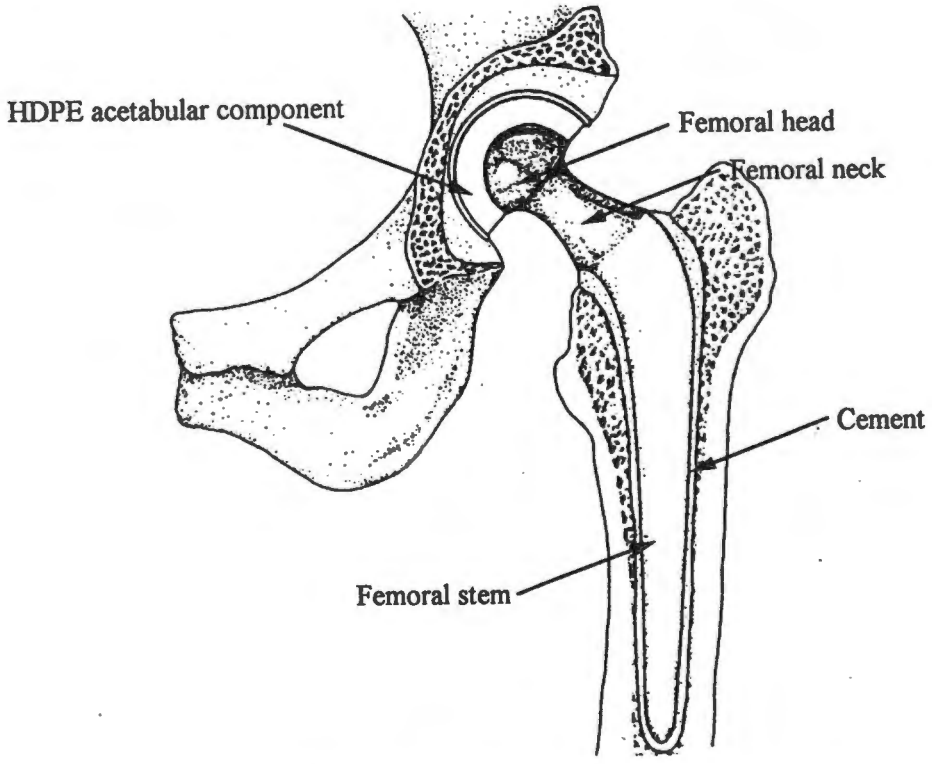

Figure 1.1 Total hip arthroplasty (Starke, 1996)..

The approach that Charnley employed was to secure the implant (both femoral and acetabular components) within the surrounding bone by means of bone cement. He used a polymethylmethacrylate (PMMA) bone cement, which is still commonly used today. However, a number of problems have emerged with this method. Griss (1984) categorised the reasons for revision surgery, and concluded that aseptic loosening was the primary reason, resulting in more than half of all revisions. Stem fracture and septic loosening are also notable problems, with septic loosening, or infection, being considered to be a very serious problem. Many investigators have identified bone cement as being the weak link in the implant system (Harris, 1991; Park, 1995), although some disagree (Müller, 1992). The most common causes of aseptic loosening of cemented implants include differing properties of cement, implant, and

bone, abrasion particles, biocompatibility of materials used, implant design, and surgical technique (Ducheyne, 1984). Other problems receiving increasing attention are toxicity of the MMA monomer remaining after polymerisation, and thermal necrosis of bone during polymerisation (Park *et al.*, 1995; Griss, 1984).

With the development of improved cementing techniques, implant fixation success rates have improved to 97% in some circumstances. Nevertheless, fixation remains a problem in the long-term, and other methods of implant fixation were introduced. The most notable of these was the advent of the cementless, or porous-coated, implant. This method relies on the ingrowth of bone into a porous coating to achieve fixation between implant and bone. Thereafter, it relies on the normal bone turnover processes to maintain a strong bond - one that will hopefully last indefinitely.

Bone tissue is in a continuous process of growth and remodelling, with old or damaged bone being removed and new tissue being deposited. The removal, or resorption, is carried out by osteoclasts, while deposition is effected by osteoblasts. The activity of these cells is determined by such factors as genetic coding, hormonal and metabolic effects, presence of disease, medicinal factors, and mechanical loading. While all of these are important, the effect of mechanical loading is particularly relevant, and is known as Wolff's Law. When physical loading is reduced, a net resorption of local bone tissue occurs, while increased loading results in a net gain of bone tissue. Also, the trabeculae of the deposited bone are orientated in such a way as to best carry the applied load.

The initial design of cementless implants was one in which the entire surface was covered with a porous coating. A serious problem immediately emerged: excessive bone resorption took place around the proximal regions of the implant. The reason for this was that stress transfer due to loading took place mostly in the distal regions of the implant - also confirmed by the fact that bone deposition was increased distally. This phenomenon, known as stress shielding, is due to the difference in stiffness between the implant material and surrounding bone tissue. An attempt to alleviate this problem was made by confining the area of the porous coating to the proximal third of the implant surface, as shown in Figure 1.2. This approach greatly reduced the problem, although not altogether solving it. One important complication was the observance of the formation of a fibrous tissue layer, especially around

the smooth areas (distal two-thirds) of the implant. This is believed to be due to large relative displacement between implant and bone, approximately 150μm being sufficient (Spector, 1988). Fibrous tissue forms when the relative motion between implant and bone is too large for bone ingrowth to occur. Although the fibrous tissue can be stable, it has a low Young's modulus and does not transmit stress well. This fibrous tissue can, and often does, form within the porous coating. It is therefore desirable to restrict relative motion and thus ensure a bond of maximum bony ingrowth.

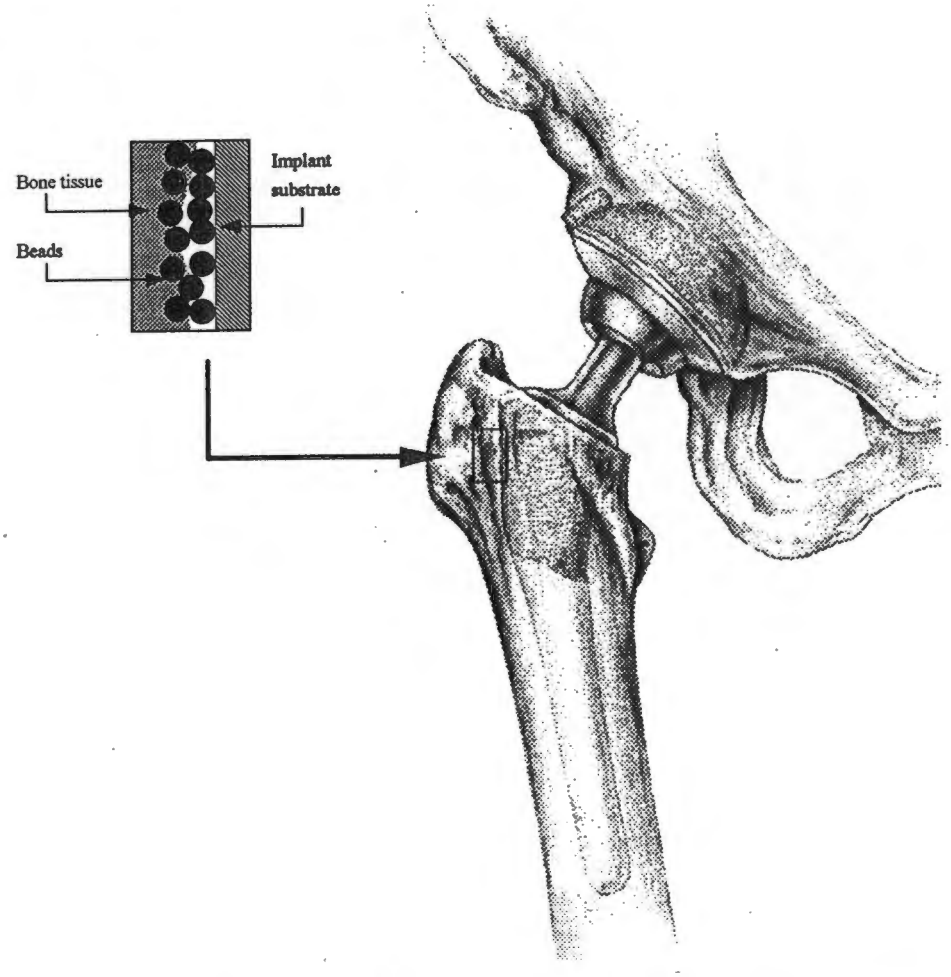

Figure 1.2 Porous coated hip implant (Starke, 1996).

Although mostly successful, cementless implants do have certain problems. One disadvantage is that recipients must remain inactive for a period of time post-operatively -- typically longer than in the case of a cemented implant. The length of time before load-bearing can begin varies considerably. Another problem is that porous-coated implants are notoriously difficult to remove, and substantial bone damage often occurs during removal. In fact, orthopaedic surgeons normally suggest that fixation of implants should not be too strong, so severe is the problem (Park, 1995). Because cementless implants rely so heavily on the performance of

host bone, these implants are best suited to the young and elderly (above 60) who are in good physical condition and with good bone stock. Other problems include excessive ion release (due to the increased surface area of the porous coating), pain, and possible foreign-body reaction to the wear particles of the metals or polyethylene. It can thus be seen that substantial obstacles do still exist, although some people believe that porous-coated implants may yet become more reliable than their cemented counterparts.

Computer-based numerical modelling has proved to be a useful tool in gaining understanding of the response of bone to a stimulus. Many numerical models have investigated remodelling activity in cortical and cancellous bone, when subjected to loading, and these have tended to be generalised studies, not related directly to implant-bone interaction. Such studies are obviously valuable (and necessary) in understanding and hence predicting bone activity. However, very few numerical models have been developed for predicting the growth rate of tissues into an implant's porous coating (i.e. the time-based evolution of the implant-bone interface). Furthermore, very little effort has been given to evaluating the accuracy of these numerical models objectively, and this research project is thus aimed at evaluating one such numerical model.

Histological retrieval studies have highlighted a number of important aspects regarding porous-coated implant fixation. It should be noted, however, that such studies tend to vary considerably, with regard to aspects like implant type and design, materials used, method of preparation of retrieved samples, age of patient, and length of implantation time before retrieval. Nevertheless, these studies are extremely valuable in establishing facts regarding bone ingrowth (and thereby contributing to the development of future implant design), as well as providing data that can be used to evaluate the accuracy of numerical models. The latter reason is of particular importance in this study. The most striking revelation of implant retrieval studies is that clinically stable porous-coated implants very often have minimal bone ingrowth, in some cases less than 10%. Furthermore, there is little or no consistency in the specific sites at which this ingrowth does occur. Most studies show extensive fibrous tissue presence within the porous coating. Indeed, it appears that limited bone ingrowth and extensive fibrous tissue ingrowth is adequate for fixation (Cook *et al.*, 1988; Collier *et al.*, 1992). Also noteworthy is the fact that the fibrous tissue in some cases had orientated itself in

a particular direction. This indicates that the fibrous tissue does transmit a small amount of load.

Many investigations have been directed at studying the bone density around an implant radiologically, especially for detecting stress shielding and hence bone resorption. As has been stated, little attention has been given to comparing numerical model predictions with the actual findings of retrieval studies or radiological imaging studies, specifically regarding the implant-bone interface. It is thus the purpose of this project to evaluate the predictions of one particular numerical model. The model to be tested was developed at the Centre for Research in Computational and Applied Mechanics (CERECAM), at the University of Cape Town. A 2-dimensional model of the reconstructed hip joint was constructed, using the finite element package ABAQUS. The hip joint analysis considered the activity at the medial and lateral borders of the femoral stem. The femoral implant used in the model was a PCA (Howmedica, Inc.) femoral component, in which the proximal third is covered with porous coating. The loading history was based on typical forces of the single-legged-stance phase of normal gait. The model predicts depth of bone ingrowth, and interface stress for various times post-operatively. The purposes of the current research project may thus be stated as being:

- To evaluate the effectiveness of using plane X-ray images in assessing the type and extent of tissue ingrowth into a porous coating
- To evaluate the effectiveness of using image analysis software in assessing tissue types and degree of mineralisation
- To use plane X-rays to quantitatively measure the extent of mineralised bone and fibrous tissue ingrowth into the medial and lateral borders of the porous coatings of femoral stems of total hip arthroplasties (in which the porous coating covers the proximal third of the stem)
- To evaluate the accuracy of the numerical model, emphasising both the accurate predictions and the shortcomings of the model
- To develop an algorithm capable of identifying trabecular bone pattern. This is considered to be a task complimentary to the primary one above, and is thus not comprehensive.

Chapter 2 LITERATURE REVIEW

2.1 Bone Morphology and Physiology

2.1.1 Bone structure and morphology

Bone is a dynamic connective tissue that plays various critical roles in the body. Bones provide structural rigidity and protect internal organs. They also provide attachment for skeletal muscles, thus enabling the body to move. Furthermore, they play a biochemical role by providing a reservoir for calcium, phosphorus, and other agents. Bone tissue has unique structural and mechanical properties that allow it to fulfil these roles. It has an excellent capacity for self-repair, and can adapt its structure in response to the mechanical demands placed on it. It can thus be seen that bone is a very complex tissue type, with a range of equally complex functions.

Bones are composed of tissue that exhibits two structural types: cortical and cancellous bone. Cortical (or compact) bone commonly makes up the shafts (diaphyses) of long bones and the thin shells of the bone ends, as shown in Figure 2.1. Cancellous (or spongy) bone occurs in the ends of long bones (epiphyses), and is continuous with the inner surface of the cortical shell. Cancellous bone has a particularly noticeable porous structure (Figure 2.2), resulting from a network of connecting rods or plates of bone tissue, called trabeculae. The interstices between trabeculae are filled with bone marrow. The distinction between the two types is made by the relative density, or volume fraction of solid material. Cortical bone typically has a relative density of 70 to 95%, and cancellous bone 10 to 70% (Carter and Spengler, 1978; Gibson, 1985).

Bone is a specialised connective tissue made up of cells and an organic extracellular matrix of fibres and ground substance. The fibres are a protein, collagen, and make up approximately 95% of the extracellular matrix. They are tough and pliable, and have little capacity for extension. The ground substance surrounds the collagen fibres, and serves primarily as a cementing agent. It is made up mainly of protein polysaccharides called proteoglycans. A

distinguishing feature of bone is its hardness and rigidity. This is due to its inorganic component, in the form of mineral salts, which is embedded within the organic matrix. This mineral component consists mainly of calcium and phosphate in the form of hydroxyapatite crystals. It is this mineral component that gives bone its compressive strength, while collagen provides its tensile strength.

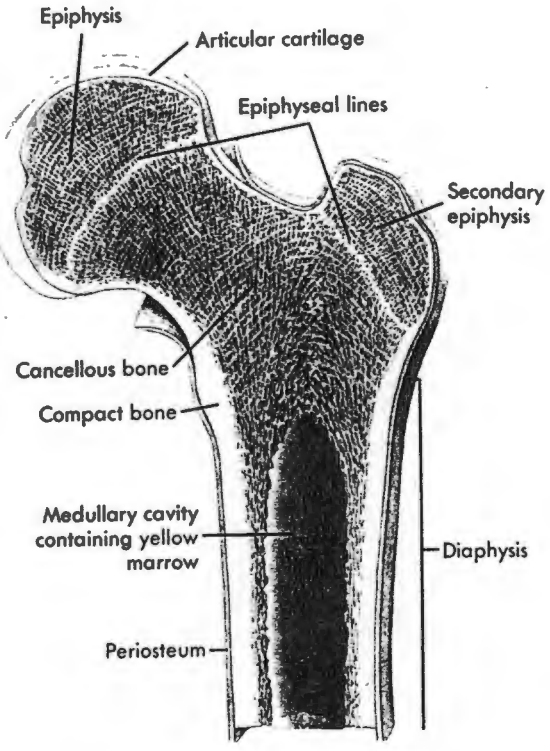

Figure 2.1 Gross structure of long bone (Seeley *et al.*, 1992).

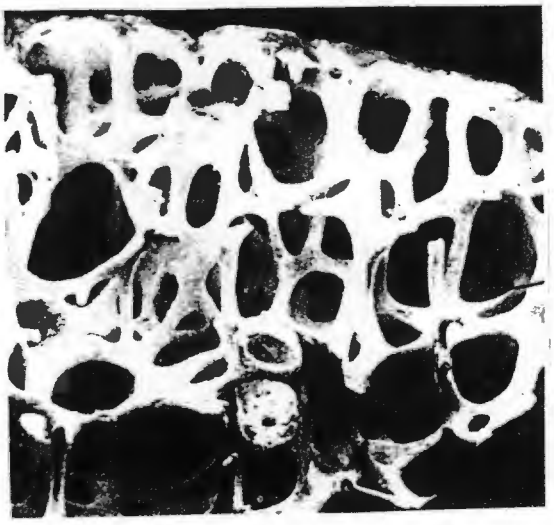

Figure 2.2 Trabecular bone structure (Gibson, 1985).

On a microscopic level, the structural unit of bone is the osteon, or haversian system (Figure 2.3). In the centre of each osteon is a haversian canal, which contains blood vessels and nerve fibres. Surrounding the canal are concentric layers (lamellae) of mineralised bone matrix. Along the boundaries of each layer, or lamella, are small cavities called lacunae, each containing one bone cell, or osteocyte. A network of small channels (called canaliculi) interconnects lacunae, and hence osteocytes. Each osteocyte receives nutrients through these channels, ultimately from the haversian canal. Osteons usually run longitudinally, but they branch and anastomose extensively.

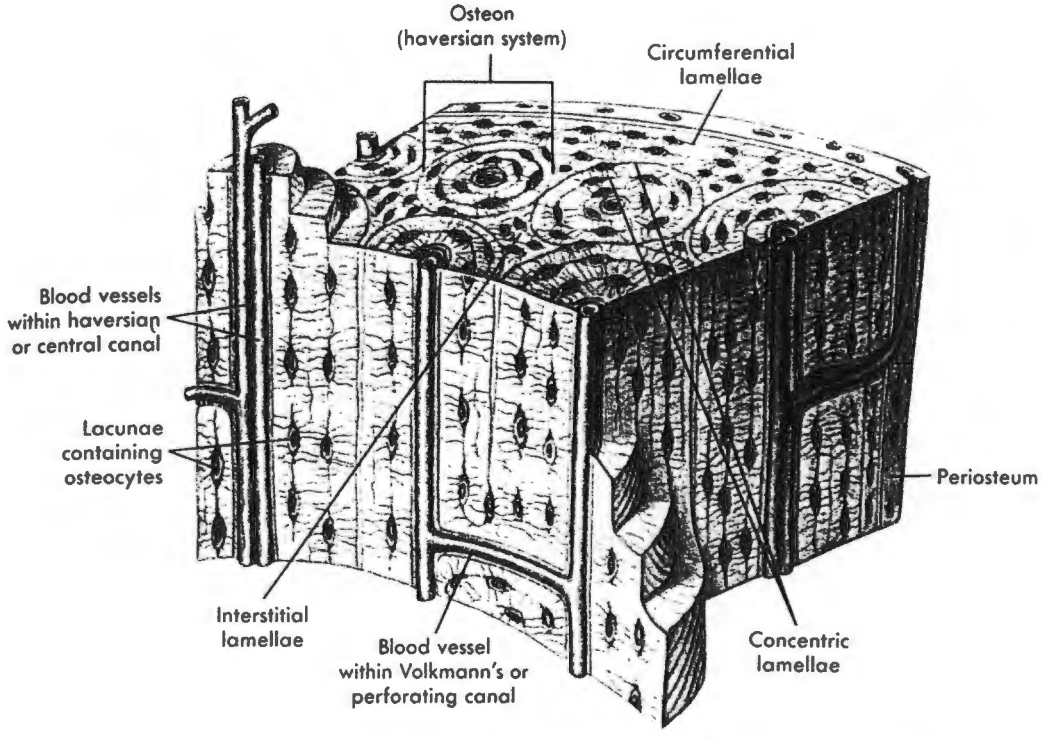

Figure 2.3 Microscopic structure of bone (Seeley *et al.*, 1992).

2.1.2 Bone repair and remodelling

Osteogenesis, or bone formation, is a complex process that is characterised by the migration, differentiation, and modulation of particular cells. Bone tissue originates as mesenchyme, an undifferentiated, loosely organised tissue, whose individual cells can migrate to various parts of the body. Osteogenic cells are derived from mesenchyme, and differentiate into osteoblasts or chondroblasts, which secrete a bone matrix that subsequently ossifies into bone tissue. There are primarily four cell types involved in the formation and maintenance of bone: osteoblasts, osteocytes, fibroblasts, and osteoclasts. Osteoblasts are responsible for the formation of new bone tissue, and do so by apposition onto pre-existing bone surfaces. They secrete the organic part of the bone matrix, as well as contributing to the mineralisation process. Osteoblasts eventually become enclosed within the matrix they create, and become osteocytes. Osteocytes are responsible for the maintenance of bone, and are less active than osteoblasts. They are interconnected by canaliculi, which allows for information transfer. Fibroblasts are involved in the formation of fibrous tissue (collagen), and are particularly active during wound healing. Although several cell types produce collagen, fibroblasts are the most active and widespread. Osteoclasts are involved in the resorption of old or damaged bone, initially dissolving the minerals and then degrading the collagen.

Bone activity can be classified into two processes, broadly referred to as "repair" and "remodelling". The repair process refers to the healing response that is stimulated by, in the case of an implant, a surgical wound. This entails the removal of dead or damaged bone cells (and other cells), and the formation of new bone tissue. The new tissue usually fills the space between the implant and the existing bone. This healing response continues for approximately 4 to 6 weeks post-operatively (Spector, 1988; Hollister *et al.*, 1994), although some investigators suggest longer times are necessary (Collier *et al.*, 1992; Park *et al.*, 1995). Thereafter, the bone is maintained by the bone remodelling process. Bone remodelling refers to the process of the removal of old or damaged bone tissue (by osteoclasts), and the deposition of new tissue (by osteoblasts or fibroblasts). These cell types operate simultaneously, and may result in a net increase or decrease in the amount of bone tissue, depending on the degree of activity of each. The activity of these cells is determined by many factors, including genetic coding, hormonal and metabolic effects, presence of disease, medicinal factors, and mechanical loading.

The effect of mechanical loading is particularly noteworthy: when physical loading is reduced, a net resorption of bone tissue occurs, while increased loading results in a net gain of bone tissue. Furthermore, the trabeculae of remodelled bone become aligned in specific directions, depending on the direction, magnitude, and duration of loading. This is in accordance with Wolff's Law, which states that a bone being bent by a mechanical load will modify its structure by bony deposition in the concavity and resorption in the convexity (Chamay and Tschantz, 1972). Gibson (1985) suggested that the symmetry of bone structure depends on the direction of applied load, while the density of the bone in a particular location depends on the magnitude of the load.

2.1.3 Tissue Biomechanics

A good understanding of the mechanical characteristics of bone and fibrous tissue is extremely important, especially in understanding the effects of implanting a prosthesis into a bone. Furthermore, the complex viscoelastic and anisotropic nature of bone requires that any numerical analysis of bone be formulated very carefully. This subject is vast, and only a very brief summary of the most important aspects is presented here.

Mineralised bone tissue

Bone is a viscoelastic and anisotropic material. Its viscoelasticity is reflected in its strength dependency on the rate and duration of loading (i.e. strain rate). It is able to carry greater loads (and store more energy) when these loads are applied more quickly. Carter and Hayes (1977) postulated that the longitudinal (the direction parallel to the majority of trabeculae) strength and stiffness of mineralised bone is approximately proportional to the strain rate raised to the power 0.06. Bone's anisotropy refers to the fact that its elastic properties and strength depend on the orientation of its microstructure. It is stronger when loaded longitudinally. It is, however, approximately isotropic in the transverse direction (Carter and Spengler, 1978).

The most important mechanical properties of bone, from a functional point of view, are its strength and stiffness. A good understanding of these and other properties can be gained from examining bone's response to loading (Figure 2.4). It should be noted that cortical and cancellous bone are very similar in composition (Carter and Hayes, 1977), with cancellous bone being slightly less mineralised (Carter and Spengler, 1978). However, each type can also vary considerably in microstructure, porosity, mineralisation, and bone matrix (Carter and Spengler, 1978). Furthermore, the various types of bone (woven or lamellar) make generalisations regarding bone mechanical properties very difficult. Nevertheless, certain

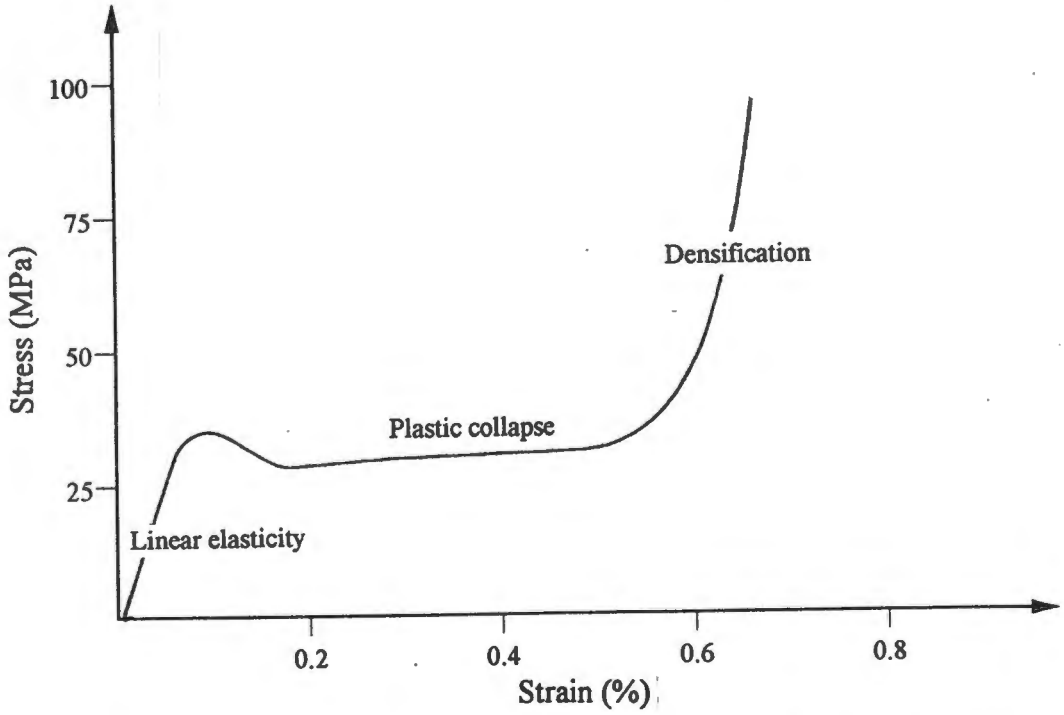

Figure 2.4 Typical compressive stress-strain curve for cancellous bone (Adapted from Gibson, 1985).

principles of bone mechanics remain true, and are worth noting. The initial "linear elastic" region is common to most materials, and occurs here when the cell walls either bend or compress axially. They return to their original size and shape when the load is removed. The second, flat part of the curve corresponds to "plastic yielding" of the bone, a state where cells tend to remain in their deformed shape after loading is removed. Here brittle fracture of the cell walls occurs, and the cells collapse. At higher loads, the cell walls touch one another, and the bone strength increases due to the compact state of the bone. This is responsible for the sharp increase in the stress-strain curve. The area under the curve constitutes the energy absorbed in the process.

The geometry of a bone greatly influences its mechanical behaviour. In tension and compression, the stress generated and the stiffness are proportional to the cross-sectional area. A larger area results in a stronger and stiffer bone. In bending, however, both cross-sectional area and the distribution of bone tissue around a neutral axis affect the mechanical behaviour. These two factors are inherent in a measure called area moment of inertia. A large area moment of inertia results in a bone being stronger and stiffer. This also applies to torsional loading, where a cross-section with a larger area moment of inertia will experience less shear stress than a cross-section with a smaller area moment of inertia. This is why stress fractures of the tibia tend to occur distally, where the area moment of inertia is smaller.

Fibrous tissue

The mechanical properties of fibrous tissue are particularly important, as fibrous tissue commonly forms during wound healing, and in particular, around implants. Fibrous tissue consists of densely-packed collagen bundles, forming a mat-like structure. Hori and Lewis (1982) conducted tests on fibrous tissue, and found it to be weak in tension and shear, while exhibiting highly non-linear behaviour in compression. Their compression tests showed it to be very compliant, with large deformations at small loads. Its modulus of elasticity was found to be approximately 0.17MPa, orders of magnitude lower than the 17GPa of cortical bone and the 1.6GPa of cancellous bone (Huiskes *et al.*, 1992).

2.2 Joint Replacement

2.2.1 Introduction

The purpose of a joint is to provide normal anatomical structure while allowing a range of motion, with no pain, for an indefinite length of time. People can usually manage sufficiently well with impeded function of joints, but pain is often the factor that persuades them to undergo joint replacement. Joint pain is commonly caused by disease, most notably osteoarthritis and rheumatoid arthritis. Osteoarthritis is a chronic joint disease, characterised by degradation of the articular cartilage and changes in the underlying bone. Eventually, the cartilage becomes worn down to such an extent that the underlying bone is exposed, and function is severely impaired. Rheumatoid arthritis is an auto-immune disease, characterised by inflammation of the synovial membrane and articular cartilage, as well as presenting various systemic effects. In its advanced stage, it can even result in fusion of bone that was previously underlying the cartilage. Both diseases are crippling in terms of joint function and excruciating pain levels, and joint replacement almost always goes a long way to alleviating these problems. In fact, the ultimate goal of total joint replacement (TJR) may be defined as being the long-term restoration of pain-free function of joints.

Total joint replacement can be performed on almost any joint of the body. The most common are total hip arthroplasty (THA) and total knee arthroplasty. Initial THA's were performed as follows: the natural femoral head was removed and the proximal medullary canal broached, to allow implantation of the femoral stem. On the acetabular side, the natural acetabulum was reamed to make place for the artificial acetabular socket. Both components were anchored within the surrounding bone with the aid of bone cement. This was the approach made famous by John Charnley in the late 1950's. Charnley also gave much attention to the size of the femoral head: if the head was large, friction was increased, and if the head was smaller, pressures were increased and dislocation became common. Charnley experimented with various sizes and found an optimal head size to be 22.2mm. It was a combination of this and the materials he used that led to the replacement becoming known as "low friction arthroplasty". Charnley used a steel femoral component (with a highly-polished head) and a high-density polyethylene acetabular cup. He initially even experimented, unsuccessfully, with

teflon. The high-density polyethylene is still commonly used today, although it has been somewhat refined.

Investigations into a direct chemical bonding method have also been undertaken (Park *et al.*, 1995). In this method, biologically active materials (with chemical properties similar to those of bone) coat the implant surface. This coating reacts with the bone it contacts, quickly forming a strong bond, with no fibrous tissue formation. Agents being tested include hydroxylapatite and tricalcium phosphate, and progress appears to be good (Collier *et al.*, 1992). Problems do exist, however, a notable one being the difficulty in coating the implants.

2.2.2 Cemented Joint Arthroplasty

When implanting the femoral component into the proximal femur in THA, the medullary canal is broached to a size slightly larger than the femoral stem. This results in a space between implant and bone, and this space is filled with bone cement. The cement commonly used is a polymer, polymethylmethacrylate (PMMA), which acts not as a glue, but as a grouting agent. In other words, the cement does not bond directly to the implant and bone; it forms an interlocking "bond" by filling the intertrabecular spaces of bone and completely surrounding the implant stem. If this interlocking is successful, relative displacement at the implant-cement and cement-bone interfaces will be eliminated, and load will be distributed over the largest possible area.

Many investigators have identified bone cement as being the weak link in the implant system (Harris, 1991; Park, 1995). Furthermore, the implant-cement interface is commonly viewed as initiating failure (Harris, 1991), with loosening beginning here and perhaps eventually leading to fracture of the cement mantle. Most investigators describe bone cement as being brittle (Spector, 1988), with some noting its low fatigue strength (Park *et al.*, 1995). Improved cementing techniques, such as the use of medullary plugs, pressurised cement application, and centrifuging cement before use (to eliminate air bubbles formed during mixing), resulted in significant improvements in fixation results. Harris (1991) reported on the incidence of femoral component loosening being reduced from between 30 and 40% at 10-year follow-up, to 3% at 11-year follow-up, using these techniques. Still more advanced techniques, called third-generation cementing techniques, claim even greater success. Other problems peculiar to bone cement are the toxicity of the methylmethacrylate monomer remaining after polymerisation

(Galante *et al.*, 1971), and thermal necrosis of surrounding bone during polymerisation (Griss, 1984; Park *et al.*, 1995).

It is worth noting that not all investigators are convinced that bone cement is the cause of failure. Müller (1992) and Coventry (1992) believe that the polyethylene (PE) material is the weak link, and more specifically, the foreign-body reaction to the PE wear debris. Müller refers to this problem as "polyethylene disease". Harris (1991) also noted the problem of particulate debris, even regarding it as being the primary problem leading to loosening.

Griss (1984) conducted a survey categorising the reasons for revision surgery of the hip joint, and found aseptic loosening to be the primary reason, resulting in 52.1% of all revisions. Stem fracture (13.2%) and septic loosening (11.1%), or infection, are also serious problems. Infection, in particular, is a very serious condition, as it cannot easily be treated. The most common causes of aseptic loosening of cemented implants include differing properties of cement, implant, and bone, abrasion particles, biocompatibility of materials used, implant design, and surgical technique (Ducheyne, 1984). Late loosening, specifically, is a considerable problem, and along with the other problems, contributed to the search for a more durable method of implant fixation.

2.2.3 Cementless Joint Arthroplasty

Although cemented arthroplasties have been highly successful, their durability in the long-term and their suitability for younger, more active, recipients is questionable. For these reasons the cementless, or porous-coated, implant has been introduced. This method relies on the ingrowth of bone into a porous coating to achieve fixation between implant and bone. Thereafter, it relies on the normal bone turnover processes to maintain a strong bond. The intention is that this bond will last indefinitely, as the bone restructures itself in response to the load experienced, especially in the case of the more active patient.

The surgical implantation of a cementless prosthesis is similar to that of the cemented one, except that the implant cavity is broached to a size slightly smaller than the implant. This requires that the implant be pressed firmly into the cavity, and is called an interference fit, or press-fit. This results in close bone-implant apposition, which is a more stable state in which bone ingrowth can begin.

Implant design

Porous-coated hip implants are typically wedge-shaped (i.e. tapering distally) in the femoral stem region. This shape aids bone-implant apposition when the implant carries a load. This is beneficial both in the early post-operative stage and later, when stress transfer will stimulate bone remodelling activity. Sadegh *et al.* (1993) claim that a compressive strain in the direction perpendicular to the direction of ingrowth is necessary for that ingrowth to occur. The wedge-shaped femoral stem is believed to provide this necessary strain field.

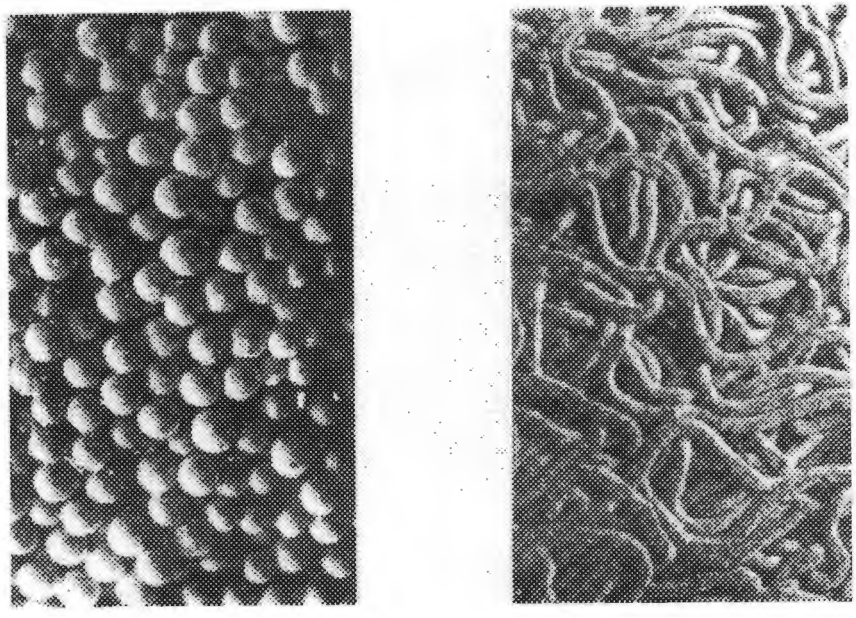

(a) (b)

Figure 2.5 Types of porous coating (a) Beads (b) Wire mesh (Park *et al.*, 1995).

The porous surface may be one of several types. The two most common types are metal alloy beads and wire mesh, both of which are shown in Figure 2.5. In the former case, spherical or irregularly-shaped beads are sintered onto the surface of the implant. The beads range in diameter, typically between 50 and 200μm. The wire mesh consists of interwoven wire fibres which form a porous sheet that is bonded onto the implant surface. A notable advantage of this type of porous surface is that the regular geometry is ideally suited to numerical modelling analysis. Furthermore, it provides ingrowth fixation strength comparable to the beaded coating type (Pedersen *et al.*, 1991). The pore size in both types is particularly important, as osteons must be able to fit in the pores for maximum bond strength. Osteons are approximately 75μm wide, resulting in pore sizes typically being between 100 and 350μm wide (Park *et al.*, 1995).

The initial design of cementless implants was one in which the entire surface was covered with porous coating, in an attempt to maximise bone ingrowth. However, a serious problem immediately became apparent: excessive bone resorption took place around the proximal regions of the implant. This resulted in weakened fixation proximally, which was a possible, and even probable, cause of eventual implant loosening. The reason for the proximal bone resorption was that stress transfer (due to loading) took place mostly in the distal regions of the implant. This was also confirmed by the fact that bone deposition was increased distally. This phenomenon, known as stress shielding, is due to the differences in stiffness between the implant material and the surrounding bone tissue. An attempt at alleviating this problem was made by confining the area of the porous coating to the proximal third of the implant surface. This approach reduced the problem, although not altogether solving it. Sumner and Galante (1992) noted that proximal bone loss still occurred, and that it could be appreciable. It was noted that even within the reduced porous-coated area, bone ingrowth was less apparent proximally, and bone hypertrophy was common around the distal boundary of the porous coating (Cook *et al.*, 1988; Collier *et al.*, 1992). Engh and Bobyn (1988) also made note of the important fact that these implants would be easier to remove than the fully-coated type, should it become necessary. Another important observation was the formation of a fibrous tissue layer, especially around the smooth distal regions of the implant. Although the fibrous tissue can be stable, it does not transmit stress well. It is thus desirable to restrict fibrous tissue formation and maximise bony ingrowth.

Some implant designs incorporate a collar below the neck of the femoral stem. This has the advantages of restricting relative motion between implant and bone, as well as providing more surface area for proximal stress transfer and bone ingrowth. A study by Whiteside *et al.* (1988) showed that subsidence is significantly decreased and hence pain occurrence would be expected to be reduced. A certain degree of subsidence is desirable, however, as it aids in anchoring the implant (Spector, 1988), and the current trend is not to incorporate a collar.

Interface motion and tissue types

There are primarily two tissue types to be found surrounding an implant: mineralised bone tissue and fibrous tissue. Fibrous tissue forms when the relative displacement between implant and bone is too large for bone ingrowth to occur. The magnitude of relative displacement resulting in fibrous tissue formation is a subject of some debate. Pedersen *et al.* (1991) claim

that a few tens of microns are sufficient, while Bobyn *et al.* (1982) and Spector (1988) believe that displacements above 150μm result in fibrous tissue formation. A fibrous tissue capsule, up to 2mm thick (Collier *et al.*, 1992), is often formed around the smooth surfaces (distal two-thirds) of femoral stems.

The area around the implant is divided into seven regions (Gruen zones 1 to 7), and the monitoring of implant-bone apposition in each region is undertaken to assess the likelihood of implant loosening. Radiolucent lines associated with fibrous tissue typically occur in the proximal regions of the implant stem (Cook *et al.*, 1988; Collier *et al.*, 1992), particularly in Gruen zone 7. An examination of the proximal regions is thus of particular significance.

Fibrous tissue can, and usually does, also form within the porous coating. Fibrous tissue has a low Young's modulus, and does not transmit stress as well as bone does. The presence of fibrous tissue within the porous coating is not, in itself, a problem. In fact, most clinically stable implants have extensive fibrous tissue presence within the porous coating, in some cases more than 90% (Collier *et al.*, 1992). Cook *et al.* (1988) analysed 90 retrieved implants and found that none had more than 10% bony ingrowth. They also noted that the fibrous tissue in some cases had orientated itself in a particular direction, indicating that fibrous tissue is capable of transmitting a small amount of load. They concluded that limited bone ingrowth and extensive fibrous tissue ingrowth is adequate for fixation. However, in terms of a good long-term prognosis, a greater proportion of bony ingrowth is desirable.

Interface strength

The strength of the bond at the implant-host tissue interface is obviously of great importance in implant fixation. Studies have been restricted to animal experiments, however, which are not reliable indicators of human bone strength. Nilles *et al.* (1973) implanted porous-coated cylinders into the cortices of dog femurs, and measured the forces required in pushing them out. They found shear strength to attain a reasonably constant 15MPa after 6 weeks. Bobyn *et al.* (1980) conducted almost identical shear strength tests on canine femurs, and included implants of various pore sizes. They concluded that the optimal pore size produced a shear strength of approximately 17MPa. They also hypothesised that the shear strength of canine cortical bone (approximately 60MPa) multiplied by the porosity (approximately 0.3) should provide an estimate of the shear strength of the bond (18MPa). Clearly, the strength of the

interface bond is dependent on several factors, both biological and mechanical, and bond strength varies accordingly.

The strength of a fibrous tissue bond is also important. Bobyn and Wilson (1982) undertook peel strength tests on fibrous tissue attached to a porous surface. They found the maximum peel strength to be 0.27MPa, at 16 weeks. An interesting observation made was that the bond strength was very similar to the tensile strength of the fibrous tissue, suggesting that failure was dominated by failure of the tissue itself, not of the bond. This would seem to correlate with the predictions of Pedersen *et al.* (1991), who claim that the most superficial tissue of the interface (i.e. tissue on the outermost part of the porous coating) carries a large proportion of the load.

Stress shielding (Osteopenia)

Stress shielding refers to a reduction in the stress levels within bone surrounding an implant, due to the fact that the more stiff implant carries the majority of the stress. Bobyn *et al.* (1990) found that pronounced bone resorption due to stress shielding occurs in at least 20% of cases. It would seem reasonable that the use of an implant with the same stiffness as bone would result in the system being as close to the normal femur as possible. It was this notion that led to the development of more flexible implants, and the use of the term "isoelastic", implying "equal elasticity". This reasoning is not quite correct, however, for this reason: when two objects of equal stiffness are joined, the composite object has twice the stiffness of the individual objects, assuming the interface between the two is uniform and well-bonded. This suggests that implants should be appreciably more flexible than bone. Bobyn *et al.* (1992) conducted canine experiments, to establish the effects of flexible implant stems, and concluded that the implant itself should have a bending stiffness of approximately one-half to one-third that of the human femur.

Morscher and Dick (1983) reported on 9 years of clinical experience with an "isoelastic" implant. They found that some proximal stiffness was necessary, to effectively transmit forces between pelvis and femur. This produced excellent results: a study of 40 femoral stems showed no revisions necessary for loosening, and no distal tip stress transfer occurred. They did concede, though, that their oldest sample was only 4.5 years - not long enough to draw any

significant conclusions. Carter *et al.* (1984) also confirmed that the use of a lower modulus material created a less abnormal distribution of stresses in the surrounding bone.

Bobyn *et al.* (1990) conducted a canine study on 8 animals, in which stiff (normal) and flexible femoral components were implanted bilaterally. Results indicated that femurs with flexible stems consistently showed 25 to 35% less bone resorption than the stiff stems. Furthermore, severe resorption occurred mid-stem in 3 stiff stems, with no such occurrence in the flexible ones. Although these results are very encouraging, two serious problems exist: failure due to fatigue is common in the long-term, and the increased relative displacement at the implant-bone interface restricts bone ingrowth. These are significant and unacceptable problems, and have led to distrust of these implants in the clinical setting.

The stiffness of an implant is determined primarily by its size, geometry, and material. Implant size has long been recognised as being a primary stiffness determinant (Bobyn *et al.*, 1990). Engh and Bobyn (1988) found femoral stems of diameter 13.5mm or more to have a 5-fold higher incidence of pronounced bone resorption than those with a diameter of 12mm or less. It is also common for a more flexible implant to be made from a material with a lower Young's modulus - another reason for titanium being popular. The geometry of an implant is reasonably complex: most femoral stems taper down towards their distal ends, which results in the distal region being more flexible than the thicker proximal region. Also, the changing geometry of the femur results in a range of stiffness properties there. It can thus be appreciated that the joining of these structures produces a complex and unpredictable stress pattern. Indeed, Morscher and Dick (1983) stated that ideal isoelasticity is impossible, as bone is an anisotropic material while all other commonly used biocompatible materials are isotropic.

Interestingly, it has also been found that femoral stems that are two-thirds or fully porous-coated resulted in a 2-fold to 4-fold higher incidence of pronounced bone resorption (Engh and Bobyn, 1988). The reason for this was explained as the increased stiffness due to the more extensive interface bonding. This is a remarkable paradox, since it is generally desired that bone ingrowth should be extensive. The ideal implant should thus be appreciably less stiff than bone when implanted, and "become more stiff" as bone ingrowth occurs. Of course, this may not be physiologically possible at all. It would seem, then, that a suitable balance in the extent of bone and fibrous tissue ingrowth is desirable for long-term fixation and stability.

Problems

Certainly the biggest problem facing cementless implants is that of loosening, resulting from stress shielding and ensuing bone resorption. However, the difficulties usually begin at surgery. Park (1995) comments that the precise nature of the surgery makes it inherently unforgiving (more so than a cemented implant). The risk of infection follows immediately, although this is common to both types of implants. Thereafter the recipient may have to remain inactive for some time post-operatively, although this depends primarily on pain experienced, and varies considerably. Another problem is that porous-coated implants are notoriously difficult to remove, and substantial bone damage often occurs during removal (Bobyn *et al.*, 1992; Park *et al.*, 1995). In fact, orthopaedic surgeons normally suggest that fixation of implants should not be too strong, so severe is the problem (Park, 1995). Because cementless implants rely so heavily on the performance of host bone, these implants are best suited to the young and elderly (above 60), in good physical condition and with good bone stock. This immediately excludes a large portion of possible users. A problem gaining increasing recognition is the release of an excessive number of ions from the metal, due to the significantly increased surface area of the porous coating (Park, 1995). Yet another sizeable problem lies in the foreign-body reaction to the wear particles, either metal or polyethylene (Harris, 1991). This, too, can eventually lead to implant loosening (Müller, 1992).

Perhaps the biggest problem of all lies in our lack of understanding of what is necessary for an implant to be successful in the long-term. Pedersen *et al.* (1991) even commented that the relative contributions of biologic repair stimuli and "Wolff's Law" remodelling towards early bone ingrowth remain undefined. Studies have shown certain design features to be desirable, but the incorporation of many of these simultaneously has proved to be very difficult, with the "perfect" implant seemingly out of reach. It can thus be seen that substantial obstacles do exist, but many people believe that porous-coated implants may yet become more reliable than their cemented counterparts.

2.3 Numerical Modelling

Computer-based numerical modelling has proved to be a powerful tool in gaining understanding, and hence predicting, the response of bone to a particular stimulus. Where animal experiments and clinical trials require a great deal of time and expense before conclusive

results emerge, numerical modelling allows quick extraction of comprehensive data. Of course, this technique has certain limitations, but such strides have been made in this field that few implant designers would venture to produce an implant without prior testing on a numerical model.

Although various numerical methods can be used in the simulation of bone activity, the finite element method (FEM) is commonly preferred. It was first introduced into orthopaedic biomechanics in 1972, and has since become a well-established tool for research and design purposes (Huiskes and Chao, 1983; Weinans *et al.*, 1990). Although no attempt is made at elaborating on the principles of the FEM here, a brief explanation is provided. When an object is subjected to loading, stresses are generated throughout the structure. The distribution of these stresses depends on the loading configuration, the geometry of the structure, and the properties of its materials. Furthermore, the stresses are affected by the interaction of the structure with the environment (boundary conditions). The stress distribution is evaluated by a mathematical model, which incorporates all of the above parameters. This model mimics the real structure, with a certain degree of refinement. The solution procedure involves combining the structural descriptions and mathematical equations, based on the principles of continuum mechanics, to give the stresses.

When using the FEM, the geometrical structure is defined first. This is done by dividing the structure into a number of elements, connected at specific points, called nodes. The boundary conditions and loading configurations are then described as displacements and forces, respectively, at specific nodes. An example of a FEM mesh is shown in Figure 2.6. Every element is then assigned material properties (moduli of elasticity), and a loading history may also be specified. With all this necessary information, the computer program then calculates the stiffness characteristics of each element and assembles the element mesh, incorporating all mutual nodal forces and displacements. A variety of element types are available, for both 2-dimensional and 3-dimensional structures. These element types differ in their number of nodes and shapes. The solution obtained is approximate in that it converges to the exact solution as the number of elements used increases. This is referred to as the accuracy of the model. The validity of the model refers to the precision with which the structural descriptions (geometry, loading, etc.) mimics the real structure. Both are responsible for a certain degree of deviation

from the real structure. The validity can be assessed by experimental verification, while a convergency test gives an indication of the accuracy of the model.

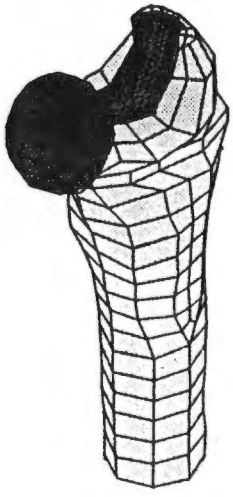

Figure 2.6 Example of Finite Element mesh (Verdonschot *et al.*, 1993).

Since its initial application to simple stress distribution patterns, numerical modelling has progressed significantly, along with the advances made in computer technology. The enormous value of computer-based modelling lies in its ability to relatively quickly evaluate (to a greater or lesser degree of accuracy) the expected results of a particular implant design and loading geometry. The expected stress distributions and magnitudes at the implant interface were of particular interest, as were the effects of material flexibility and bone flexibility. The development did not remain confined to stress analysis, however. The incorporation of a bone growth algorithm into the predicted strain patterns allowed bone growth patterns to be predicted. This was then modified to analysing bone ingrowth into a porous-coated surface. In this way, a dynamic system, with a boundary that changes its position over a period of time, can be modelled. Although significant progress has been made, some problems have made this development less than straightforward.

Sadegh *et al.* (1993) note that the existing literature deals largely with the chemistry, biology, and surface science of the implant-bone interface, with much less material relating to the mechanical aspects thereof. Indeed, the literature commonly examines the effect of various degrees of ingrowth, without considering the development of that ingrowth. Weinans *et al.* (1990) modelled the effects of a fibrous tissue layer between the cement and bone. Markolf *et al.* (1980) did a similar analysis, examining implant subsidence when a cemented implant was

surrounded by an elastic layer. Pedersen *et al.* (1991) conducted a 2-dimensional FEM study of interstitial bone stress as a function of ingrowth depth and wire mesh geometry. In these studies, as in almost all such numerical modelling studies, the model begins with an assumed ingrowth state, not considering the development of the ingrowing material.

The study by Sadegh *et al.* (1993) is one exception. They used the boundary element method (BEM) to predict the final shape of remodelled mature bone into several cavity designs. They claim that the BEM is superior to other numerical methods in problems involving moving and evolving boundaries. They acknowledge, too, that significant assumptions have to be made in such a model, and cite this as a primary problem in numerical modelling in general.

FEM analyses may be accomplished in 2-dimensional (2-D) or 3-dimensional (3-D) space. The 3-D analysis requires appreciably more computational time, and is therefore more expensive. These models are also more difficult to formulate. The biggest problem with the 2-D model is the deviation from the normal 3-dimensional stiffness characteristics of the structure. These factors have resulted in extensive use of 2-D models, with adaptations to more closely mimic the real 3-D structure (Carter *et al.*, 1984). Dalstra *et al.* (1995) claim that the femur can be well analysed using an adapted 2-D model.

2.4 Motivation for this study

It is obviously very important to know how accurately a numerical model mimics the real situation. Remarkably few analyses have been conducted in this regard. Initial attempts at evaluating numerical models were confined to comparing surface stress and strain measurements of intact bones with the predictions of various numerical methods, such as simple beam theory. Valliappan *et al.* (1977) compared the predictions of a 3-D FE model of the femur with the strains measured on the surface of a cadaver specimen. They found the two to agree very well, even though some discrepancy was evident. In 1981, Huiskes *et al.* compared the predictions of beam theory with measured strains on the surfaces of cadaver femurs. They found beam theory to produce "excellent agreement" in the femoral shafts, with less agreement at the geometrically more complex ends. Rohlmann *et al.* (1983) compared a 3-D FE model with experimental results of femoral cadaver specimens. They compared stress and strain patterns (under several loading conditions) in both intact femurs and femurs with

endoprostheses, and found the intact femur results to correlate much better than the ones containing prostheses. Nevertheless, in both cases the FE model was deemed to achieve "reasonable agreement" with the experimental results. Carter *et al.* (1984) conducted a study involving both a 2-D FEM analysis and canine femoral head surgery, and concluded that their computer simulation exaggerated the changes in stress fields.

More recently, Verdonschot *et al.* (1993) compared a 3-D FEM model with laboratory experiments on cadaver femurs containing implants. They found a load-transfer analysis to correlate very closely with the experimental results. Their analysis of implant stability was less similar, with some quantitative differences being found. Significantly, they noted that the conclusions drawn from the FE studies and the laboratory experiments were the same, and concluded that the FEM can effectively be used for design evaluation of hip prostheses, even though some quantitative deviations may be present. Dalstra *et al.* (1995) evaluated a 3-D FE model of the pelvic bone, by comparison with measured surface strains on a cadaver pelvis. Although noting some discrepancies, they found "reasonable agreement", and the basic ability to predict stress and strain distribution realistically. Weinans *et al.* (1993) compared a 3-D FE model with canine experiments, after a simulation time of 2 years. They compared both the trabecular structure and bone density of bone surrounding a femoral stem, and found the computer simulation to perform "surprisingly well". They, too, concluded that although quantitative predictions did not correlate perfectly, computer simulation remains a versatile tool for the pre-clinical testing of prosthetic designs.

All studies showed some degree of deviation of computer simulation predictions from experimental findings. Some studies noted that the computer simulations tended to exaggerate the stress and strain patterns (Carter *et al.*, 1984; Dalstra *et al.*, 1995), although others claimed that this was not the case (Verdonschot *et al.*, 1993). Almost all studies emphasised that qualitative validation was preferred. Sadegh *et al.* (1993) believe that a quantitative comparison is unreasonable, for primarily two reasons. Firstly, physical and biological parameters (on which the predictions rely), such as the modulus of elasticity of trabecular bone and the remodelling rate constant, are not known sufficiently accurately. Secondly, and perhaps more importantly, the history of mechanical loading is extremely difficult to measure, especially in a long-term animal study. It will be noted, too, that none of the above studies concern the evaluation of a computer simulation model that predicts the growth of a bone surface, as in the

case of bone ingrowth into a porous coating. It would seem that no documentation on such studies exists, and hence the motivation for this study. It can thus be appreciated that the evaluation of a particular numerical model is no simple task, due to the problems described. Furthermore, it is equally difficult to compare one numerical model with another, as each model has its own assumptions and physical and biological data.

Chapter 3 MATERIALS AND METHODS

3.1 Introduction

This chapter begins by documenting the predictions of the numerical model being tested. It then describes some initial experiments that were undertaken to establish the best method of assessing tissue types, before describing various techniques used in the final algorithm chosen. Some details of the patients who participated in the study are also provided. A major part of this chapter is devoted to the various algorithms that were investigated in extracting the relevant information from the images.

3.2 Predictions of numerical model

The numerical model uses a 2-dimensional, plane stress finite element model, shown in Figure 3.1 (Starke, 1996). It incorporates a side plate to simulate the stiffness provided by the cortex, which is lost by the use of the 2-D approximation. In this way it better mimics the real 3-D structure. This is a simplification that is common in contemporary FEM models. Regions of cortical and cancellous bone (green and orange, respectively) can be clearly seen. The interface between the implant and the bone is shown in red. The cortical and cancellous bone have mechanical properties that are assumed to remain constant, while the properties of the interface are allowed to vary, as it develops. In this way, only the interface evolution is analysed. The side plate is given the material properties of cortical bone.

The loading on the proximal femur is extremely complex and varied, with forces being applied by an array of muscles, as well as being transmitted through the acetabulum. A person of average mass is considered in this analysis. The numerical model considers three loading cases, the most important being the single-legged stance phase of normal gait. This is considered to be the worst case loading condition occurring during normal activity, when loads transferred across the hip joint are at their greatest. The second and third loading cases are those occurring at the extreme ranges of motion of the joint, and are considered to be the extremes of normal activity. The first case is applied for 50% of the total number of load cycles, while the second and third cases each carry a 25% weighting.

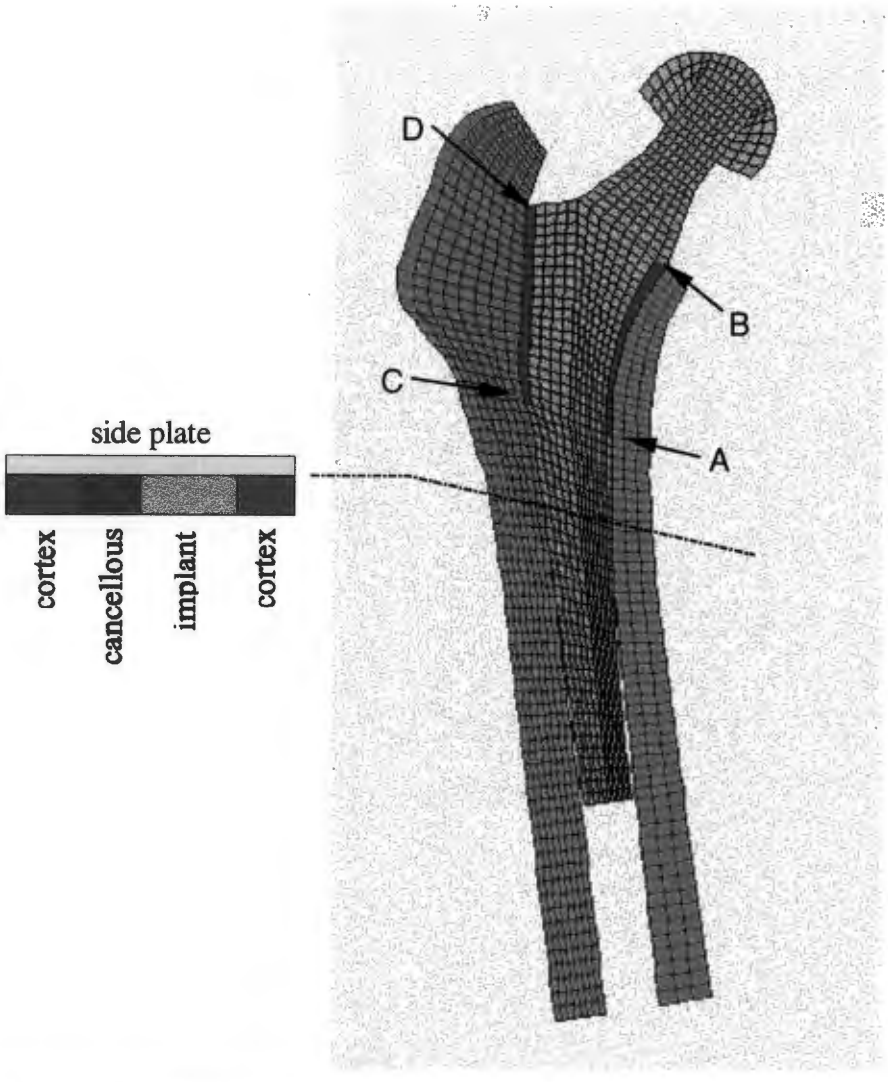

Figure 3.1 Finite element mesh of the reconstructed proximal femur (Starke, 1996).

Two analyses of the hip joint were undertaken. The first allows a 14 day rest period before loading begins, which is the more realistic option. The second assumes loading to begin immediately post-operatively. In this study, only the first analysis (which includes the 14 day rest period) is assessed, as this more closely resembles the actual rest period of the patients who were studied. The predictions of the numerical model are shown in Figure 3.2 and Figure 3.3, for the lateral and medial borders, respectively. Both graphs also show the evolution of the interface at time intervals of 40, 80, 120 and 160 days after surgery.

The interpretation of these graphs is obviously of critical importance. In particular, the fluctuations must be interpreted correctly. Both graphs begin (0 days) with complete apposition of implant to bone, represented as 100%. This value then begins to decrease with time, and fluctuations start to develop. Although the fluctuations in the graphs appear to

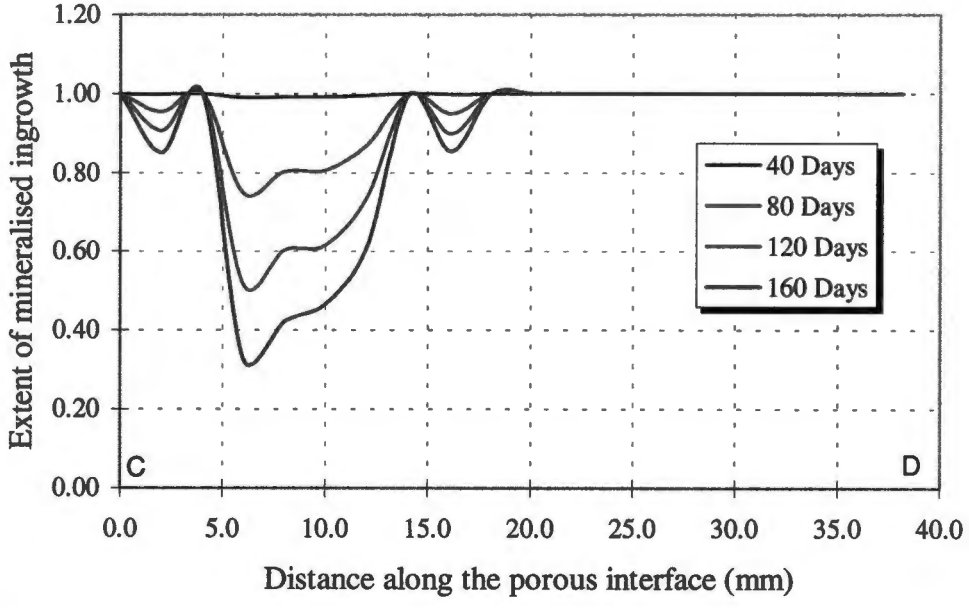

Figure 3.2 Extent of mineralised tissue ingrowth along the lateral porous surface (including a rest period of 14 days) (Starke, 1996).

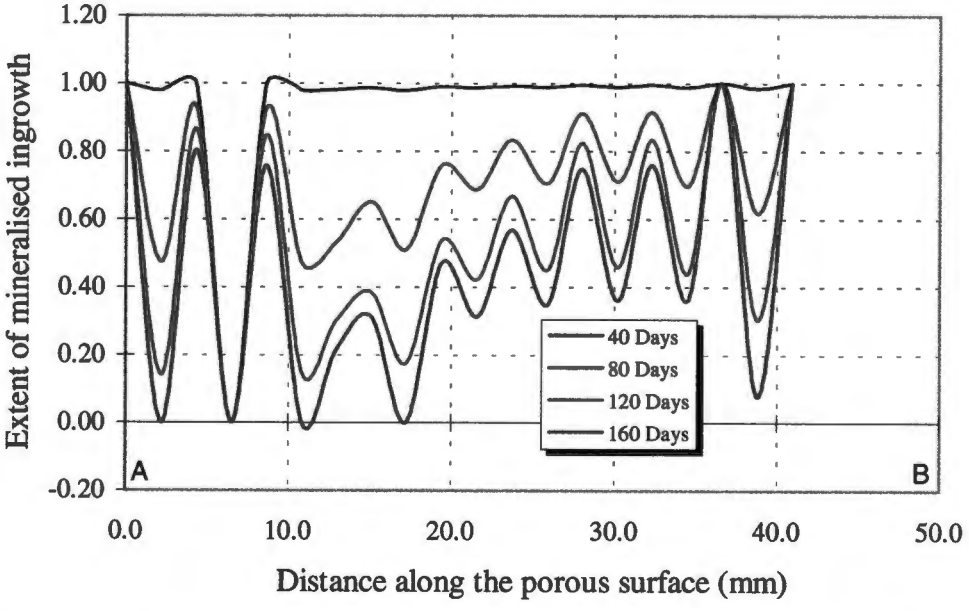

Figure 3.3 Extent of mineralised tissue along the medial porous surface (including a rest period of 14 days) (Starke, 1996).

suggest that the mineralisation of the bone varies, and even becomes zero in places, this is regarded as an incorrect interpretation. The fluctuations are a result of the inherent functioning of the numerical model, and the predictions should be translated into a mean

around which the graph fluctuates. This "averaged" version of the graph at 160 days is shown in Figure 3.4, for the medial porous surface.

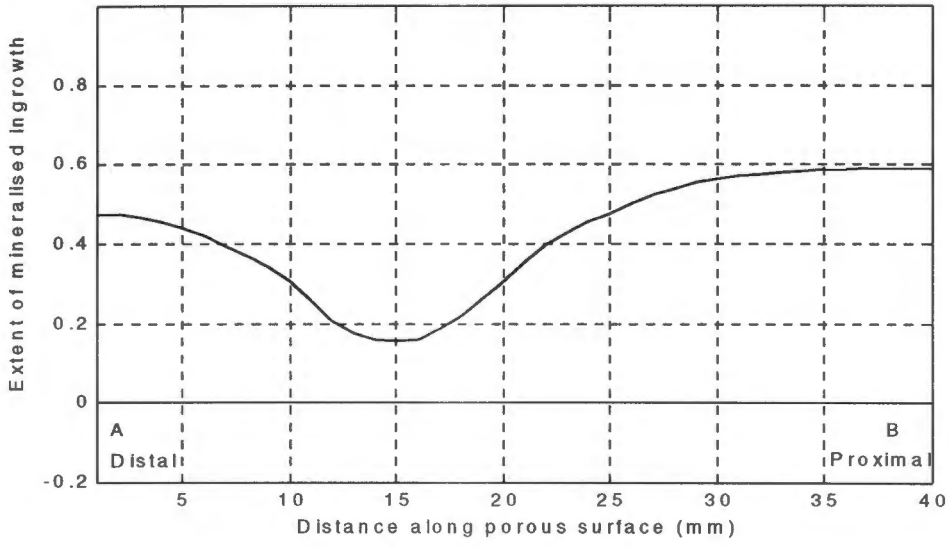

Figure 3.4 Prediction of numerical model with fluctuations averaged (160 days).

In this case, the prediction remains above zero throughout, which implies that only bony tissue is formed, to a greater or lesser degree of mineralisation. If the graph had dropped to below zero, this would have indicated that fibrous tissue would be expected to form. Another point to note is that the above graphs use a time unit of one day. In fact, this can be interpreted less strictly, with the trends over time being more meaningful. In Figure 3.3, the graphs are clearly converging (i.e. successive graphs become closer together), and stop at 160 days because a threshold has been reached. Thereafter, the graphs are not expected to deviate significantly from this position.

3.3 Initial Experimental Investigations

3.3.1 Computer Tomography

It was initially hoped that Computer Tomography (CT) would prove to be a suitable method of imaging, as cross-sectional imaging seemed ideal for the task. Some experimentation was thus done with this method. Two femurs containing implants were borrowed from the Anatomy Museum at UCT Medical School, and a retrieved porous-coated implant was borrowed from Prof. Walters (orthopaedic surgery). All three specimens were tested in a CT scanning machine at Groote Schuur Hospital. The specimens were scanned in both air and in

a container of water (to simulate the *in vivo* case of an implant in a patient). Results were disappointing, however, with a great deal of artefact being created, due to the ferro-magnetic properties of the stainless-steel implant, and virtually no meaningful detail was visible. Even the rough porous surface was indistinguishable from the smooth surfaces. Also, a great deal of shadowing was created in the long axis of the cross-section, further blocking out any detail. Several radiologists at the unit believed the task to be impossible using present-day CT equipment. It was therefore concluded that CT would not meet our imaging requirements.

3.3.2 Dual Energy X-ray Absorptiometry

A brief investigation of Dual Energy X-ray Absorptiometry (DEXA) was undertaken, with limited success. DEXA is typically used to measure bone mineral density, often in regions around implants, to measure changes in bone density due to stress shielding from the implant. The bone mineral density is a good indicator of the quality of bone stock. It became apparent, however, that the resolution of this method was very limited. DEXA is typically used to measure bone density in seven specific zones around the implant. This density is measured from the edge of the implant to the outer perimeter of the bone cortex. However, these regions cannot be made sufficiently small to be of use in this study. The smallest area possible was approximately 3.5mm x 3.5mm, where this study required zooming in to a significantly smaller area (less than 0.1mm). If it were not for this problem, DEXA may well have been ideal for the task. An interesting prospect is that if this study provides routines capable of measuring bone density around implants from X-rays, at a higher resolution than DEXA allows, it may prove to be a superior or preferred technique. Nevertheless, with present technology, DEXA was found to be unsuitable for analysing bone ingrowth into a porous coating. For the aims of this study, it has no advantages over conventional plane X-ray images. Appendix D provides an example of the results of a DEXA scan.

3.4 Materials

3.4.1 Patients studied

Ten patients who took part in a previous study (Breckon, 1993) were contacted, as they had implants suitable for this study. They all had Zimmer Anatomic cementless femoral implants (made of Titanium), with the proximal third of the implant consisting of a wire mesh porous

coating. Seven of these patients agreed to participate in this study, and their demographics are provided in Table 3.1.

SUBJECT	AGE	SEX	MASS	HEIGHT	DIAGNOSIS *	OPERATION DATE
1	64	M	75 kg	1.70 m	RA	8 November 1993
2	47	F	46 kg	1.57 m	OA	25 October 1993
3	53	M	98 kg	1.74 m	OA	18 October 1993
4	59	M	58 kg	1.78 m	OA	1 November 1993
5	53	M	90 kg	1.88 m	OA	18 October 1993
6	65	M	70 kg	1.76 m	OA	22 November 1993
7	35	F	72 kg	1.59 m	OA	18 October 1993

* RA = Rheumatoid Arthritis; OA = Osteoarthritis

Table 3.1 Details of patients included in the study.

3.4.2 Questionnaire

A questionnaire enquiring about details of each patient's activity levels was drawn up, and filled in by each patient. The questionnaire is shown in Appendix B. It was decided to use a questionnaire format rather than other methods (such as verbal exchange), as this would provide the patients with more time to consider the question. Ease of completion is considered to be an advantage in using the questionnaire method (Berdie and Anderson, 1974). Also, the questionnaire was not deemed to be difficult to understand or to answer. One major drawback of using mail questionnaires is low response rate (Salant and Dillman, 1994). However, it was judged that in a study such as this, with relatively few subjects to be questioned, and a short questionnaire, the data would be gathered without difficulty. The content of the questionnaire was very important, as the predictions of the numerical model were based on specific loading conditions, most notably the single-legged stance phase of normal gait. A comparison of the loading conditions used in the numerical model with the actual activity of each patient may explain, at least to some extent, discrepancies in the findings.

It was decided that the information to be extracted was essentially the following: weight (and

weight changes), age, activity levels, bone disease, and overall health. The questionnaire did not address the issue of bone disease, as some information in this regard was already known, and the patients might not have known all relevant details of their bone disease. The emphasis of the questionnaire was on assessing the type and regularity of activity of the subjects.

Several aspects were noted as being of particular importance in the questionnaire (Oppenheim, 1966; Social and Community Planning Research, 1972), and given attention in the construction of the questionnaire. Accuracy (also referred to as validity) refers to the relevance of the questions asked, i.e. whether they extract useful information. Reliability is also important in this regard, and relates to whether the questions are well-understood, and would produce the same response if asked several times. Resolution, or sensitivity, refers to the capacity of the questionnaire to extract specific details on a subject, for example, to distinguish between one long walk of an hour, or several short walks totalling an hour. It was also attempted to make the questionnaire as unbiased as possible, with no leading or suggestive questions. It was also emphasised that the patients should be completely honest and not provide answers that they thought were "correct", or what the questioner wanted to hear.

The issue of conducting pilot studies (pre-tests) was also considered, but it was decided that the information required was not of an extremely detailed nature, and possible answers seemed to fall neatly into various categories. Also, the questions asked were simple enough and it was not expected that major errors should occur. Furthermore, if misunderstandings or confusion did occur, these could be cleared up over the telephone at a later stage. The short questionnaire and number of patients were conducive to this type of follow-up.

3.4.3 Plane X-rays

It was eventually decided that plane X-rays would suffice for the purpose of observing bone ingrowth. This is, after all, the method that the orthopaedic surgeon uses (very successfully) in assessing both the extent of bony ingrowth and the formation of fibrous tissue.

The success of a study of this nature depends to a large degree on the quality of the X-ray images. For this reason, much attention was given to the X-ray film used. It was decided that

double-emulsified, green-sensitive, ortho-chromatic film would be used. This is the film typically used in Groote Schuur Hospital for diagnostic X-rays. Furthermore, the intensifying screens used at the hospital are considered to be of "good" quality.

Each of the patients came to Groote Schuur Hospital for the X-ray scan. Several images were taken at different settings (kV and mAs), to acquire images that best show the edges of the implant and the trabecular bone structure. With higher kV settings, the edge of the implant is better defined, but the trabecular bone patterns are less clear. Conversely, with higher mAs settings, the bone trabeculae are clearer, but at the expense of implant edge clarity. A trade-off thus exists between the voltage and mAs settings, and the intention was to take X-rays with acceptable implant definition and trabecular bone definition. For the first patient, further images (30° internal rotation and 30° external rotation) were taken, after which it was decided that there was no advantage in these views, especially as the numerical model only predicted bone ingrowth at the medial and lateral borders of the implant. Hence, emphasis was placed on the acquisition of a few good quality images, rather than on a greater number of images at different angles and settings.

3.4.4 Scanning of X-rays

For the purpose of analysis, each X-ray image was scanned (digitised). A scanner of sufficiently high resolution was essential, and a suitable scanner (Nikon LS-4500AF Film Scanner) was found to be available at the Electron Microscope Unit at UCT, under the direction of Professor Sewell. This scanner is capable of scanning up to 8.5μm/pixel (3000 pixels/inch). After some experimental scanning at 25.4μm/pixel (1000 pixels/inch), it was decided that 33.33μm/pixel (762 pixels/inch, or 30 pixels/mm) would be used. This decision was based on how efficiently (time-wise and memory-wise) the image analysis software could manage the resulting file. This resolution was more than adequate for our purposes, bearing in mind that the pore sizes of the porous coating are in the region of 75 to 100μm.

The scanner required that the X-rays be cut to a size of no more than a rectangle of 127mm by 101.6mm (5 inches by 4 inches). Prof. Walters (orthopaedic surgery) suggested that we include as much of the image distal to the porous coating as possible, as this was also important in determining the extent of implant fixation. The section of the X-ray that

contained the relevant detail (the proximal femur, from the top of the porous coating to approximately 127mm distally) was therefore cut out and scanned. The acetabular component was not under analysis and was not included. The images were scanned in an upright position, with the implant running from top to bottom. It was found that if the X-rays did not completely fill the 127mm by 101.6mm area being scanned (i.e. light was able to shine around the sides of the X-ray), the edges of the scanned image appeared lighter than they would otherwise have been. Care was thus taken in ensuring that the area around the X-ray being scanned was completely covered.

The images were recorded in the TIFF format, so as to avoid compression of the images. Each file was approximately 6 Megabytes in size. The images were recorded in the conventional 8-bit format, which allowed for a grayscale resolution of 0 to 255. Using a different approach (e.g. a 12-bit format, or cropping out the highest grayscale values, such as the implant) would have allowed for a greater grayscale resolution, but this was judged to be unnecessary. The range of 0 to 255 proved to be more than adequate, as features were easily distinguished in this range. A greater grayscale resolution would not have provided more information, nor made the existing information any clearer. It was more important to achieve adequate resolution in the spatial sense (i.e. pixel size), as this allowed for close analysis of intensity differences in a very precise location.

The resolution of scanning requires further comment. It would be ineffective to scan X-rays at a very high resolution, where these X-rays themselves are of significantly lower resolution. In other words, if there is not sufficient clarity of detail in the original image, then scanning at a high resolution becomes pointless. The resolution of the X-ray machine is thus important, and two measures were taken to assess this resolution. The first was to analyse a section of an X-ray that included some of the steel cables used to re-attach the greater trochanter. These cables are made up by winding together several thinner wires. These thinner wires could be clearly seen on the X-ray, and were measured in pixel widths. This dimension was then converted to millimetres, resulting in a resolution of approximately 300μm. This approach, however, only measures the wire thickness, and does not indicate that this is the highest possible resolution of the machine. The second method was more accurate in determining the resolution. A very thin crack was noticed in one of the implants, during an initial investigation (Section 3.3.1). This crack was barely visible on the X-ray, but was clear when magnified

using the image analysis software. The width of this crack varied between 2 pixels (50μm) and 3 pixels (75μm) along its length. It should be noted, however, that this resolution was achieved on a dry bone specimen with incorporated implant, outside of the body, where the X-ray machine could be positioned close to the specimen. In the case of the live patients, this was not possible, and it was unrealistic to expect that such resolution could be achieved. Nevertheless, a resolution between these two values would appear to be realistic, and the X-ray machine was considered to be adequate for the purposes of this study.

3.4.5 Software and computer used for analysis

Several options were investigated regarding the analysis of the scanned images. The Digital Image Processing (DIP) laboratory at UCT's Department of Electrical Engineering (under Prof. de Jager) had various software packages that were made available to us. Two software programs were investigated -- Khoros 2.0 and Advanced Visual Systems -- and were found to be useful but not ideal for our purposes. Khoros is a visual programming language, and incorporates numerous image processing capabilities. The perceived power of the Advanced Visual Systems software was in its ability to zoom in and out of a 3-dimensional representation of an image. However, neither software was found to have any distinct advantages over other image processing means, and were tentatively set aside. It was finally decided that MATLAB (The MathWorks Inc., 24 Prime Park Way Natick, MA, USA) would be used, as images are essentially matrices containing image intensity values. Furthermore, MATLAB is extremely conducive to programming, more so than the aforementioned packages.

MATLAB 5.1 and the Image Processing Toolbox (version 1.0) were installed on a Pentium computer (100 MHz), as both memory and sufficient speed were essential for the processing of the large images. It was found that frequent memory errors occurred using the conventional 16MBytes of memory, and memory was thus upgraded to 32MBytes.

3.5 Methods: Analysis of Images

All images were scanned in the position shown in Figure 3.5, with the implant running more-or-less from top to bottom, and bone densities varying on the left and right sides of the implant. In this figure, the porous coating can be clearly seen, with notches at each extreme.

Furthermore, for analysis purposes (and because computer memory space was a concern) the images were cropped into smaller areas, the width including one edge of the implant (including the porous surface) and the surrounding bone, as shown in Figure 3.6. In other words, each image was cropped down the centre, through the implant, resulting in each X-ray being reduced to two images -- a medial and lateral side, including the porous regions. As can be seen in Figure 3.5, the lateral porous coating is completely obscured from view by the screws and cables used to re-attach the greater trochanter. The lateral porous coating is only about half the length of the medial side, and covers almost exactly the hidden region in the figure. This was the case in almost all the images, and thus only the medial porous coating was analysed. Image intensities vary between 0 (corresponding to black) and 255 (corresponding to white). The implant absorbs most of the X-rays, and appears white, while air does not absorb X-rays at all, and appears black. The attenuation in bone lies between these two, and produces various shades of gray. Lighter gray thus indicates bone of higher density, while darker gray indicates lower bone density. Fibrous tissue appears relatively dark, similar to low-density bone, and the distinction between the two forms the essence of this thesis.

Figure 3.5 Example of original image.

Figure 3.6 Cropped image for analysis.

The procedure that was used to assess the images is provided in the remainder of this chapter. However, a short summary may be useful at this stage. Three methods that were found to be effective at identifying particular traits were chosen for the analysis. The **first** was to plot the grayscale values of a line immediately adjacent to the porous coating (i.e. at the implant-bone interface). This provided information regarding the bone intensity at the interface, but was not

sufficient on its own to identify regions of radiolucency. It was thus merely a sound basis on which to build. The **second** method was to analyse the profiles of rows across the implant (i.e. horizontally in Figure 3.6). This was effective in identifying regions of radiolucency (fibrous tissue formation). This was then applied to the first graph, reducing it in those regions where radiolucency was found. This combined graph was deemed to be a realistic representation of what could be seen on the images. A **third** approach was developed, but not used in the final assessment. Here the magnitudes of the slopes (gradients) of the fall-off in intensity from the implant to the surrounding bone were calculated. It was found that this parameter was effective in identifying regions of high bone density and probable good bone ingrowth. It was decided not to use this method, however, as those regions of good bone density were sufficiently well identified by the first approach. The following sections include an example of one of the patients, and illustrate each procedure as it is applied.

3.5.1 Features sought in X-ray images

The correct assessment of the condition of the implant is based heavily on the features sought on the X-ray image, and the guidance of an orthopaedic expert is thus of vital importance. Prof. Walters (orthopaedic surgery) provided valuable assistance in this regard. Although there are several factors to be considered in assessing such an X-ray, one feature is particularly important, and is described here. The most obvious and reliable indicator of fibrous tissue formation is the presence of a continuous radiolucent zone, an example of which is provided in Figure 3.7. This zone is typically represented by a darker line immediately adjacent to the implant, and a sclerotic line of hardened bone just beyond that. In Figure 3.7, the implant lies on the right (white), with the sclerotic line lying a few millimetres to the left. The darker band in between the two is fibrous tissue. This feature indicates definite fibrous tissue formation, and was thus given a great deal of attention in the present analysis. It is important that the radiolucent line be continuous, otherwise it may not indicate fibrous tissue formation. Also, a radiolucent line without an associated sclerotic line does not necessarily indicate the presence of fibrous tissue. Hence the intensity of the sclerotic line is particularly important. This study therefore gave considerable weight to assessing this parameter.

Figure 3.7 Typical example of sclerotic bone with fibrous encapsulation.

3.5.2 Profiles parallel to the edge of the implant

The first approach was to extract and plot the tissue densities along lines parallel to the edge of the implant. Such graphs are significant, as differences in the tissue density in different regions provide valuable clues about the extent of osseo-integration and stability of the implant. Furthermore, this is almost exactly what the numerical model predicts. Figures 3.2 and 3.3 show that the numerical model plots the extent of bone mineralisation along the edge of the porous surface, expressed as a percentage. This experimental analysis measures the bone density on a scale of 0 to 255, and then normalises this, to correspond to the numerical model.

The approach was first to establish the position of the edge of the implant, and then to use this line as a template to extract the corresponding grayscale values from the original image. The correct identification of the edge of the implant was very important, as several approaches in the analysis used this as a starting-point. The identification of this line was first achieved through the use of several of the edge detection routines in the Image Processing Toolbox. In short, the process was first to identify those regions having grayscale values of between 240 and 254. These values were chosen as they exclude the regions that are definitely implant (value 255) and include the higher regions, which are mostly bone, but also include some of the outer periphery of the implant. This was an effective starting point, because the sharp drop-off at the edge of the implant resulted in there being no possibility of confusing bone with implant. The result was several broad but broken areas, in the form of a binary image (*i.e.* where "1" represented a "chosen" pixel, and "0" a rejected one). These were then adjusted with several successive Toolbox routines, to produce a reasonably consistent line, representing the edge of the implant. These routines included area filling,

bridging of gaps, removing isolated pixels, and thinning of the line. However, use of these Toolbox routines required a significant amount of time and memory (as each of them processed an entire binary image the same size as the original), and thus other methods were investigated.

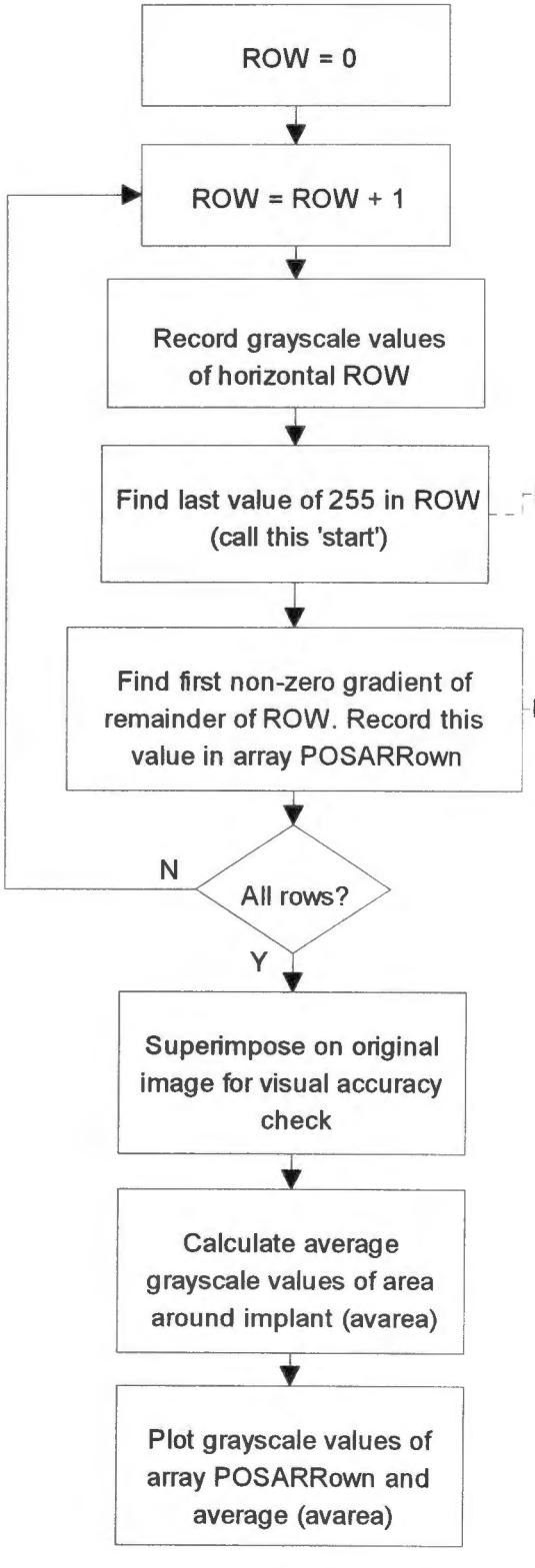

This results in a jagged edge being identified, and accounts for any irregularities in the implant before the final fall-off at the edge.

This was necessary because in some cases the fall-off at the edge of the implant was gradual, and the MATLAB routine rounded off values, thus still measuring these as being zero. Later methods (particularly those in Section 3.5.3) required finding the first zero after the edge of the implant, and it was necessary to eliminate possible zero gradients at the edge of the implant.

Figure 3.8 Algorithm for detecting edge of implant.

Several MATLAB routines and functions were written, and proved to be altogether more efficient in producing the desired results. Not only were these routines quicker, but they also used up less memory, making use of fewer variables. An outline of the algorithm is described in the following flowchart in Figure 3.8.

As a means of expanding on the descriptions, an example of one of the patients is presented, and carried through each procedure. Figure 3.9 shows the shape detected as the edge of the implant. It should be noted that this figure has been rotated anti-clockwise by 90°, compared to Figure 3.6. The detected edge is shown as a white line, although in practice this line is only a visual method used to confirm whether a suitable line has been extracted.

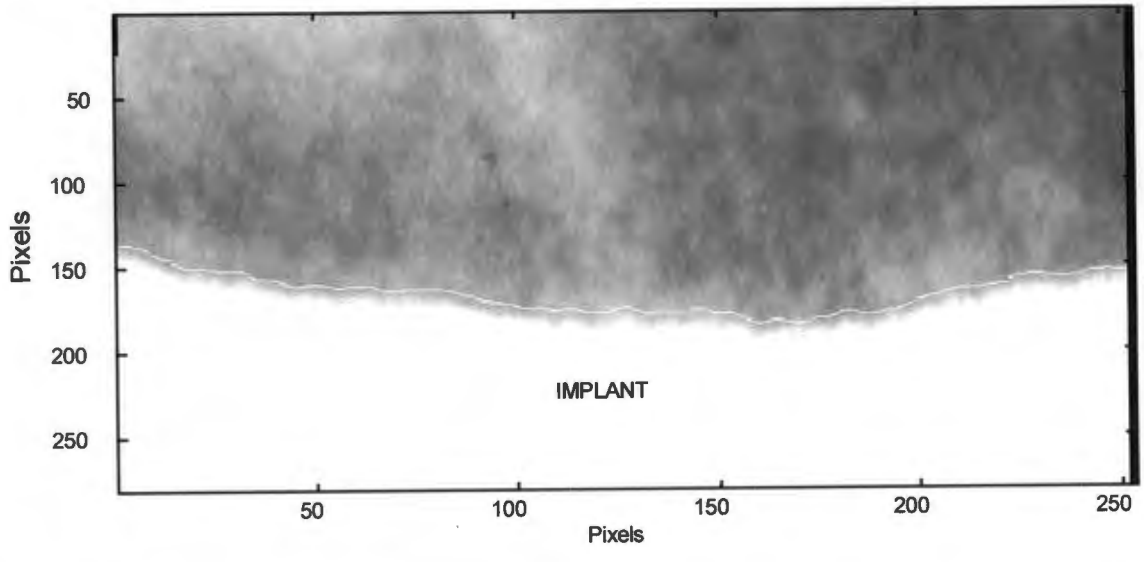

Figure 3.9 Section of X-ray image showing shape of detected implant edge (white line).

The line defining the edge of the implant was used as a template, and was moved away from the implant slightly, so as to be sure that only biological tissue was being included, and no implant material. The distance that this template was moved away from the implant varied slightly between images, but was generally between 330μm and 400μm (10 and 12 pixels respectively). The grayscale values at this new position were then extracted. This was done using a Toolbox routine that extracted the intensity values from the original image, at the specified points. This resulted in the extraction of the grayscale values along the edge of the implant, which were then plotted. A further useful procedure was to extract grayscale values along several lines parallel to the original line. This resulted in plots of grayscale values along lines a specific distance away from the implant. This could also be done for a succession of

distances, thus effectively showing bone density as a function of distance away from the implant. The grayscale values extracted from the example image are shown in Figure 3.10. The correlation is reasonably good, with regions of higher density around the implant appearing as peaks, and regions of lower density appearing as troughs. The higher regions tend to correlate very well with what is assessed as being good bony ingrowth, but the troughs merely indicate low-density tissue. There is no obvious distinction between low-density bone and fibrous tissue. For this reason, further information was necessary to refine the graph, and this is documented in the following section. It will be noted that a mean is shown in Figure 3.10. This is the mean of the grayscale values of an area immediately adjacent to the implant, 20 pixels wide. This was intended to provide a benchmark that would allow a judgement to be made as to whether tissue was fibrous or bony. In other words, if an average of the surrounding tissue density was known, it was anticipated that regions lying below this mean would indicate fibrous tissue, and those lying above it, bony tissue. Although providing something of a benchmark, this approach did not prove to be as effective as was hoped. In Figure 3.10, there were two regions of clear radiolucency (between pixel positions 90 - 280 and 890 - 990), but as can be seen, these regions (particularly the first) do not lie clearly below the mean. Even raising the mean slightly does not result in those radiolucent zones falling neatly below the mean.

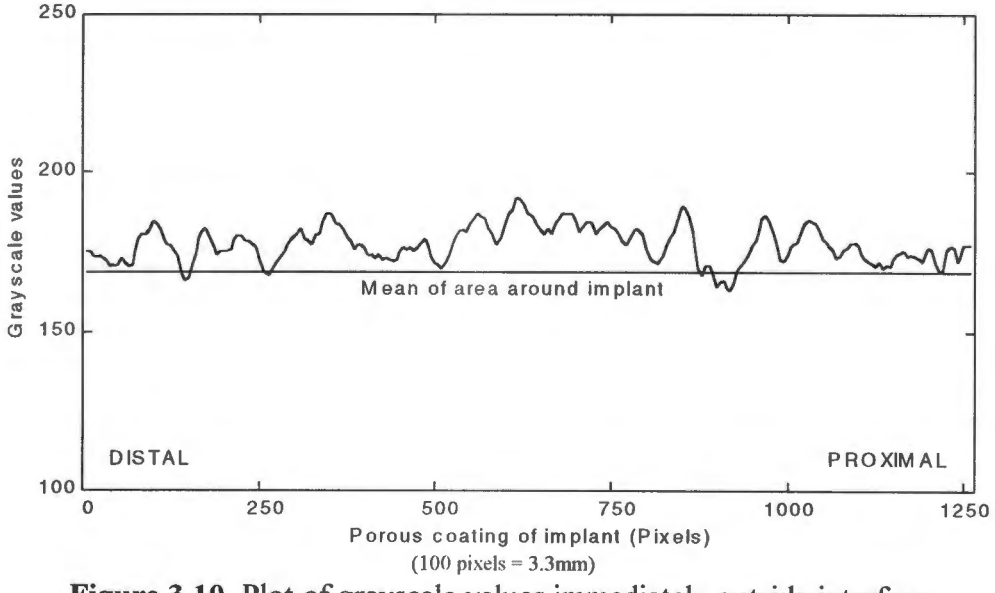

Figure 3.10 Plot of grayscale values immediately outside interface.

This method was thus judged to be a "pure" method, but limited in that there was no reliable

benchmark for comparison. Bone densities in different regions of the implant could be effectively compared with one another, but it was difficult to quantify whether a particular density represented good bone density or possibly fibrous tissue. One means of acquiring a benchmark was the identification of regions of known fibrous tissue formation (described in Section 3.5.3). In this case, the graph could be positioned such that those regions identified as fibrous tissue lay below a threshold, this threshold distinguishing the bone from the fibrous tissue. This method was effective in identifying regions of higher tissue density, but ineffective in identifying fibrous tissue. However, it was a sound basis on which to build, and with the addition of information from others, provided a good indication of the tissue density at the interface.

3.5.3 Profiles along horizontal rows

The second approach was to consider the image profiles along each horizontal row. Across one row (assuming the image is positioned as shown in Figure 3.6), intensities begin at a maximum at the implant (white), and then decrease to near-zero (black) on the right, as in Figure 3.11. The maximum value of 255 occurs throughout the implant itself (metal), with a sharp drop-off at the edge of the implant. Of particular interest is the possible presence of a radiolucent line immediately adjacent to the implant. This is commonly associated with a sclerotic line of hardened bone just beyond the radiolucent line. This would provide substantial evidence for the presence of fibrous tissue. Two methods were used to judge whether such a radiolucent zone existed. Both methods that were adopted examined the typical shape of the intensity profile of the implant and surrounding bone.

Method 1: Use of associated gradient plot

The first method made use of the intensity profile and its associated gradient plot. An example of the general shapes of each are shown in Figure 3.11. The gradient plot indicates where the slope of the intensity profile becomes positive, negative, and zero. The zeroes are particularly useful in determining points of local minima and maxima of the intensity graph. Moving from left to right in the gradient plot, the graph is initially zero where the intensity remains constant at 255. At the edge of the implant, the gradient quickly becomes negative, reaching a minimum at the position of the steepest negative slope. It then increases (becomes less negative), and crosses the x-axis at a point where a local minimum occurs in the intensity

graph, and represents the bottom of the "trough" of the radiolucent zone. The gradient plot continues to increase, through the maximum positive slope, and then decreases again, crossing the x-axis at a corresponding local maximum in the intensity graph, the top of the sclerotic "ridge". Thereafter, the gradient plot converges to zero as the grayscale values becomes more consistent. The region of greatest interest is the region between the first local minimum and maximum.

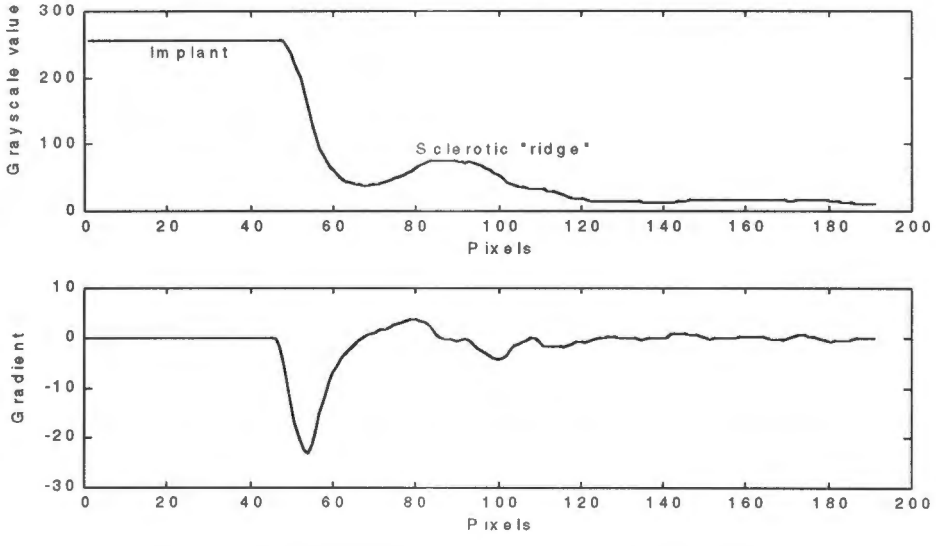

Figure 3.11 Example of row profile and gradient.

The above description is, of course, an ideal case, with no complicated shapes. In reality there are numerous variations in shape that make this analysis more difficult. A robust method, capable of accommodating all possible variations in shape and emerging with the correct assessment, was necessary for analysing the images. A quantitative measure was required to assess whether there were any signs of a sclerotic line. The first step was to examine the image and establish the approximate width (in pixels) of any radiolucent zones. This width is used to narrow down the region of interest, thus saving processing time, and eliminate the effect of possible outlying regions of high density bone, such as the cortex. Although detracting from the automation of the process, this step was necessary to optimise the performance of the procedure. The process thereafter was to examine each row as shown schematically in Figure 3.12.

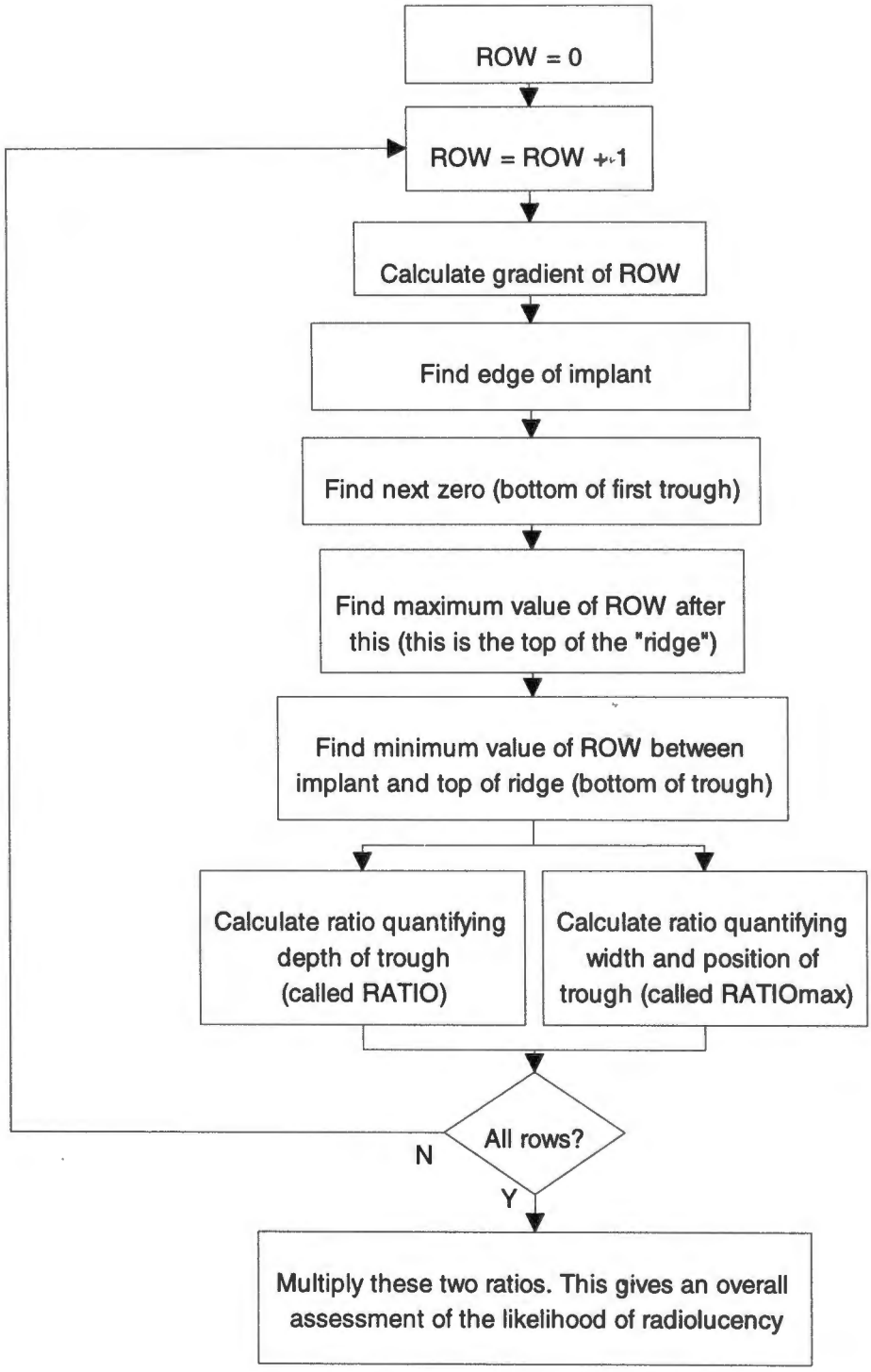

Figure 3.12 Algorithm for quantifying regions of radiolucency.

A high value of this ratio indicates that a significantly deep and wide radiolucent zone has been detected, and low values indicate that neither has been found. Middle-range values imply that either only one ratio is high, or both are average, and this is a region of less marked radiolucency. This method is effective in identifying regions of radiolucency, but the opposite

is not true -- low values do not necessarily indicate good bone density. For this reason, all positions at which the graph is less than a threshold were reset to that threshold. This threshold was usually the mean plus one standard deviation, thus extracting only the regions of definite radiolucency. In other words, the graph was "cut" through the centre (approximately), and only the top half retained. This graph was then inverted (because radiolucent zones are used to *reduce* the grayscale plot), and positioned such that the threshold value equalled 1. This was necessary so that when this graph was multiplied by another, it would only alter the other graph in those regions not equal to 1 (i.e. in regions of radiolucency). Figure 3.13 illustrates the example. It can be seen that those regions corresponding to radiolucency (particularly positions 90 - 280 and 890 - 990) that were not picked out by the first method (Figure 3.10), have been clearly identified by this method.

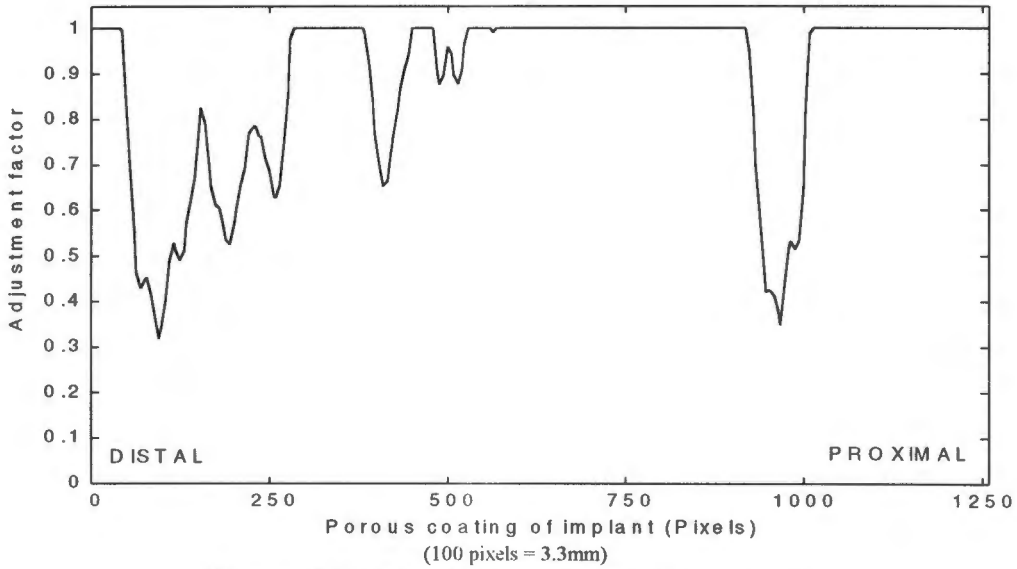

Figure 3.13 Identified regions of radiolucency.

Initially analyses were carried out on each individual row. It was found, however, that if each group of five successive rows was averaged, the effect was two-fold. Firstly, small discontinuities higher up in the profile were smoothed, usually enough that they were not recognised at all. Secondly, the actual row profile became more consistent. By this is meant that even in a region where a definite radiolucent zone exists, some row profiles do not display a typical radiolucent shape. With this averaging method, these inconsistencies were filtered out. The averaged five rows provided a more realistic representation of the actual appearance of the region. Initially, only a part of each row was averaged -- from the implant edge to a point 100 pixels away. However, this required a great deal of processing time

(approximately 15 minutes). This would seem to be an unacceptable length of time, especially bearing in mind that there is only one feature being identified, and only the porous coated region was being examined. Also, as this diagnostic tool develops, more features will need to be extracted, and this running time would then become a significant restriction. However, it was found that averaging the entire row did not detract from the result, and it required much less processing time (approximately 3 minutes). Hence, this was the approach that was used.

This method of analysing row profiles proved to be the most robust of those attempted, but at the expense of complexity and time. This routine required the longest time to run, and the MATLAB code was generally more complex than the other routines.

Method 2: Correlation with known radiolucent profile

The second method used to test for the presence of a radiolucent line was to analyse the shape of a row profile by comparison with the shape of a known profile. Model profiles of both radiolucent zones and bone ingrowth were used. Due to there being many different possible shapes of radiolucent profiles (both in height and position), it was necessary to use several models for radiolucency. It was hoped that a row profile would correlate significantly better with one type of model profile, and differ significantly with the other, and thus be effective in distinguishing between regions of radiolucency and bone ingrowth. Some of the model radiolucent lines were pointed out by Prof. Walters earlier in the investigation as being good examples of radiolucent zones. The correlation was carried out using a MATLAB routine which statistically correlates 2-dimensional arrays.

For comparison, the arrays were required to be of the same length. For an accurate assessment, it was necessary to extract corresponding regions from each profile, as this would ensure that the correlation was due to the detail of the profile alone, and not the overall shape. In other words, if the sample profile was one which began at a particular point in the row, then comparing this to a sequence that began in a different position would obviously result in little correlation. Only if the two sequences began in exactly the same position could the profiles be meaningfully compared. Hence, the starting point chosen was the edge of the implant. The length of the array was 100 pixels (corresponding to 3.3mm on the X-ray), as most radiolucent zones would occur within this width. The procedure was to acquire a correlation coefficient for every fifth row (for memory- and time-saving reasons), and to store

these coefficients in an array. The plotting of this array of coefficients produced peaks corresponding to regions where correlation was high, and troughs where correlation was low.

Although this method seems to have a sound basis, there were a number of problems. Firstly, the fact that rows being compared had to be of the same length was a serious problem, as they could not easily be lengthened or shortened to a corresponding length. There were thus gray areas where correlation with either model graph could not be reliable. A second problem was that the method tended to be biased towards correlating better with the bony ingrowth profile. By this is meant that all of the image radiolucent profiles correlated well with the model bony profiles, with the model radiolucent profiles performing only slightly better. This was due to the fact that the radiolucent profiles and the bony profiles were very similar. Both had a steep drop-off at the edge of the implant, and a flattening out lower down in the profile. The only difference was the trough and ridge in the case of radiolucency. This had the result that any profile of more-or-less this shape correlated well with both graphs, and the correlation with the bony profile was generally better than desired. This method was thus more effective at identifying regions of bony ingrowth than fibrous tissue ingrowth.

Due to these problems, and the fact that this routine was reasonably time-consuming to run, it was decided not to use this algorithm. There were already other effective ways of detecting bony ingrowth, and it was thus not necessary to use this approach.

3.5.4 Slopes of the fall-off at the edge of the implant

A third approach investigated but not used in the final analysis was to examine each row profile, and find the steepest slope of the fall-off at the edge of the implant. It was thought that the steepness or shallowness of this slope would provide an indication of the tissue type immediately surrounding the implant. It soon emerged, however, that this method was effective at identifying regions of good bone ingrowth into the porous coating, but ineffective at identifying radiolucent zones. Initially, this method was used to enhance the grayscale plot in those regions displaying definite bone tissue formation. The adjustment was made in a similar manner to the previous one, except that in this case these regions were increased. The maximum slope was calculated and recorded for each row, and the plotting of these data resulted in peaks in regions of good bone ingrowth. As in the case of the radiolucency plot,

this graph was not allowed beyond a particular threshold. In this case, that threshold was the mean of the values, and any values smaller than the mean were reset to the mean. This graph was then positioned such that the threshold had a value of 1. Initially, this graph was combined with the previous one for radiolucency, thus forming a graph of all adjustments necessary to refine the original grayscale plot. The combining of the two graphs was done by multiplication, as this left the graphs unchanged in those regions where both values were 1. An example of this is shown in Figure 3.14. It will be noticed that the previous data from Figure 3.13 is almost undisturbed. In fact, with some adjustment, this representation is almost sufficient on its own to quantify the image data, and this approach may prove to be preferable in future analyses.

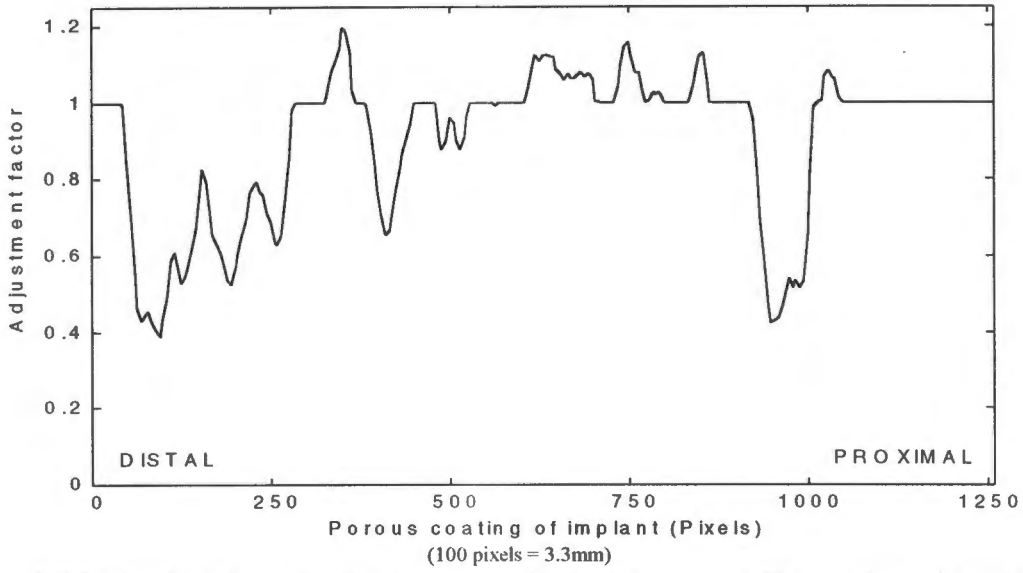

Figure 3.14 Combined graph of adjustments for both bony and fibrous tissue identification (Note: this graph was not used in the final method).

This graph was only used in the initial stages of investigation, and not in the final analysis, for two reasons. Firstly, the original grayscale plot provided a good representation of those regions showing good bony ingrowth, more than adequate for the aims of this study. Secondly, it was not desirable to distort the data unnecessarily. This adjustment would have increased only those regions of definite bone formation, and thus distort the data somewhat. Due to these reasons, it was decided not to include this procedure in the final analysis. Thus, only the data pertaining to the radiolucent line (Figure 3.13) was used to adjust the original grayscale plot of Figure 3.10.

When these two graphs (Figures 3.10 and 3.13) were combined as described above, this had the effect of reducing the grayscale plot only in those regions where radiolucency was detected. The final result is shown in Figure 3.15. Comparison of this graph with the original grayscale plot of Figure 3.10 shows that the basic shape is retained (although it has been stretched), with those regions requiring adjustment having been altered. However, this graph is not a pure representation, in the sense that it is very difficult to judge the percentage of bone mineralisation that the extremes exhibit in reality. In other words, it is difficult to assess whether the maximum value in the original grayscale graph indicates good bone ingrowth, or whether the graph should be stretched vertically. For this reason, it was decided to normalise the data, so that the largest positive values are made to equal 1. It is realised that this is not a completely true reflection of the actual case, but it was essential to be consistent in manipulating the data, and to position the graphs such that they could all be effectively compared with one another. With these problems in mind, it will be appreciated that the shape of the graph is its most important asset. Regions of high values indicate good bony ingrowth, and negative regions suggest that fibrous tissue formation is likely. Furthermore, the positive and negative regions differ somewhat in interpretation, and this is explained in greater detail in Section 4.1.

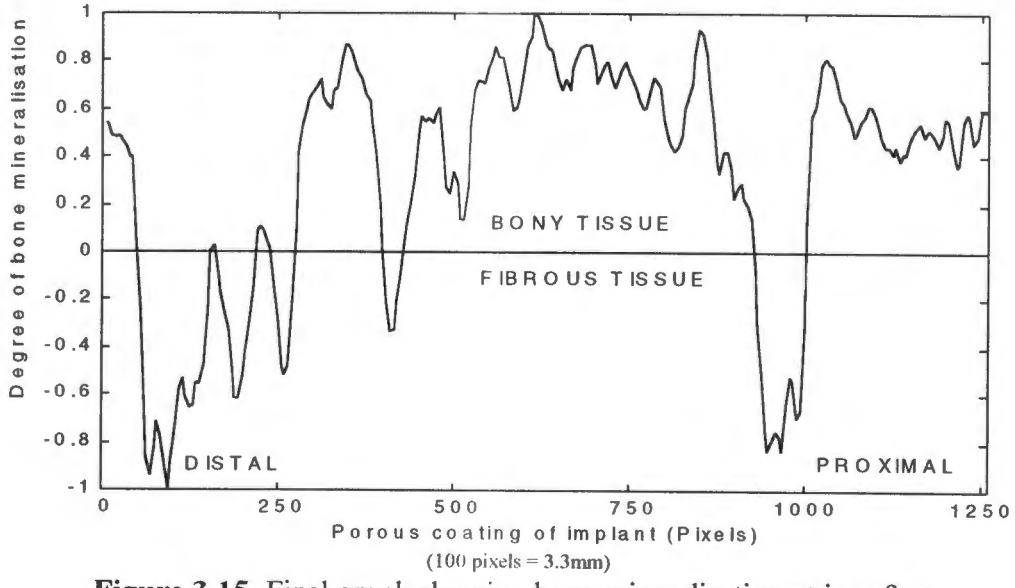

Figure 3.15 Final graph showing bone mineralisation at interface.

3.5.5 Three-dimensional representations

The fourth approach was to plot a 3-dimensional representation of the area around the implant. This was not strictly a 3-D picture, but rather a 3-D representation of a 2-D image.

In other words, a matrix value of 255 was recognised as being "high", and plotted as such, while smaller values were plotted at lower "height". This provided a "mountain range" view, where regions of higher bone density appeared as spurs and hills, and regions of lower density appeared as troughs, valleys, or low-lying areas. An example of this view of a sclerotic line is shown in Figure 3.16. This was a useful way of visualising the changes in bone density around the implant. A particularly noticeable feature was that of radiolucent zones appearing as troughs between the implant and the outlying sclerotic "ridge". It was soon realised, however, that this representation was essentially only good for visualisation, and not very useful for extracting quantitative data. Furthermore, the process of displaying a 3-D representation requires a great deal of memory and time (a 1.4MByte image took approximately 8 minutes to be displayed). Nevertheless, it was a valuable exercise in assessing the general bone density around the implant.

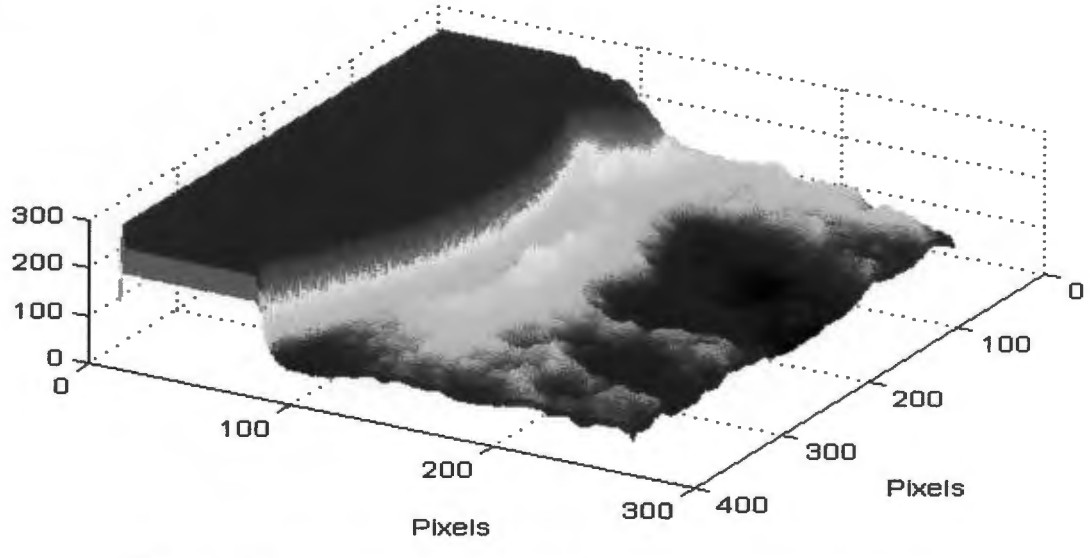

Figure 3.16 Example of 3-D view (showing sclerotic "ridge").

The area to be plotted as a 3-D representation was not extracted simply as a rectangle adjacent to the implant. This method would have resulted in the mountain range either including some edges of the implant, or excluding some areas of surrounding bone, or both. This, of course, was not desirable. Hence, the approach that was taken was first to identify the line representing the edge of the implant (as described previously), and then to extract the grayscale values on that line. This line was then moved away from the implant, one pixel at a time (i.e. each line parallel to the previous one), each time extracting the grayscale values. This was continued until a suitably large area was included. This approach resulted in a

precise representation of the surrounding bone, excluding the implant itself and including all immediately surrounding bone.

MATLAB provided several routines for better visualising the 3-dimensional view. It allowed for the construction of various colourmaps, resulting in particular heights being represented by particular colours. This was useful in enhancing certain features of the "mountain range". Also, the ridges could be "raised" using some of the routines that adjusted the intensity, contrast, and brightness of the original 2-D image. Other routines allowed contour plots to be drawn, but these proved to be too dense to be a useful representation -- there was simply too much fine detail in the image for such a plot. Zooming in to an image was also possible, although this was somewhat inefficient, and required a few seconds between each image representation. There was also the possibility of presenting a "fly-by" effect (what an aeroplane would see when looking down on the mountain range while flying overhead), but this didn't appear to have any distinct advantages over the static representation, and furthermore required a significant amount of time and memory.

Chapter 4 RESULTS

This chapter presents the extracted data from all seven of the patients studied. It presents only the final graphs resulting from the techniques and algorithms described in Chapter 3. It also includes the final data relating to the time study. Also included is an assessment of each patient's activity levels, which has obvious implications for the correlation of the findings with the numerical model.

4.1 Interpretation of graphs

Section 4.2 presents the extracted bone mineralisation at the implant-bone interface. However, their interpretation of these graphs requires elaboration. The graphs range from -1 to +1, where positive values represent bony ingrowth, and negative values represent fibrous tissue formation. This was done because the numerical model was presented in this way and correlation between the two is thus more meaningful. However, physiologically the development of the tissue at the interface will follow one of two routes, either towards bone formation or fibrous tissue formation. Thus the transition from positive values to negative values is not strictly continuous - low density bone is not necessarily "close" to becoming fibrous tissue. A more realistic interpretation is that in the positive half (top), higher density represents higher bone mineralisation (as one would expect), but in the negative half (bottom), lower values represent the width or clarity of radiolucent zones. In other words, a small negative value indicates fibrous tissue formation, where the radiolucent line is narrow or not marked, while a large negative value indicates a wide or marked radiolucent line. In the positive region, the interpretation is as one expects, namely that higher values represent greater bone mineralisation, and lower values indicate less mineralisation, but still definite bone formation. The positive regions of the graphs have been scaled (i.e. "stretched") so that their maximum values are +1, but this is not strictly true. Great difficulties were experienced in determining whether the maximum tissue density in a particular graph constituted 100% bony ingrowth, and if not, what this value should be. It was thus decided that this approach was the best means of presenting the data.

4.2 Tissue density graphs of patients

One of the main objectives of this study was to determine whether any correlation existed between the numerical model and the actual findings. A statistical assessment of this

correlation was not practical, as the exact data from the numerical model was unavailable. Also, these two parameters are of differing dimensions and cannot easily be compared. Furthermore, a qualitative assessment was more than adequate for this purpose. To provide an approximate quantitative assessment of the agreement of the graphs with the numerical model, a rough scale has been drawn up. Five degrees of correlation have been used, defined as follows:

- Excellent agreement: the graph and the numerical model correlate almost perfectly, with both the shape and the position of the graphs matching extremely well.
- Good agreement: the overall shape of the patient graph and the position of the graph are similar to the numerical model.
- Some agreement: there is either a vague overall correlation, or parts of the graphs correlate to a limited degree.
- Poor agreement: there is extremely limited correlation between the graphs, with only a suggestion of correlation in a part of the graphs. The graphs are generally dissimilar.
- No agreement: no correlation whatsoever exists between the graphs. The graphs appear to contradict one another.

Each graph has been assigned the most appropriate level of this range. This is, of course, a qualitative assessment of each of the graphs, and is thus not a true quantitative evaluation. For the reasons given above, it is felt that this is the most appropriate means of describing the correlation. The prediction of the numerical model is presented again in Figure 4.1, for comparison purposes.

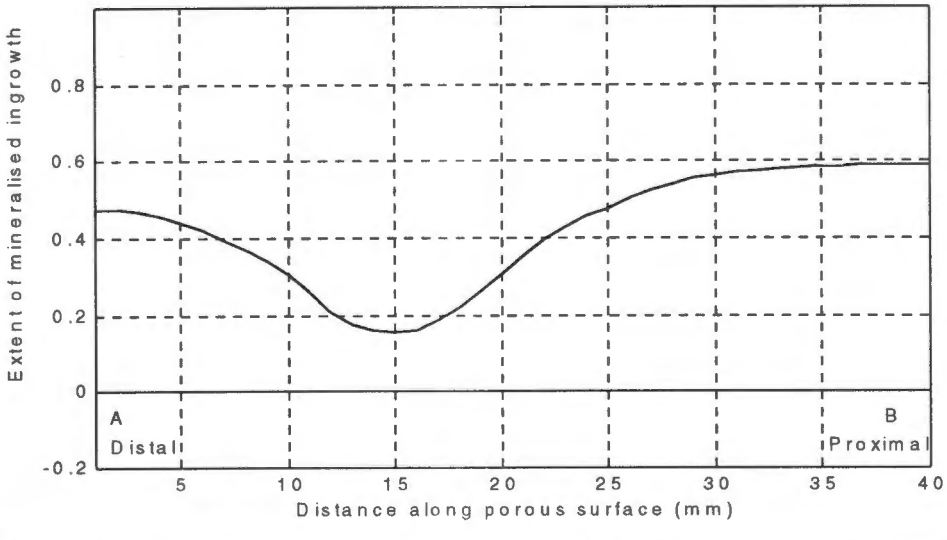

Figure 4.1 Prediction of numerical model with fluctuations averaged (160 days).

4.2.1 Patient 1

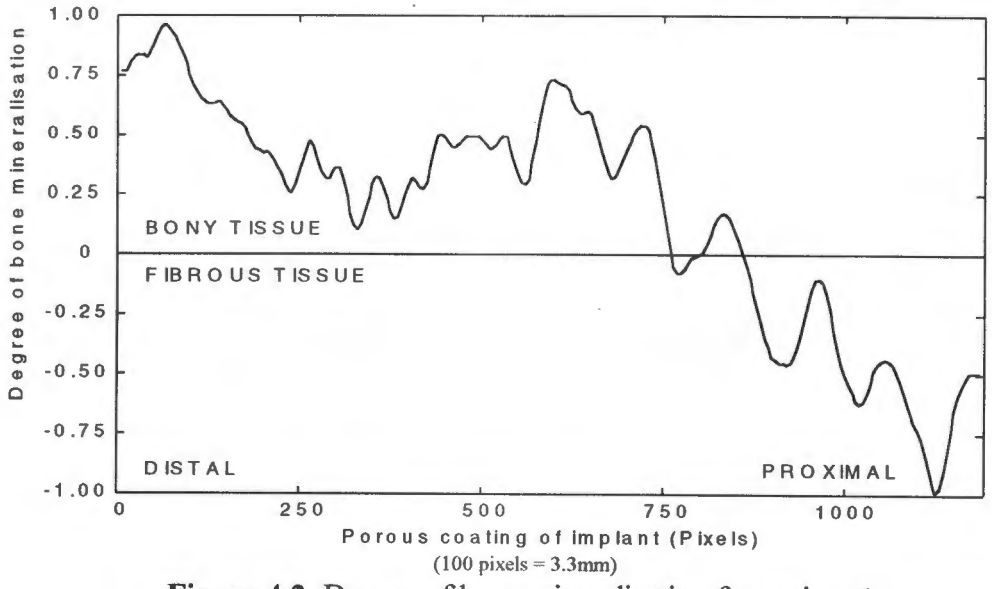

Figure 4.2 Degree of bone mineralisation for patient 1.

Patient 1 (Figure 4.2) showed a high degree of mineralisation in the distal regions of the porous coating, with a sharp drop-off when moving proximally. The bone then becomes more dense again in the mid-porous region, before another sharp drop-off where fibrous tissue becomes predominant. The distal half of the porous coating thus displays reasonable correlation with the numerical model. The proximal half, however, shows no correlation at all and so overall agreement is poor.

4.2.2 Patient 2

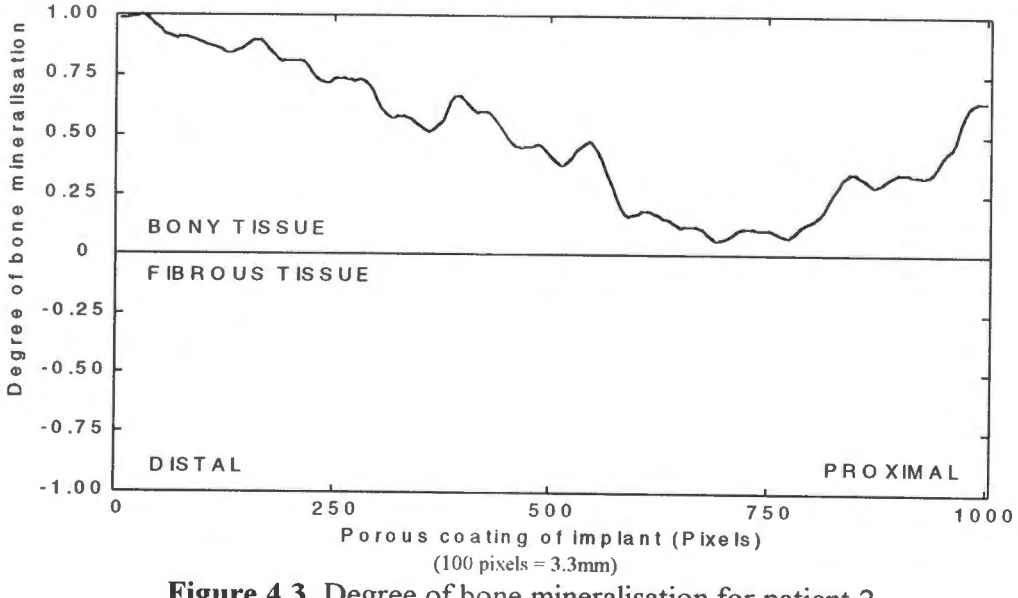

Figure 4.3 Degree of bone mineralisation for patient 2.

Patient 2 (Figure 4.3) has bony ingrowth throughout the length of the porous coating, as does the numerical model. The distal half correlates well with the numerical model, and the proximal half is not dissimilar. The least degree of mineralisation occurs approximately two-thirds of the distance to the proximal end, whereas the numerical model predicts that this trough should occur more distally. There is good overall agreement.

4.2.3 Patient 3

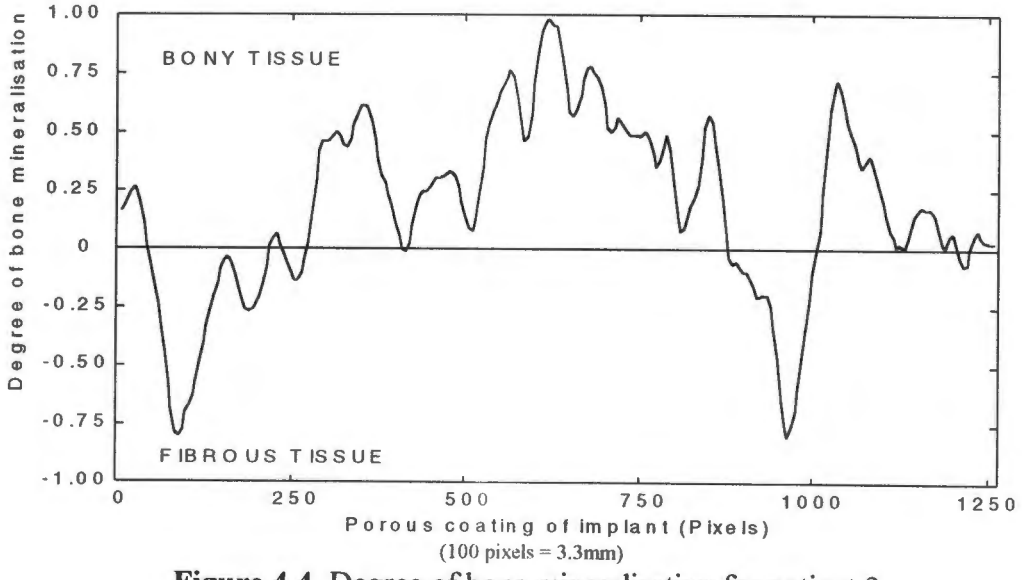

Figure 4.4 Degree of bone mineralisation for patient 3.

Patient 3 (Figure 4.4) displays no correlation with the numerical model. The porous coating has regions of fibrous tissue formation, but these are not even located in regions of low bone density in the numerical model. Overall, there is no agreement.

4.2.4 Patient 4

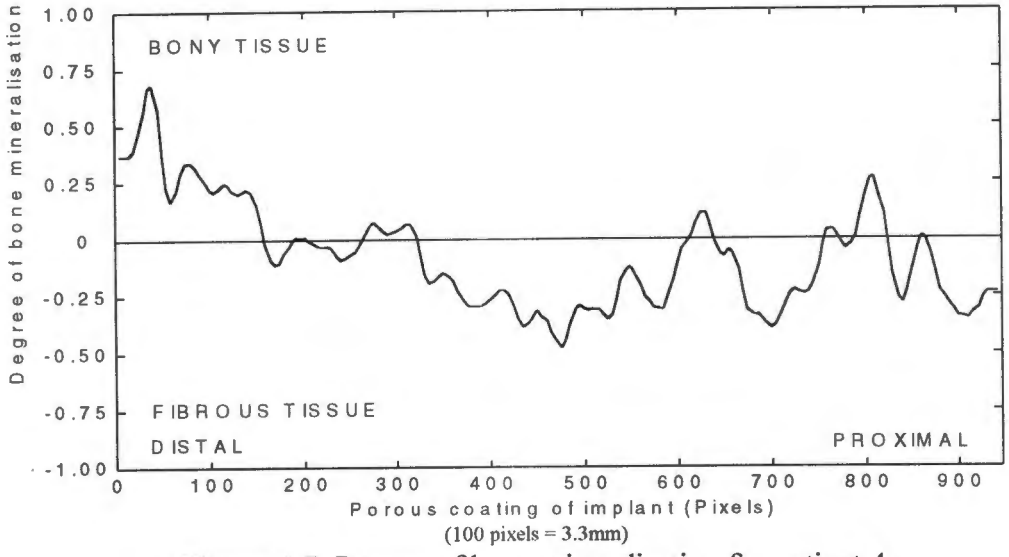

Figure 4.5 Degree of bone mineralisation for patient 4.

Patient 4 (Figure 4.5) displays an overall profile that is similar to the shape of the numerical model prediction, but the two are situated at different levels. More than half the length of the porous coating is covered with fibrous tissue, where the numerical model predicts none. The distal half has the best correlation, although actual mineralisation values are lower than the model. There is some agreement in overall terms.

4.2.5 Patient 5

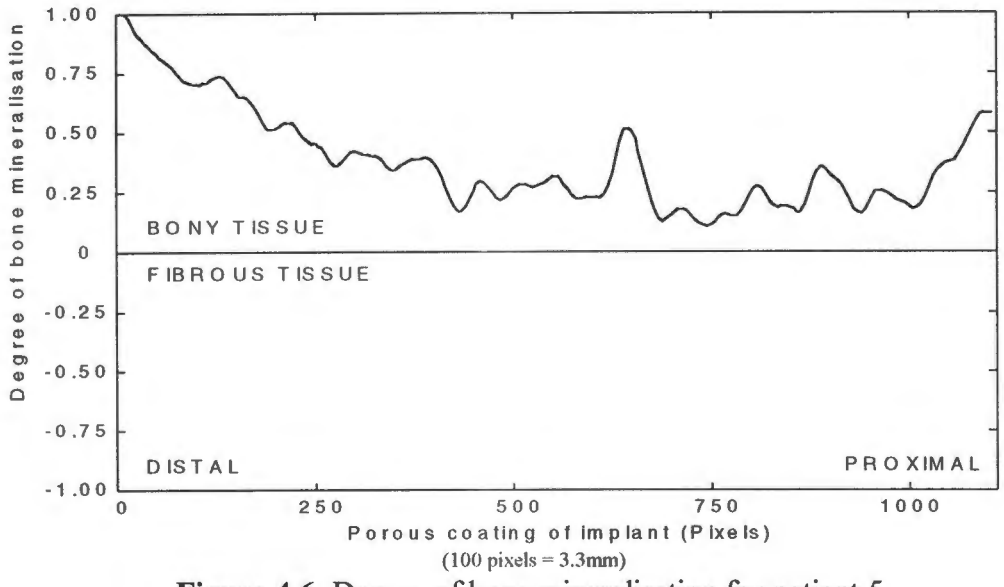

Figure 4.6 Degree of bone mineralisation for patient 5.

Patient 5 (Figure 4.6) shows good agreement with the numerical model. The distal half, in

particular, compares very favourably. The bone density in the proximal half is slightly lower than the prediction of the model. There is, however, a very gradual increase in the tissue density in the proximal end of the porous coating. There is bone tissue throughout. The overall agreement is good.

4.2.6 Patient 6

It should be noted that the X-ray image used for the analysis of patient 6 was one taken two months post-operatively. This was because there was a problem with the X-rays taken when the patient came in. There was a fault with the X-ray machine, and this resulted in fine light and dark bands appearing across each of the images. These were unsuitable for analysis with the software, as the bands produced wavy lines when plotted. The image used was thus not one of those taken during this study, but a previous one. Two months may be too soon to indicate reliably what tissue type has formed at the interface. Nevertheless, this was overcome by comparing the graph with the numerical prediction at 80 days.

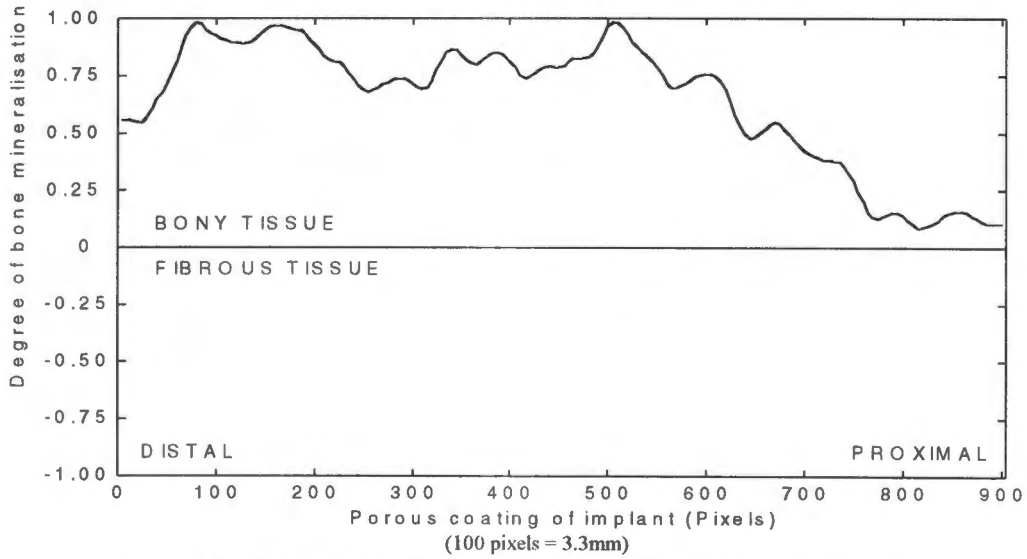

Figure 4.7 Degree of bone mineralisation for patient 6.

Patient 6 (Figure 4.7) displays high bone density in the distal half, and bone formation throughout. There is a slight decrease from the distal high moving proximally, but this is limited, and increases again almost immediately. The general shape is dissimilar to that of the numerical model, but there is some overall agreement.

4.2.7 Patient 7

The X-ray image used for patient 7 was taken eight months post-operatively. This was done because the patient did not agree to come in for the X-ray, but it was established that a previous X-ray was of a sufficiently good quality to make an analysis of this patient worthwhile. This has the result, however, that this graph differs slightly from the others, and may not be a good indicator of the type of tissue that eventually forms under the assumed conditions. The tissue might still be in the process of becoming a particular type, and not had enough time to stabilise.

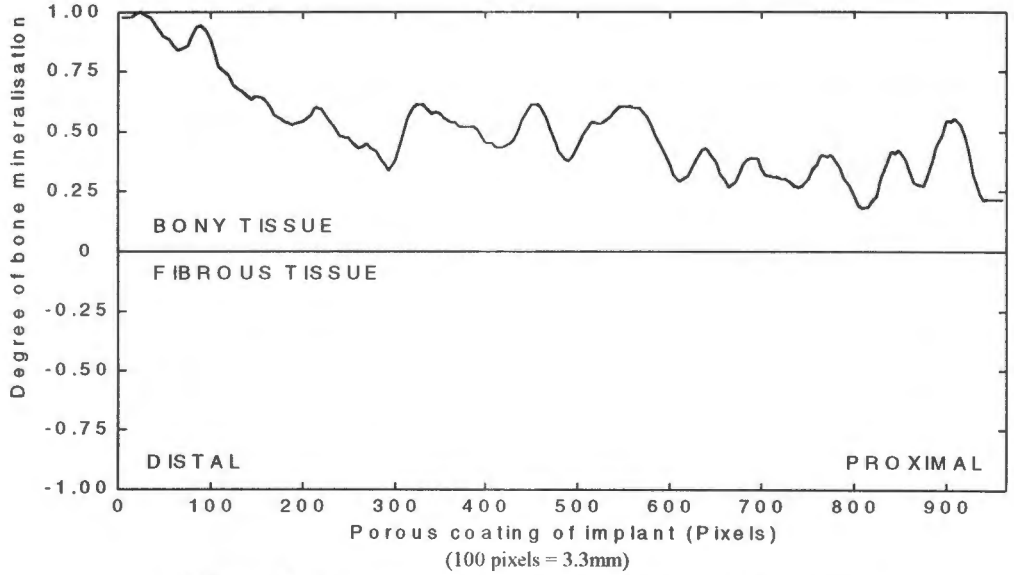

Figure 4.8 Degree of bone mineralisation for patient 7.

Patient 7 (Figure 4.8) has bony ingrowth throughout the length of the porous coating. The distal half compares well with the numerical model, with a maximum at the distal end that drops off when moving proximally. The proximal half has slightly lower tissue mineralisation than predicted, and does not increase towards the proximal end. There is some overall agreement.

4.3 Tissue density changes over time

A time study of the density of the tissue around the implant was also undertaken. It was thought that having information about the changes in tissue density over time may provide clues as to whether fibrous tissue or bony tissue was likely to form, or was in the process of forming. In other words, if the tissue density in a particular region was found to be increasing over a period of time, this may indicate that good bony ingrowth would ensue. Conversely, decreasing tissue density may indicate that fibrous tissue was in the process of forming.

All of the past X-rays of the patients who participated in this study were acquired and examined. It was found that only one of these patients (patient 4) had a sufficient number of X-rays of good quality to make a time study feasible. This patient's X-rays from four previous occasions were used, along with the fifth which was taken during this study. The chosen X-rays had been taken 10 days, 24 days, 73 days, 200 days and 1300 days post-operatively. A significant problem with this study was that the X-ray machine settings of those X-rays taken previously (the first four) were unknown. The X-ray images varied somewhat, with some being lighter than others. This had the result that they could not be meaningfully compared with one another. Figure 4.9 shows the grayscale plots of lines immediately adjacent to the implants in each image. These have been extracted as described in Section 3.5.2, with no enhancement (Sections 3.5.3 and 3.5.4). The enhancement has not been done so as not to distort the data at all, thus making comparison most meaningful. Hence, the shapes of the graphs of Figure 4.9 are accurate, but their positions relative to each other are not.

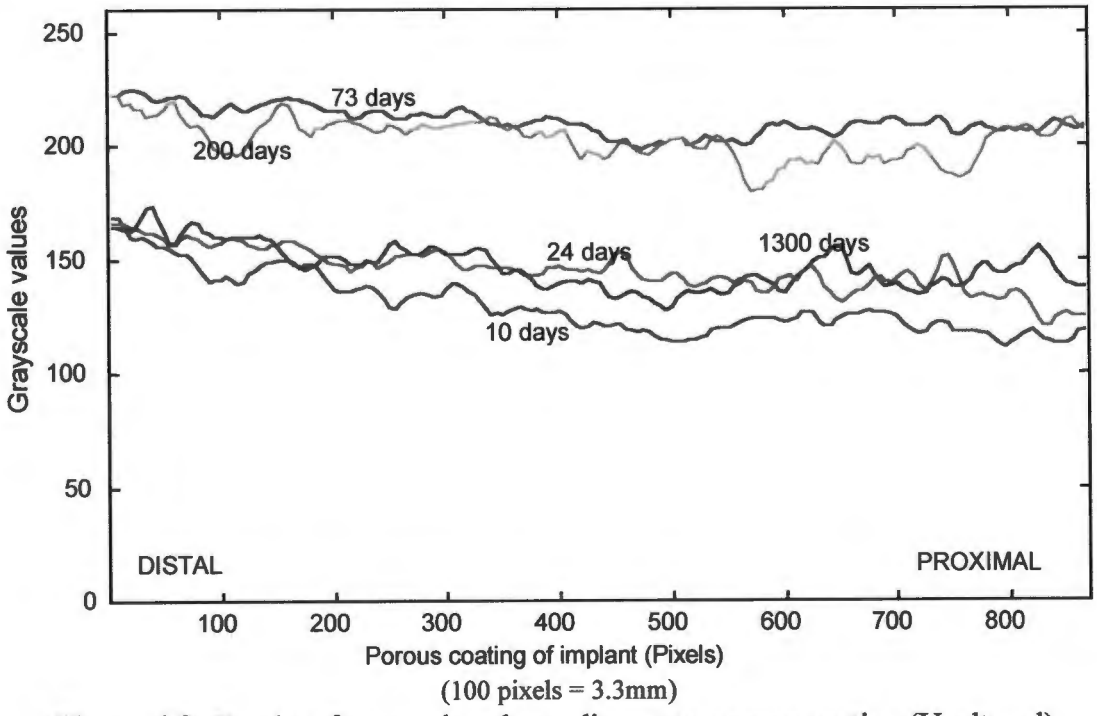

Figure 4.9 Graphs of grayscale values adjacent to porous coating (Unaltered).

The images required a benchmark for comparison purposes, and a sample of the density of the bone cortex was used for this purpose. From each image, corresponding sections of the cortex were extracted as samples. The intention was to adjust the above graphs by plotting each one relative to its sample density. In fact, two sample regions were used from each image, and these values averaged. The samples were taken from the lateral, mid-stem regions of the bone

cortex, as stress shielding from the implant is less here than on the medial side. The densities (grayscale values) of each sample were then calculated, and these results are shown in Table 4.1. The ratios shown are those factors that reduce the sample value to the smallest of the sample values (e.g. 208x0.8125=169). The averaged ratio will be multiplied by each of the graphs, thus appropriately normalising each graph to a level comparable with the others.

Time post-op. (days)	Sample 1 (grayscale)	Ratio 1	Sample 2 (grayscale)	Ratio 2	Average Ratio
10	208	0.8125	164	0.8415	0.8270
24	180	0.9389	146	0.9452	0.9420
73	232	0.7284	184	0.7500	0.7392
200	232	0.7284	184	0.7500	0.7392
1300	169	1.0000	138	1.0000	1.000

Table 4.1 Grayscale values of sample regions.

Each graph multiplied by its average ratio produces the graphs of Figure 4.10. When compared with Figure 4.9, it can clearly be seen that the graphs have converged to a common level. It should be noted that this process has reduced the grayscale values, and has thus distorted the data slightly. This is unfortunately unavoidable in a normalisation process such as this. However, this is not a significant alteration as it is not the actual values that are sought, but rather the trends -- how the graphs behave compared to one another.

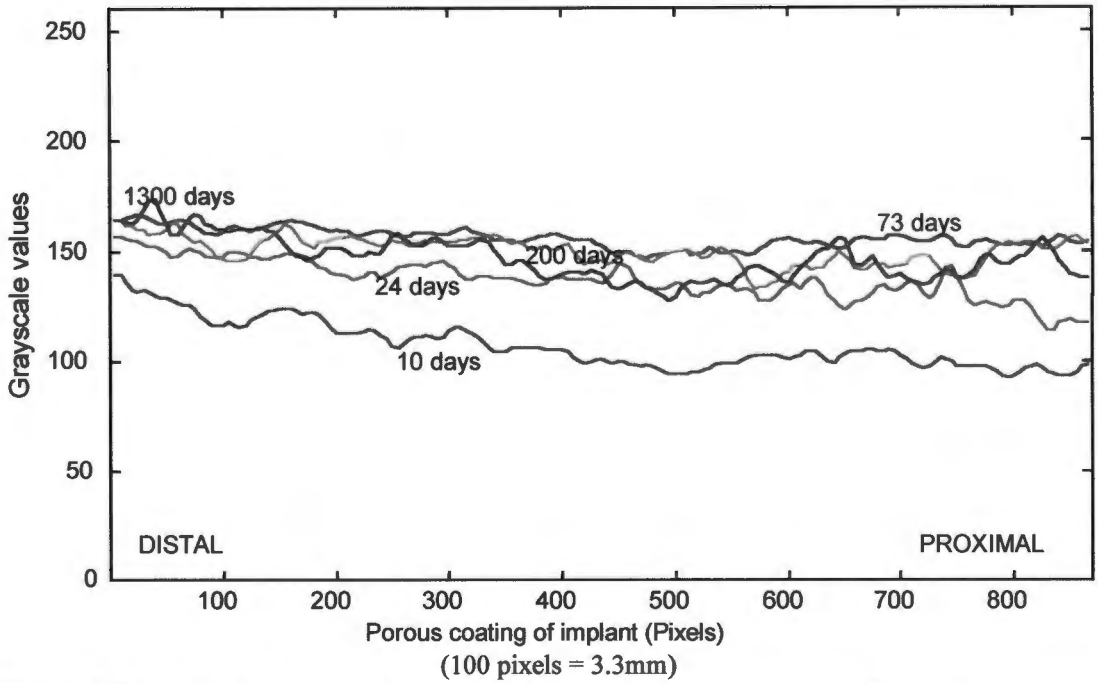

Figure 4.10 Graphs of grayscale values adjacent to porous coating (Intermediate stage).

There is an inaccuracy with the above procedure. The process relies on the fact that the density of the bone cortex does not change over a period of time. This is may be a doubtful assumption, especially considering that this patient was diagnosed with osteoarthritis. The problem was overcome by acquiring information about the patient's bone density. This data was provided by the osteodensitometry group at Groote Schuur Hospital. The information was acquired using DEXA, and an example is shown in Appendix D, although not for the same patient. The relevant region is zone 6, and the patient's bone density in this region is shown in Table 4.2. The times at which these data were recorded (8 days, 100 days, 192 days and 1107 days post-operatively) correlated well with those required in this study. The data for the second image was acquired by interpolation of the data of the first and third recordings.

Time post-op. (days)	Density of bone cortex (g/cm^2)	Ratio 3	Final Ratio
8	1.727	0.8217	0.6795
(24)	1.698*	0.8357	0.7872
100	1.562	0.9085	0.6716
192	1.419	1.000	0.7392
1107	1.469	0.9960	0.9660

* This value was acquired by interpolating the surrounding data

Table 4.2 Bone cortex density changes over time.

The ratio in the Table 4.2 is calculated in the same way as before, with the ratio being the factor that reduces each density value to the minimum value (e.g. 0.8217x1.727=1.419). This again has the effect of adjusting the values to a comparable level. Ratio 3 is then multiplied by the previous graph (Figure 4.10), thus further correcting the benchmark. This produces the final result, shown in Figure 4.11. In practice, it was simpler to combine the two relevant ratios, without constructing the intermediate graph. Multiplying these ratios (the average ratio of Table 4.1 and ratio 3 of Table 4.2) results in a final ratio, shown in Table 4.2. This is the actual value that was applied to the original data, and produced the result in Figure 4.11.

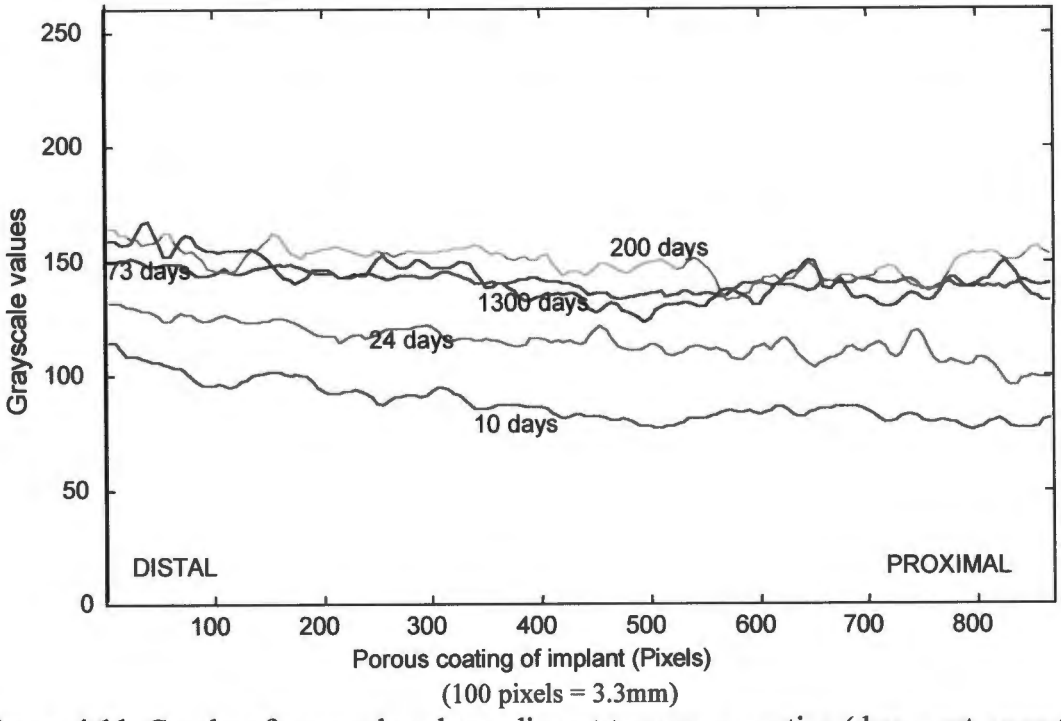

Figure 4.11 Graphs of grayscale values adjacent to porous coating (days post-operatively).

4.4 Loading of implants

The activity levels of the patients were assessed by means of a questionnaire (Appendix B), and were found to vary considerably. Some patients were extremely active, taking part in several sports, including running, hiking, cycling, and others. Other patients only undertook sedentary tasks. Furthermore, the patient's body masses varied greatly, ranging between 46kg and 98kg. It was thus necessary to compute a numerical factor that would quantify the activity levels of the patients. Some activities, such as running, place proportionately greater forces on the hip joint than others, such as swimming. Hence, each activity was assigned a hip stress rating between 1 and 5, shown in Table 4.3. The regularity of activity was also important, and thus another factor was used, according to the questionnaire options. Here the factors 1 to 5 represented occasionally, monthly, fortnightly, weekly, and daily, respectively. These two factors (stress and regularity) were then multiplied to produce a factor indicative of their activity level in that sport. For example, a patient cycling on a weekly basis would score 3 x 4 = 12 for that activity. This produced an activity factor that was based on both the type of activity and the regularity of that activity.

Activity	Stress rating (on hip)
Swimming	1
Cycling	3
Athletics	5
Golf	4
Soccer	5
Rugby	5
Hiking	4
Squash	5
Bowls	2

Activity	Stress rating (on hip)
Cricket	3
Running	5
Tennis	4
Weights	1
Climbing	2
Table tennis	2
Canoeing	1
Volleyball	1

Table 4.3 Stress ratings assigned to various activities.

It was felt that the amount of walking or standing that a patient did in a typical day was also important, as these activities contribute to forces experienced by the hip joint. However, all of the patients indicated that they spent in excess of 2 hours per day walking or standing. It was thus decided to use the patient's description of their activity levels in general. This question offered the responses very active, active, average, inactive, and sedentary. These responses were allocated the values 5, 4, 3, 2, and 1 respectively, and were multiplied by 3 to give them suitable weighting. This factor was then added to those of the sporting activities, resulting in an overall activity factor for each patient. This data is summarised for all patients in Table 4.4, where only those sports activities shown were undertaken by the patients.

Patient	Swimming	Cycling	Gym/weights	Hiking	Running	Table tennis	Canoeing	Volleyball	General Activity (Standing & walking)	Overall Activity Factor
1									Average (9)	9
2									Average (9)	9
3	W(4)	D(15)	D(5)						Very active (15)	39
4		W(12)		O(4)	W(20)	M(4)	M(2)		Active (12)	54
5	W(4)	D(15)		O(4)					Very active (15)	38
6	O(1)		2W(6)	O(4)				W(4)	Active (12)	27
7									?	(Moderate)*

*This patient could not be contacted; hence this assessment comes from a previous study.

(O=Occasionally; M=Monthly; F=Fortnightly; W=Weekly; D=Daily; Numbers in brackets indicate points for that activity).

Table 4.4 Summary of activity levels of patients.

It can be seen that there is no strict maximum value to this range. The following scale was thus used to categorise the activity levels of the subjects. This was judged to be a more appropriate indicator of activity levels.

Factors 0 - 15: Inactive

Factors 16 - 30: Moderate

Factors 31 - 45: Active

Factors >45: Extremely active

The patient's activity factors tended to fall towards the centre of these ranges, resulting in these descriptions being good indicators of activity levels.

4.5 Summary

Table 4.5 below provides a summary of the data collected in this study, and is discussed further in Chapter 5.

Subject	Age	Sex	Mass (kg)	Days until weight-bearing (walking)	Activity Level	Agreement with Numerical Model	General Tissue Type
1	64	M	75kg	5 (7)	Inactive	Poor	Bony + Fibrous
2	47	F	46kg	180 (180)	Inactive	Good	Bony
3	53	M	98kg	90 (90)	Active	None	Bony + Fibrous
4	59	M	58kg	90 (180)	Very active	Some	Fibrous
5	53	M	90kg	15 (30)	Active	Good	Bony
6	65	M	70kg	? (90)	Moderate	Some	Bony
7	35	F	72kg	?	(Moderate)*	Some	Bony

* This patient could not be contacted; hence this assessment comes from a previous study.

Table 4.5 Summary of patient profiles extracted from the study.

Patient 1 is a male of average weight, and has low activity levels. He displays both bony and fibrous tissue formation, which would seem not to be a contradictory result. The agreement with the numerical model was found to be poor. Patient 2 is the lightest subject in this study, a female weighing only 46kg. Furthermore, she is relatively inactive, and based on these parameters, one would expect little bony ingrowth into the implant. However, osseo-integration is good, with only a small section displaying low-density bone, and no evidence of fibrous tissue formation. Agreement with the numerical model is good. Patient 3 is the heaviest patient participating in the study, a male of 98kg. He is active, and one would thus expect that there would be significant stimulation of the bone surrounding the implant. However, X-rays

reveal some clear radiolucent zones associated with fibrous tissue. This would seem to suggest that activity levels are only a small factor in determining whether tissue ingrowth will be bony or fibrous. Furthermore, there is no apparent agreement with the numerical model at all. Patient 4 is a relatively light male, who is extremely active. X-rays of the implant reveal significant fibrous tissue formation. Some correlation with the numerical model exists. Patient 5 is an active and relatively heavy male. He has extensive bone formation around the porous coating of the implant, with no fibrous tissue apparent. There is good agreement with the numerical model. Patient 6 is a male of average weight, whose activity levels are moderate. He displays bony ingrowth throughout the implant, with low-density bone in the proximal region. There is some correlation with the prediction of the numerical model. Patient 7 is the youngest subject in the study, a female weighing 72kg. Her activity levels were assessed as being moderate, and she displays bone ingrowth throughout the implant. There was found to be some agreement with the numerical model prediction.

Chapter 5 DISCUSSION

This chapter begins by describing in greater detail some of the features which were sought on the X-rays. It then discusses the techniques and algorithms used in the study, the correlation of the findings with the numerical model, and an assessment of the time study. Finally, possible reasons for differences between the findings and the model are provided.

5.1 Features of X-ray images

The correct assessment of the condition of the implant is based heavily on the features sought on the X-ray image. The guidance of an orthopaedic expert is thus of vital importance, and Prof. Walters (orthopaedic surgery) provided valuable assistance in this regard. It is important to realise that the orthopaedic surgeon has as his main concern the stability of the implant -- whether it is secure, or possibly becoming loose. Our aim, however, was to identify the presence of either mineralised bone or fibrous tissue surrounding the porous coating of the implant. Whether the implant is possibly becoming loose was not important in this study. Nevertheless, the features that would indicate the possible presence of fibrous tissue and/or bone include the following:

- The presence of a radiolucent line has been described in Section 3.5.1, and is the most important feature to be recognised. Also worth noting is that although the radiolucent line is darker than the sclerotic line, it still contains some speckles of what appears to be bony tissue, even in the centre. Bearing in mind that bone and fibrous tissue cannot form in the same region, and that fibrous tissue should appear almost black, these speckles must be attributed to bone in the foreground and background, and not in the radiolucent zone itself. The speckles in the radiolucent line are particularly enhanced by the higher density of the sclerotic line of hardened bone in the foreground and background, with a smaller contribution from the bone cortex. This is of particular significance for this study, as it represents a distortion of the actual tissue density at the implant-bone interface.
- Normal X-ray features (an implant that is considered to be secure) include calcar resorption, radiolucent zones up to 2mm in width, cortical thickening, periosteal reaction, endosteal sclerosis, and subsidence of the implant (Manaster, 1996).
- The most reliable radiographic signs of implant loosening include progressive subsidence, migration, or tilt of the component, bead shedding, cortical hypertrophy, endosteal bone

bridging at the stem tip, endosteal scalloping, and a radiolucent zone wider than 2mm. In particular, a radiolucent zone becoming wider with time is an indication of probable implant loosening. Furthermore, revision arthroplasties often display wide radiolucent zones, and these cases may require separate analysis (Manaster, 1996).

- Physiologically, the development of tissue will follow one of two routes: either the tissue will become mineralised and form bone, or it will not mineralise, and become fibrous tissue (Starke, 1996). However, an implant that displays the typical signs of bony ingrowth may also include the presence of fibrous tissue at the implant-bone interface. Although the fibrous tissue lies adjacent to the implant, it is not considered to be integrated with the implant. Similarly, fibrous encapsulation may also include some bony tissue. The important factor is the tissue type that dominates the integration of the implant. This point correlates well with the findings of Collier *et al.* (1992), who observed that an implant encapsulated in fibrous tissue often displays more stability than might be expected.
- In some cases, the presence of darker areas adjacent to the implant is not indicative of radiolucent zones. Such darker areas may be due to the body's response to granuloma. This is a pathological condition in which the bone is eroded by biological processes, and may result in darker regions surrounding the implant. It is thus essential to distinguish between granuloma and fibrous tissue formation. However, the distinction between the two conditions using image analysis software is beyond the scope of this study. To overcome this problem, each of the X-rays was examined by an orthopaedic surgeon, to assess whether any such cases did exist, and if so, to exclude them from the study. In fact, none of the patients showed this condition, and all were included. Another possible cause of an apparently darker area immediately adjacent to the implant is that the bone may simply be of a low density. In this case, the presence of a clear sclerotic line provides the distinction between low-density bone and fibrous tissue.
- High density tissue cannot be fibrous tissue -- it must be bone. Regions of higher density tissue around an implant are indicative of bone formation, and if these are in close apposition to the implant, then this is a good indication that bone ingrowth into the porous coating has occurred. Low density tissue (relative to the higher regions) suggests fibrous tissue, but this is not a clear distinction.
- The trabecular bone pattern is also an indicator of bone ingrowth into the implant. Bone trabeculae lying in a more or less superior-inferior direction, with a slight curving inwards

towards the implant, suggest that the force transmitted from the tapered implant is mostly downwards and slightly outwards, as expected. Regions of the porous coating that include this trabecular bone pattern imply that good bone ingrowth has occurred. It is for this reason that attention has been given to the analysis of trabecular bone pattern in this study (Appendix C).

5.2 Assessment of techniques used

The techniques that were used in this study were described in detail in Chapter 3, and an overall assessment of their effectiveness is presented here. Several methods were investigated. The aim of all methods was the identification of, and distinction between, fibrous tissue and bony tissue at the implant-bone interface. It was found, however, that some methods were more effective at identifying one tissue type, and less effective at identifying the other. In fact, in most cases these methods were remarkably ineffective at identifying one of the tissue types. For this reason, these methods were used only to identify the tissue type at which they were effective, and ignore the other. In this way the strengths of each method were optimised, and the weaknesses ignored.

The basis on which all results were built was the extraction of the grayscale values at the implant-bone interface. This entailed the identification of the edge of the implant, and the plotting of the grayscale values at this interface. High densities on an X-ray (light gray) indicate good bone mineralisation, and low densities (dark gray) indicate low tissue density. It would seem logical that densities below a particular value could indicate possible fibrous tissue formation. However, the assessment of the value of this threshold is extremely difficult, because there are significant contributions to the observed bone density at the interface from surrounding bone. In other words, at the implant-bone interface on an X-ray, the observed tissue density is not the actual density at that interface. There is a significant contribution from the bone cortex, as well as from bone between the cortex and the implant (in the foreground and background). In particular, the sclerotic line of hardened bone that is associated with fibrous tissue contributes greatly to the observed density within a radiolucent line. It is this factor that results in the tissue density in the centre of a radiolucent zone (where fibrous tissue has definitely formed) appearing lighter than even the regions of definite bony ingrowth. This is a severe deviation from an ideal situation, and appears to occur in all cases

of radiolucency. A logical means of correcting this distortion is to identify regions of definite radiolucency, and acquire a measure of the intensity of the sclerotic line in these regions. This intensity (or a factor thereof) can then be subtracted from the measured grayscale values in those regions. A further difficulty is that there are contributions from both the foreground and the background. It is thus arguable that a value of twice the average of the sclerotic line should be subtracted. This approach was tested, but in practice was found not to be reliable: when subtracting the average grayscale value of the sclerotic line from the radiolucent line, the resulting value was often found to be negative. Subtracting twice this value almost always resulted in a negative value. Furthermore, this method results in large density differences in regions where the tissue changes from bony to fibrous, which is highly unlikely in reality, and this was the main reason for not using this method. Hence, a slightly different approach was taken in this study -- one which didn't result in such a marked change from bony tissue to fibrous tissue. This method is believed to have much merit, and it would seem that such an approach is the purest method of analysis. The method requires further development before acceptable results might be acquired. For the present study, however, the actual method that was used was deemed to be more suitable.

In practice, it was difficult to identify the interface precisely. The distinction between the implant material and surrounding tissue was extremely difficult. The method employed was to use the line identifying the edge of the implant as a template, and move this line away from the implant slightly, so as to be sure that only biological tissue was being included, and no implant material. The grayscale values at this new position were then extracted. The distance that this template was moved away from the implant varied slightly between images, but was generally between 330μm and 400μm. Figure 3.9 illustrates that although this was not the exact interface between the implant and surrounding bone, it was clearly close enough to the implant to be an accurate reflection of the tissue mineralisation at the interface. In cases where a sclerotic line existed, the interface was positioned such that it lay in the centre of the radiolucent line. This method was judged to be a sound basis on which to build, because the X-ray image merely provides information regarding the tissue density through that specimen. In this study, the degree of mineralisation of the tissue was sought, and this was exactly the parameter that was indicated by the lightness or darkness of the X-ray. Furthermore, this routine was relatively simple and quick to run, and did not require as much memory space as some of the other routines. Although it was effective at identifying regions of good bone

formation, it had the drawback of being ineffective at identifying fibrous tissue.

Due to distortions in grayscale values for the above reasons, additional methods were required to identify tissue types. The identification of good bone formation was effective with the grayscale plot described above, and thus a method of identifying fibrous tissue was critical. The first method used to identify fibrous tissue was by analysing the profiles of rows across an image (i.e. from the implant to the surrounding tissue). A typical profile indicating fibrous tissue encapsulation was the presence of a continuous sclerotic "ridge" of hardened bone situated within a few millimetres of the implant edge (see Figure 3.7). Two approaches were taken in assessing whether this feature existed. Both were obviously geared towards the identification of fibrous tissue only. The first was to quantify the shape (depth and position) of the radiolucent trough and sclerotic ridge, described in Section 3.5.3, Method 1 (see also Figure 3.12). It was not a perfect method, however, and tended to exaggerate some areas above others, where this was not clearly the case. It also sometimes incorrectly identified certain regions as having a radiolucent profile, where an outlying area of higher density bone was identified as a sclerotic ridge. Although these problems were reduced as much as possible, they were not eradicated completely.

The second approach was to correlate the overall shape of the profile of each row with a model shape. The model shapes included ideal shapes of both radiolucent zones and good bony ingrowth. This method had certain problems, however. One was that it tended to be biased towards the bony ingrowth profile. By this is meant that when correlating a slightly radiolucent shape (i.e. a shallow trough and low sclerotic ridge) with the model shapes, the correlation with the bone shape was relatively high, and often approximately the same as the correlation with the radiolucent shape. The method did not effectively distinguish between the two shapes. Another significant problem was that the correlation routine required that the two arrays of data be of the same length. This had the result that if this method was to be successful, a vast number of model shapes would be required, so as to cover a wide range of array lengths. Furthermore, even with just a few sample shapes, this method was time-consuming. This method was thus found to have some merit, but was less effective than the first approach, and was not used in the final analysis.

Another approach that was investigated (but not used in the final analysis) was to identify

regions of good bony ingrowth. The method examined the slope of the fall-off from the edge of the implant. Each row profile was analysed, and the steepest slope calculated and recorded. Steeper slopes were associated with less mineralised tissue (fibrous tissue or low-density bone), and flatter slopes with higher mineralisation (bony ingrowth). The plotting of these values produced peaks in regions of good bony ingrowth, and troughs in other regions. The technique was found to be very effective at identifying good bony ingrowth, but less effective at identifying radiolucent zones. Initially it seemed that this method might be capable of distinguishing between low-density bone and fibrous tissue. However, no clear evidence emerged that this might be true. It may yet be shown to be an indicator of both fibrous tissue and bone formation, but this was not established beyond doubt during this study. Initially, this method was used to enhance (raise) the grayscale plot of the interface (in bony regions), but it was judged that this parameter was effectively identified by the grayscale plot alone. Also, it was not thought desirable to distort the data unnecessarily. Hence, this approach was developed and tested, but not used in the final method.

5.3 Correlation of numerical model and X-ray images

The interpretation of the graphs has important implications in assessing correlation, and Section 4.1 elaborates on data interpretation. Due to the nature of the analysis and some of the problems encountered, the graphs have been "stretched" somewhat in certain regions. This has the result that a quantitative comparison becomes less meaningful. Furthermore, it is important to note that the numerical model tested in this study only presents one loading situation, and thus the numerical model and the patient data clearly cannot be compared quantitatively. The literature review reveals that most investigators believe a qualitative assessment of the results to be more appropriate (Carter *et al.*, 1984; Verdonschot *et al.*, 1993; Sadegh *et al.*, 1993; Dalstra *et al.*, 1995). Hence, in this study quantitative correlations are used insofar as is reasonable, with qualitative approaches being used otherwise. It should also be realised that one of the reasons for this project being undertaken was that there is very little literature dealing with evaluating numerical models. This has the result that linking this work with the literature is somewhat limited.

Of the seven patients studied, four showed no fibrous tissue formation at all, one displayed mostly fibrous tissue formation, and the remaining two showed both bony and fibrous tissue

formation. The numerical model (see Figures 3.3 and 3.4) suggested that only bony tissue would form (to a greater or lesser degree), and this is true of four patients. Only one patient displayed extensive fibrous tissue encapsulation. In this sense, some correlation with the numerical model was apparent, but this was clearly limited.

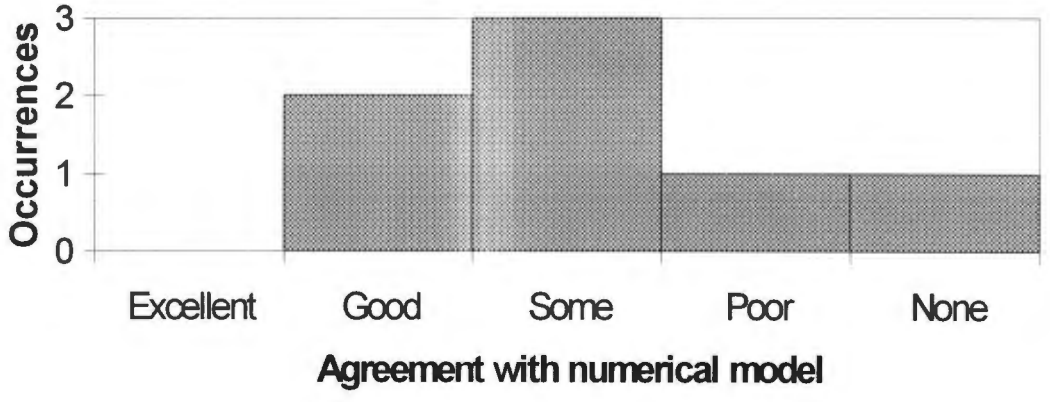

Figure 5.1 Correlation of observations and numerical model.

Figure 5.1 provides a visual summary of the correlation between the numerical model and the actual observations. This assessment indicates that no graphs show excellent agreement, two have good agreement, three have some agreement, one has poor agreement, and one shows no agreement. Overall, the graphs are reasonably evenly spread across the five categories, on average slightly below the centre of the range (towards poor correlation). It should be noted that no graphs have excellent agreement with the numerical model, and one shows no agreement whatsoever. The remainder fall into the middle three categories, indicating that there is a limited degree of agreement between the numerical model and the practical findings. The numerical model has not proved to be an accurate method of predicting the type of tissue formation, but it also doesn't clearly contradict the observations. It thus appears that the finite element method may yet prove to be a useful (and possibly accurate) method, but the parameters in this particular model do not mimic the actual cases sufficiently well to be considered reliable. This is in part due to the fact that there was a great deal of variation in the ages, masses, and activity levels of the patients studied, while the numerical model only considers one loading case. Other contributing factors are discussed in Sections 5.5 and 5.6. A 3-dimensional model may be significantly more accurate and reliable, and only further studies will determine the usefulness of this method.

Two patients display good correlation with the numerical model. It will be noted that one is male and the other female. The two female subjects in the study both have predominantly bony ingrowth into the implant. The males fall into all three categories. Clearly, there is no correlation according to the male criterion, but there may be in the female case. Of course, two occurrences is not sufficient to come to any definite conclusions, but the possibility exists. It thus appears that sex is not a clear factor contributing to tissue type, or correlation with the numerical model.

It must be emphasised, however, that a sample population of only seven patients means that it is very difficult to draw definite conclusions. With fifteen to twenty patients participating, there would be much more confidence in the conclusions drawn. Also, more trends may emerge with a greater sample size. It should be appreciated, however, that acquiring such a sample size is an extremely difficult task, as one first needs to find this number of subjects with suitable implants, and then persuade these patients to participate in the study. There is almost no advantage at all for the patient, and further incentives may be necessary to persuade them to participate in such a study.

When observing all of the graphs generally, one observation is strikingly apparent. Five of the seven graphs have a maximum mineralisation value at the distal end, with a sixth arguably also displaying this feature. Only one graph (patient 3) shows low bone density at the distal end of the porous coating. This trend agrees with the numerical model, where the distal end has a local maximum which decreases gradually when moving proximally (see Figure 3.4). The reason for this pattern is that load transmission through the proximal regions of the implant (particularly Gruen zone 7) is often poor, with the distal regions carrying the bulk of the load. This finding is in keeping with those of Cook *et al.* (1988) and Collier *et al.* (1992), who found bone hypertrophy to be common in the distal regions of the porous coating. This appears to be a definite trend of the graphs. However, it is also the only obvious trend amongst the seven graphs, and this fact is somewhat disappointing.

Although not an aim of this study, it is interesting to note that there appears to be little correlation between activity levels and the type of tissue formed around the implant. One would expect load-bearing to result in stimulation of the bone surrounding the implant, and

thereby increase bone formation around the implant. However, this is not apparent in this study. Of the three patients who fall into the active and very active categories, two show the presence of fibrous tissue (and one of these extensively). Furthermore, three of the subjects who are inactive or moderately active show good bone formation (with the fourth having both bone and fibrous tissue). It is well-known that fibrous tissue is formed when micro-movement of the implant relative to the bone occurs (Bobyn *et al.*, 1982, Spector, 1988, Pedersen *et al.*, 1991). The findings of this study suggest that perhaps too much activity (or too much load over too short a period of time) might assist in the formation of fibrous tissue. Even moderate and occasional loading appears to give rise to fibrous tissue formation. Conversely, however, patient 5 shows good bone formation, and is an active person. Hence, there appears to be little correlation between these parameters. However, there are too few subjects in this study to come to a definite conclusion on this possibility, but it is an interesting observation nevertheless.

There is no apparent correlation between age and the type of tissue forming around the implant (Table 5.1). The two youngest subjects have predominantly bone ingrowth into the implant, but so does the oldest. The occurrences of fibrous tissue also do not fall towards either end of the scale, but appear to be randomly distributed across the age groups.

AGE	TISSUE TYPE
35	Bone
47	Bone
53	Bone + Fibrous
53	Bone
59	Fibrous
64	Bone + Fibrous
65	Bone

MASS	TISSUE TYPE
46	Bone
58	Fibrous
70	Bone
72	Bone
75	Bone + Fibrous
90	Bone
98	Bone + Fibrous

Table 5.1 Relationships between ages, masses, and tissue types.

There also seems to be no correlation between body mass and tissue type (Table 5.1). The lightest subject displays bony ingrowth, but the second-lightest has fibrous tissue. The other two that have fibrous tissue (as well as bone) fall in the other half of the range. This suggests

that there is no clear trend.

None of the patients in this study displayed the classical signs that would suggest that the implant was loose, or becoming loose. Yet three of the seven patients displayed fibrous tissue formation, one of these extensively. This finding agrees with those of Cook *et al.* (1988) and Collier *et al.* (1992), who concluded that limited bone ingrowth and extensive fibrous tissue ingrowth is adequate for implant fixation. Clearly, in this study, the presence of fibrous tissue has not compromised the stability of the implant significantly.

It must be pointed out that there are very many possible reasons for this apparent lack of correlation, and these are discussed in detail in Sections 5.5 and 5.6. It will be appreciated that this study correlates two measures, neither of which are irrevocably accurate. In fact, either (or even both) could deviate significantly from reality. We are confident, however, that the methods used to assess the X-ray images provide a true indication of the actual tissue mineralisation at the interface. Being confident of this, the assessment of the accuracy of the numerical model is undertaken with confidence.

It will be noted that several of the patient graphs (most notably Figures 4.1, 4.3, and 4.7) display a certain degree of fluctuation. It was decided that the fluctuations of the numerical model should be ignored, and only the means used. There would seem to be a possibility that these fluctuations may carry some meaning. From our present knowledge base on this topic, however, drawing conclusions from such vague similarities would be purely speculative. For this reason, it has been decided to adhere to the "rule" that for purposes of comparison, the fluctuations are to be ignored.

The literature review indicated that all studies showed some degree of deviation of computer simulation predictions from experimental findings. The trend was clearly also apparent in this study, with the numerical model and the actual findings not correlating well. Although there was some agreement in general, this was very limited. Many investigators used the term "reasonable agreement" to describe the correlation between the model and the experimental findings. This would be too strong a term to describe the findings of this study, where "some agreement" or "limited agreement" are more appropriate. The literature review also emphasised that studies preferred a qualitative validation, and this study gave a good

understanding of the basis for this preference.

5.4 Assessment of time study

The time study proved to be a valuable addition to the information content of the X-ray images. Those X-ray images taken during this study only provided information on the bone mineralisation at one point in time. The time study provided information as to how this mineralisation was changing, i.e. whether the tissue was becoming more dense, or less dense with time. It should be noted at the outset that no enhancements were made to these data. The data presented are simply the grayscale values at the implant-bone interface. The enhancement of this data (as done with the "static" images) would have altered the positions of the graphs relative to each other, and this was clearly undesirable.

The first two curves of Figure 4.11 (at 10 days and 24 days) clearly indicate that the tissue is becoming more mineralised with time. This would appear to be at least partly due to the bone repair process after surgery, described in Section 2.1.2. This is the body's response to injury, and entails the removal of dead or damaged bone cells, and the formation of new bone tissue at the injury site. In this case the injury site is the implant-bone interface, from where the grayscale values were extracted. This repair process typically takes place 4 to 6 weeks (28 to 42 days) post-operatively (Hollister *et al.*, 1994), although this may vary between subjects. These first two graphs fall neatly within this period, and it seems reasonable that the interface is experiencing this process. This finding is consistent with those of Bobyn *et al.* (1980), who found that bond strength increased with time, specifically during the repair process. Nilles *et al.* (1973) also demonstrated an increase in bond strength with time, although this was not confined to the repair process. The time study is also valuable simply because it illustrates the body's response to injury. It is a good presentation of the bone repair process.

The remaining three curves (at 73, 200 and 1300 days) appear to stabilise at a particular degree of mineralisation. Between 24 and 73 days, the tissue has mineralised appreciably - approximately as much as between 10 and 24 days. This may also be partly attributed to the repair process, but it is expected that this process has largely been completed. The increase in tissue density between 24 and 73 days must to a large degree be attributed to the effect of stress on the tissue. At 200 days, the tissue reaches a maximum mineralisation (in general

across the porous surface), which is, in itself, an interesting and perhaps useful observation.

There is a slight but noticeable drop in the bone density between 200 days and 1300 days. This feature may be a particularly significant one, as the X-ray at 1300 days clearly showed the formation of fibrous tissue along almost the entire length of the porous coating. This was apparent due to the presence of a radiolucent line, although this line was relatively narrow (approximately 300μm wide). It should be noted that the grayscale values of the graph at 1300 days are appreciably higher than the graphs at both 10 days and 24 days. Thus it is not the actual values that are important, but rather the trends of the graphs relative to one another. The drop in bone density from 200 days to 1300 days requires an explanation. At 200 days the X-ray displayed extensive regions of good bone ingrowth into the porous coating. By 1300 days, extensive fibrous tissue had formed. The explanation *could* be that fibrous tissue has begun forming. Unfortunately, no definite conclusions can be drawn from this study, with only one sample. Further studies are required to assess whether or not this is true. Furthermore, additional information can perhaps be drawn out. For example, it may emerge that a greater drop-off is associated with the formation of a thicker covering of fibrous tissue (i.e. a wider radiolucent line).

A limitation of this study is that there are only five time points available. The addition of another graph at a later stage (a year or more) would be valuable in assessing the possible truth of the hypothesis. Furthermore, a study with consistent time periods between sample images would provide a valuable gauge of tissue activity.

The fact that the graph after 1300 days is known to be fibrous tissue, and yet lies above the graphs of 10 days and 24 days, which are known to be bony tissue, illustrates the problem faced in the preceding section. This problem is that fibrous tissue appears not to necessarily display tissue density lower than low-density bone, and the distinction between the two becomes extremely difficult. This raises the point that the methods used in this study may not be sufficiently sensitive to automate the process of tissue differentiation completely. This may be true of the "static" case, but a computer can detect trends, i.e. detect that the graph at 1300 days is the first to decrease relative to the preceding one. Hence, it cannot yet be discarded as a tool for determining tissue types.

It will have been noticed that in each of the graphs, the general slope decreases slightly from the distal end to the proximal end. This is in keeping with the previous findings, as well as those of Cook *et al.* (1988) and Collier *et al.* (1992), namely that the distal end of the porous coating displays slightly greater bone ingrowth than the proximal regions. The proximal half of the porous coating displays approximately even tissue ingrowth.

There are two aspects of the analysis that may have distorted the data slightly. Both relate to the adjustments that were carried out to normalise the data and make them comparable. The first occurred when the samples of bone cortex were chosen. Although this was done as accurately as possible, the position of the samples did not correlate perfectly with one another. The data is gauged against this measure, and a small error will have been introduced. The second aspect is introduced because the data is further adjusted according to the DEXA studies. Although these studies ought to be accurate, their data is also imperfect, and another error will have been accumulated. However, these errors are expected to be very small, and of limited practical significance.

If it proves to be true that the time study provides a sound basis for predicting whether fibrous tissue or bone tissue is in the process of forming, then it will be a more powerful method of tissue detection than the first method. In this case, the monitoring of the tissue density at the implant-bone interface may provide a prognostic tool that could even be used in decisions relating to revision surgery.

5.5 Possible reasons for results deviating from numerical model

There are a number of reasons for a numerical model not correlating well with the actual system it aims to mimic. In this study these reasons include: simplification of biological factors that are not understood fully (including pathological conditions); assumptions inherent in the numerical model; large variations in loading conditions; and imperfect analytical methods used. In these and other processes there are significant assumptions and simplifications that are made to reduce the analysis to manageable proportions. These factors are described below.

- The numerical model used "typical" loading conditions, incorporating both the single-legged stance phase of normal gait (considered to be the worst case loading condition

occurring during normal activity, when loads transferred across the hip joint are relatively high), and the extreme ranges of motion of the joint. Actual loading conditions in the patients varied considerably, with some patients being very active, and others performing only sedentary tasks.

- The numerical model assumes a person of "average" mass. The actual patients studied had masses that varied considerably, from 46kg to 98kg. This is a very large range, and obviously differs significantly from the numerical model.
- The numerical model assumed a rest period of 14 days before weight-bearing began, whereas the actual rest periods of the patients varied between 5 days and 6 months (see Table 4.5).
- Significant assumptions have to be made in constructing such a numerical model. Physical and biological parameters, such as the modulus of elasticity of trabecular bone and the remodelling rate constant, are not known sufficiently accurately. This is commonly cited as being a primary problem in numerical modelling. Furthermore, these biological parameters may vary over time in the patient, whereas the model assumes constant values throughout. Furthermore, medication may also affect these biological variables.
- The numerical model is a 2-dimensional representation. This will clearly result in some deviation from both a 3-dimensional model and the actual human case.
- The X-ray images were not an entirely "pure" representation. The images were treated as though they showed a true cross-section of the implant-bone system (in the frontal plane). In other words, the bone appearing immediately around the medial and lateral borders of the implant was interpreted as being a reflection of the bone density in only that plane. In fact, this bone density included bone lying in front of, and behind, this plane. This had the result that it was extremely difficult to distinguish "background" bone from the bone on the borders of the implant. Although substantial effort was put into overcoming this problem, the X-ray remains an imperfect representation. Furthermore, little could be done to improve this deviation directly, i.e. by producing a more realistic X-ray image.

5.6 Other problems and limitations experienced

In addition to those points specified above, there are other aspects peculiar to this study that have resulted in some loss of accuracy of the analysis. Some of these are unavoidable, while others only became apparent during the analysis.

- In the patients studied, the lateral side of the porous coating was almost always obstructed from view by the cables and screws used to re-attach the greater trochanter. Also, the lateral porous coating is appreciably shorter than the medial side, approximately half the length. In most cases more than half of the lateral porous coating was hidden. This resulted in the assessment of the lateral side being impossible, which was unfortunate, since such additional data may have been useful.
- The consistency of the X-ray machine may require special attention in future analyses such as this. It would seem reasonable to expect the X-ray supply to vary somewhat across the length and breadth of the image. In other words, if nothing was placed in the field of view, the resulting image should ideally be absolutely consistent in grayscale tone throughout, but this is unlikely in practice. It may be worthwhile to attempt to correct this deviation, perhaps by placing strips of materials of known density in various positions in the field of view, and making adjustments in grayscale values accordingly.
- It was extremely difficult to identify accurately the interface between the implant and the surrounding bone. An X-ray image simply provides an indication of the degree of attenuation of the X-rays passing through the specimen, and cannot distinguish between particular tissue types. There was thus no way of being certain that a chosen interface included only surrounding bone/fibrous tissue, and not some of the edges of the implant. For this reason, it was important to err on the safe side, i.e. to ensure that the chosen interface was sufficiently far from the implant to exclude all of the implant. This had the result that the chosen interface was not exactly the actual implant-bone interface.
- The results of the analysis of the X-rays were not perfect. There was no way of quantitatively gauging whether the highest tissue densities for a particular patient represented good bone mineralisation or just average mineralisation. For this reason, all graphs were "stretched" until the maximum mineralisation was 100%. A similar problem existed with the formation of fibrous tissue. This is clearly a source of deviation from the actual case, and is not a perfect representation. To overcome this problem in future studies such as this, a reference "scale" (such as a stepped piece of metal) should be placed alongside each patient while the X-rays are being taken. In this way the subjects can be confidently compared with one another.
- In some images, the lesser trochanter or the screws (used to re-attach the greater trochanter) obstructed the view of the medial porous coating. In these cases the

obstructed regions were simply disregarded, which introduced an inaccuracy. This problem was unavoidable, however, as a view in the frontal plane was essential.

- There is a trade-off in the quality of the X-ray image. A sharp image is ideal for assessing trabecular bone pattern, but this sharpness is not as essential for the general assessment of the bone density. In fact, a slight blurring of the image may even be preferable, as this has the effect of "averaging" the intensity. This point has implications for the possibility of automation of the process, where high-quality, sharp images are often not the norm in a hospital setting.
- The default data format that the MATLAB Image Processing Toolbox uses during image analysis is double-precision. Unless specified otherwise, all data are stored in this format. Our analysis did not require double-precision accuracy. Double-precision is a 64-bit format that uses 8 times more memory space than the conventional 8-bit format. For our purposes, analysing large images, it was much more important to conserve memory space, and it was thus desired to keep data in the 8-bit format. However, several of the operations in this analysis used routines that required the double-precision format. In these cases the data had to be converted to double-precision, the routines run, and the data then returned to the 8-bit format. This proved to be a tedious process, and one that used memory space inefficiently. This was perhaps the only problem of real substance that was encountered in the use of the MATLAB software. Although mentioned here, this limitation is in the process of being overcome by the MATLAB authors, and this should not be a problem in the future versions.
- A great deal of variation of X-ray features exists. For example, the position of the bone cortex relative to the implant can vary considerably. The position of the greater trochanter may also vary between patients. In these cases, the density of the cortex or greater trochanter appears higher than the bone immediately surrounding the implant. This presents a problem in identifying a possible radiolucent line, as the cortical bone may be mistaken for a sclerotic line of hardened bone. Also, the overall lightness or darkness of the X-ray has an impact on the effectiveness of the algorithm in picking up the features. This requires that the X-rays first be adjusted to a suitable contrast before analysis begins. Although not a significant problem, this has implications for the possibility of automating the X-ray analysis.
- Some distortion or magnification of the actual dimensions occurs on the X-rays (typically

about 10%). In other words, 1mm on the X-ray is usually not exactly 1mm in reality. This could have been overcome by gauging dimensions from various known dimensions. The diameter of the shank of the screw used in re-attaching the greater trochanter would have been particularly useful in this regard. However, the aim of this analysis was to establish the trend of bone mineralisation from the proximal end of the porous coating to the distal end. Hence, it was not necessary (or appropriate) to calculate a magnification factor in this study.

- Imperfections in the X-ray (e.g. dirt or scratches) tend to have a relatively large effect on the analysis. Due to the high resolution examination of the X-rays, dirty spots had the effect of reducing the grayscale values significantly. This was not a problem in this analysis, as great care was taken to keep the X-rays clean and scratch-free. However, this may be a problem in the case of automation of the diagnostic process, where X-rays may be older and more scratched.

5.7 Conclusion

All the objectives set out originally were achieved in this study. Plane X-rays were found to be a sufficiently good indicator of tissue mineralisation, although not ideal. Clearly, a true cross-sectional representation of the implant and surrounding bone would have been best (such as a CT scan), but this was found to be impossible with present technology. Nevertheless, plane X-rays were successfully used in assessing the type of tissue growth into the porous coating of the implants. MATLAB was used to analyse the images, and proved to be very effective. There were no serious problems, and the software was judged to be well suited to the task. Unfortunately, an assessment of the lateral border of the implants proved to be impossible, as wires and screws used to re-attach the greater trochanter obstructed the view of the porous coating. Various algorithms were developed to analyse the data, some to identify regions of radiolucency (fibrous tissue), and others to identify bony tissue formation. Each method concentrated on its strengths, and left it's weaknesses to other methods. There was found to be some correlation, although this was limited. Also, some progress was made in the development of an algorithm to identify trabecular bone pattern (see Appendix C), although this was a complimentary objective.

The most striking conclusion emerging from this study is that the unaltered X-ray image is

indeed a good indicator of the degree of tissue mineralisation, and hence the tissue type. However, in almost all cases the information contained in the X-ray is distorted, due to the fact that a plane X-ray is not a true cross-sectional representation. In particular, the presence of a sclerotic line of hardened bone significantly lightens the appearance of surrounding tissue, including fibrous tissue. This hardened bone does not contribute only to the distinctive sclerotic line, but also to both the foreground and background of the radiolucent line, resulting in the radiolucent line appearing much lighter than it ought to. It is felt that with further development the grayscale values of these areas can be adjusted, so that this distortion is reduced. However, the adjustment is not a simple linear subtraction. While it is certainly true that something must be subtracted from radiolucent zones where these are bounded by sclerotic bone, the precise quantity to be subtracted remains very difficult to discern. Furthermore, this quantity may vary between adjacent regions. Hence, it is recommended that a study be conducted to establish whether this may be an accurate method of determining tissue density.

It became clear during this study that more subjects were required for trends to emerge. Seven subjects are simply not enough to establish whether possible trends are significant or not. There may be some difficulty in acquiring a sufficient number of subjects, however, as the implants should ideally be identical in all patients. This may prove to be a significant problem.

The longitudinal time study produced interesting results. Time studies may even prove to be a more powerful means of tissue identification than the first method, that of measuring the tissue density (grayscale values) at the implant-bone interface. Furthermore, they may have clinical implications if they can predict that either fibrous tissue or bony tissue is in the process of forming. Further time studies are necessary to assess whether they are indeed as useful as suggested by this study. These studies also provided an effective means of illustrating the bone repair process after surgery.

Chapter 6 RECOMMENDATIONS

During the course of this study, it became apparent that one of the main thrusts of an analysis of this type is to make the diagnosis of an X-ray image more automated. In an ideal case, it is envisaged that an X-ray be placed in a scanner, linked to a computer that will be able to discern the position of any possible radiolucent zones, and whether the widths of these zones are changing. For this, a database of relevant information (e.g. past X-rays of a particular patient) may be required, and this may take some time to accumulate. In fact, there are many radiological signs, both of implant loosening and biological activities, that could be assessed in this way (see Section 3.4.6.1). Some of the points below relate to a situation such as this, and it should be noted that this requires a great deal of development and time before the above scenario becomes possible. Nevertheless, these points provide some indication of the type of work that could be done:

- The adjustment of grayscale values in regions identified as being definitely radiolucent requires further development. This approach is clearly the purest method, but also represents a significant alteration of the data. In particular, the transition between regions of bone formation and fibrous tissue formation requires attention.
- The development of an algorithm to measure the width of radiolucent zones, where these exist. Good progress has been made in this regard in this study, but greater accuracy and robustness is desirable. Also, the measurement of the widths of the sclerotic line of bone may prove useful.
- It would be extremely valuable to assess whether some of the possibilities regarding time studies (described in Section 5.4) are indeed true. More time studies, and more detailed ones, are required to determine if these studies do indicate the tissue type that is forming around the implant. If found to be true, this would be a very powerful means of monitoring tissue formation.
- The development of an algorithm to assess trabecular bone pattern. The work that has been done in this analysis (see Appendix C) is only the beginning of what proved to be a very challenging task. The development of this algorithm was not given much weight in this study, as it did not directly contribute to the primary task, that of assessing the validity

of the numerical model. However, this is a useful parameter in assessing normal trabecular bone structure around an implant.

- The monitoring of the widths of radiolucent zones over a period of time. This is an important parameter in the evaluation of possible loosening of the implant. This will require that a database of information be available for comparison purposes, and will thus be difficult until such time that a sufficient number of X-rays of that patient become available. In some cases, perhaps even most cases, there may never be enough information for this to be possible. Nevertheless, it would be a very useful diagnostic tool. This aspect also has the complication that revision arthroplasties often display wide radiolucent zones, and a distinction may have to be made in such cases.
- It has been suggested that if a significant database of X-rays can be accumulated (as in the above case), perhaps it would be found that the positions at which bone ingrowth (or fibrous tissue) occurs might prove to have a degree of consistency. In other words, it may emerge that a particular class of patient (e.g. a specific age group) displays bone ingrowth at specific sites of the implant. If this were true, then suitable implants could be prescribed for specific patients, making these arthroplasties more reliable. Furthermore, appropriate implants could be manufactured to suit the needs of particular patients.
- The purest means of assessing the nature of the tissue immediately surrounding the implant is by analysing retrieved implants. Conclusions would be both easier and more meaningful with this approach. There would obviously be complications with this method, as retrieved implants may not have sufficient surrounding tissue extracted to come to substantial conclusions. Another possibility is to accumulate data from patients who have died with their implants *in situ*. A study of this type would carry much weight in assessing the validity of the numerical model.
- It became apparent during this study that the process being undertaken was not dissimilar to the DEXA process. Both are used to measure bone density at specific sites. There is a possibility that when some of the techniques used in this study are applied to an X-ray image, the results may be comparable to the DEXA results. If this is found to be true, these methods may be more convenient in assessing bone density, as it is common practice for regular X-rays to be taken, regardless of the DEXA scans. These methods may even prove to be more effective than DEXA.

APPENDIX A

MATLAB routines

The following routines illustrate the techniques used in assessing the images. While it has been attempted to include all details of these processes, some has been commented out (the % sign indicates that this line of code will be ignored by the program). In particular, those sections of code relating to the time study are commented out. This was done to make the reading of the code more clear. In practice, relevant sections of the omitted code were included in the program, depending on the task. Comments have been inserted to further clarify the purpose of each section. Many routines used are those available in Matlab (or the Image Processing Toolbox), and are thus not described here. All routines written for the purpose of this study are included in this section.

Master routine

This is the main routine that calls up other subroutines. It establishes overall control of the image characteristics.

```
clear all;                          % clears all stored variables
cd c:\warren\xrays\powell;          % locates directory containing scanned x-ray images
IM2 = double(imread('textpic.tif'));
IM2edge = double(imread('po75por1.tif'));      % reads in the image data
%% The following 5 lines relate to the time study:
%IMsamp1 = double(imread('pr10sam2.tif'));
%IMsamp2 = double(imread('pr24sam2.tif'));
%IMsamp3 = double(imread('pr73sam2.tif'));
%IMsamp4 = double(imread('pr200sa2.tif'));
%IMsamp5 = double(imread('pr1300s2.tif'));
cd c:\matlab\bin;                   % returns to Matlab directory
IM = averow(IM2);                   %Averages every 5 rows
IMedge = averow(IM2edge);           %Averages every 5 rows
[r,c]= size(IM);                    % assesses no. of rows and columns of image
clear IM2 IM2edge;

%% For time study: calculate sample average densities
%ave1 = mean(mean(IMsamp1));        %0.8270
%ave2 = mean(mean(IMsamp2));        %0.9420
%ave3 = mean(mean(IMsamp3));        %0.7392
%ave4 = mean(mean(IMsamp4));        %0.7392
%ave5 = mean(mean(IMsamp5));        %1
%%Bone cortex density
%den1 = 0.8217;
%den2 = 0.8416;
%den3 = 0.9085;
%den4 = 1;
%den5 = 0.9660;
%fact10  = ave1*den1;
%fact24  = ave2*den2;
```

```
%fact73  = ave3*den3;
%fact200  = ave4*den4;
%fact1300 = ave5*den5;

%% The following 3 sub-routines form the heart of the process: the extraction of the grayscale
values at the implant-bone interface, testing for the presence of a radiolucent line, and assessing
regions of good bony ingrowth:
%Calculate INTENSITY graph
contpl2;                    % extraction of grayscale values
%Calculate RADIOLUCENT graph
radluctest3;                % testing for radiolucent line
%Calculate BONE graph
%slopes;                    % testing for good bony ingrowth
                            % Note: this routine was not used in the final method, but has merit

%plot(arint);
%axis([0 length(arint) 0 260]);
%figure; plot(arrl);
%axis([0 length(arrl) 0 1]);
%final = multim(arint,arrl);
%figure;
%plot(final);
%axis([0 length(final) 0 260]);

%% Multiply RADIOLUCENCY and INTENSITY - this combines the two graphs, reducing
%%the grayscale plot in regions of radiolucency
fin2 = multim(RL,INTsm);            % multiplies two arrays (see 'multim' routine)
finint = fin2-min(fin2);
fin3 = finint/max(finint);  %clear fin2;
fin4 = fin3-0.5;            %clear fin3;
final = fin4/max(fin4);         %normalise data
%final = smoothodd(fin5,3);
plot(final);                % plot graph of multiplied parameters
axis([0 length(final) -1 1]);
hold on;
sep = zeros(1,length(final));
lin = sep*50;
plot(sep,'k-');
xlabel('Porous coating of implant (Pixels)');
ylabel('Degree of bone mineralisation');
set(gca,'XTickLabel',[' 0 ';' 250';' 500';' 750';'1000';'1250']);
text(110,0.12,'BONY TISSUE');
text(107,-0.12,'FIBROUS TISSUE');
gtext('DISTAL');
gtext('PROXIMAL');

%%The following pertains to the time study:
%load temp10;
%load temp24;
```

```
%load temp73;
%load temp200;
%load temp1300;
%plot(1:173,temp10(1:173),'-',(1:173),temp24(1:173),'-',(1:173),temp73(1:173),'-
',(1:173),temp200(1:173),'-',(1:173),temp1300(1:173),'-');
%axis([0 174 0 260]);
%set(gca,'XTickLabels',['  ';'100';'200';'300';'400';'500';'600';'700';'800']);
%xlabel('Porous coating of implant (Pixels)');
%ylabel('Grayscale values');
%text(5,15,'DISTAL');
%text(143,15,'PROXIMAL');
%gtext('10 days');
%gtext('24 days');
%gtext('73 days');
%gtext('200 days');
%gtext('1300 days');

%% This code combines the data for RADIOLUCENCY and good BONE ingrowth. It was
%%not used in the final method, but has a useful result.
ADJUST = multim(RL,SLOPE);
figure;
plot(ADJUST);
ylabel('Adjustments');
%%The following combines the above parameter and the original grayscale graph:
%%Multiply ADJUST and INTENSITY
fin2 = multim(ADJUST,INTsm);
fin3 = fin2/max(fin2); clear fin2;
final = fin3-0.5; clear fin3;
figure;
plot(smoothodd(final,3)); hold on;
j = 1:length(final);
plot(j,0);
ylabel('Degree of bone mineralisation');
axis([0 length(final) -1 1]);

%% Saves arrays of graphs to disk
PRt1300INTsm = INTsm;
PRt1300RL = RL;
PRt1300slope = SLOPE;
PRt1300adjust = ADJUST;
PRt1300final = final;
save PRt1300arr PRt1300INTsm PRt1300RL PRt1300slope PRt1300adjust PRt1300final;
%% End of Master routine
```

ROUTINE: averow

This function averages the grayscale values of 5 rows in an image:

```
function Y = averow(X)
[r,c] = size(X);
```

```
Y = [];
for j = 5:5:r
  ROW1 = X(j-4,:);
  ROW2 = X(j-3,:);
  ROW3 = X(j-2,:);
  ROW4 = X(j-1,:);
  ROW5 = X(j,:);
  ROW = (ROW1 + ROW2 + ROW3 + ROW4 + ROW5)/5;
  Y = [Y;ROW];
end
```

ROUTINE: multim
This function multiplies two arrays.

```
function Y = multim(A,B)

A = A';                    % transpose array
B = B';
l = length(A);
Y(1:r) = 0;
for n = 1:l
  Y(n) = A(n)*B(n);
end
Y = Y';
```

ROUTINE: contpl2
This routine plots grayscale values parallel to the implant edge, and is called up from the master routine.

```
J = image(IM);
set(J,'CDataMapping','scaled');
h = get(J,'CData');

clear POSARRown;
for j = 1:r
  ROW = IMedge(j,:);
  %% Find edge of implant
  IMPL = find(ROW==255);                % Find last occurance of 255
  start = IMPL(length(IMPL));
  POSARRown(j) = start;
%  GRADown  = steep(ROW,20);            % Find steepest profile
%  SMALLown  = min(GRADown);
%  POSown  = find(GRADown==SMALLown);       %Find position steepest profile
%  POSARRown(j)  = POSown(1);           % Record position in array
end

POSAR = smoothodd(POSARRown,5)+11;   %Position of plotted line

%% Superimpose the edge on the image (only for viewing/checking)
```

```
for j = 1:length(POSAR)
  h(j,round(POSAR(j))) = 255;
end
h3 = imrotate(h,90);
imagesc(h3,[0 255]); colormap(gray);
xlabel('Pixels');
ylabel('Pixels');
imzoom on;
gtext('IMPLANT')
set(gca,'YTickLabel',[";";";";";";";";";"]);
%pause;

%% Calculate average grayscale value of area around implant
width = 20;
val = [];
for j=1:length(POSAR)
  val = [val;IM(j,round(POSAR(j)):round(POSAR(j))+width)];
end
avarea = mean(mean(val(1:length(val),1:width)));
%break

%% Plot grayscale values of extracted line
clear i j;
i = 1:length(POSAR);
j = POSAR;
INT = impixel(IM,POSAR,i);
INTsm = smoothodd(INT,3);
maxval = max(INT(:,1));
%arint = INTsm/;

%% Stretch values over range
INTsm = INTsm - 0.5*(min(INTsm));
INTsm = INTsm * 250/max(INTsm);

figure;
zer = zeros(1,length(INTsm));
av = zer + avarea;
plot(1:length(INTsm),INTsm,'-',1:length(INTsm),av,'k-');
%plot(INTsm);
axis([0 length(INTsm)+1 100 250]);
ylabel('Grayscale values');
xlabel('Porous coating of implant (Pixels)');
gtext('Mean of area around implant');
gtext('DISTAL');
gtext('PROXIMAL');
set(gca,'XTickLabel',['  0 ';' 250';' 500';' 750';'1000';'1250']);
```

ROUTINE: radluctest3

This routine analyses the shape of the grayscale profile from implant to surrounding bone, and determines whether this shape represents radiolucency.

```
WIDE = 28;    %Pixels
RATIO = [];
RATIOmax = [];
Iminarr = [];
TOP = 30;
BOT = 1;
for j = 1:r
  ROW = IMedge(j,:);
  ROWsm = smooth(ROW,3);
  GRADgrad = gradient(ROWsm);

  %% Find end of implant => label 'start'
  IMPL = find(ROWsm==255);                % Find last value of 255 - definitely implant
  start1 = IMPL(length(IMPL));
  start2 = find(round(GRADgrad(start1:length(ROWsm)))~=0);      % Find next non-zero
slope
  start = start1 + start2(1);             % Set edge of implant to this point
  ROWsh = ROWsm(start:start+WIDE);
  clear start1 start2 IMPL;

  %% Visual check
  %  plot(ROWsh);
  %  ylabel('Intensity');
  %  axis([0 length(ROWsh)+1 0 260]);
  %  imzoom on;

  %% Find first zero => local minimum
  zer = fndzer(GRADgrad(start:start+WIDE));
  if (length(zer)>=1)
    %% Find max I between there and end
    Imax = max(ROWsh(zer(1):length(ROWsh)));
    %% Find position of Imax
    Imaxint = find(ROWsh(zer(1):length(ROWsh))==Imax);
    Imaxpos = Imaxint(1)+zer(1)-1;
    %% Find min I between 1 and Imax
    Imin = min(ROWsh(1:Imaxpos));
    %% Find position of Imin
    Iminint = find(ROWsh(1:Imaxpos)==Imin);
    Iminpos = Iminint(1);
    Iminarr = [Iminarr;Iminpos];
    clear Iminint Imaxint;
    if (((Iminpos<TOP) & (Iminpos>BOT)) & ((Imaxpos-Iminpos)~=0))
      RATIO = [RATIO;((Imax-Imin)/(Imaxpos-Iminpos))];        %Depth of radiolucent zone
      RATIOmax = [RATIOmax;((Imaxpos-Iminpos)/Imaxpos)];%Position of radiolucent zone
    else
      RATIO = [RATIO;0];
```

```
      RATIOmax = [RATIOmax;0];
    end
  else
    RATIO = [RATIO;0];
    RATIOmax = [RATIOmax;0];
  end
%  pause;
end     %End of main loop

%Multiply Depth indicator (RATIO) and Position indicator (RATIOmax)
KINK = smoothodd(RATIO,11);
%plot(RATIO);
KINKmax = smoothodd(RATIOmax,11);
%figure; plot(RATIOmax);
RL = multim(KINK,KINKmax);      %Multiply RATIO and RATIOmax
RL = 2-RL;                      %Invert graph
RL = RL/max(RL);                %Normalise

RL = smoothodd(RL,3);
avg = mean(RL);
sd = std(RL);

for j = 1:length(RL)
  if (RL(j)>avg-0.4*sd)       % Set threshold!
    RL(j) = avg-0.4*sd;
  end
end
RL = RL+(1-avg+0.4*sd);

% Stretch values
for j = 1:length(RL)
  RL(j) = 4*RL(j);              % Adjust stretching
  RL(j) = RL(j)-3;          % Adjust stretching
end

%RL = smoothodd(RL,3);
%arrl = RL;
%save ararr arrl arint;      % Save arrays as variables

%figure;
plot(RL);
axis([0 length(RL) 0 1.05]);
ylabel('Adjustment factor');
xlabel('Porous coating of implant (Pixels)');
gtext('DISTAL');
gtext('PROXIMAL');
set(gca,'XTickLabel',['  0 ';' 250';' 500';' 750';'1000';'1250']);
```

ROUTINE: slopes

This routine analyses the steepness of the decline in grayscale values from implant to surrounding bone, and assesses whether this shape represents probable bony ingrowth. Although the routine clearly has some merit, it was not used in the final method, as it was important not to distort the data in any unnecessary way.

```
val = [];
width = 40;              % Width adjacent to implant to be assessed
for j = 1:r
  ROW = IM(j,1:170);
  ROWsm = smooth(ROW,2);
  IMPL = find(ROWsm==255);
  start = IMPL(length(IMPL));
  ROWsh = ROWsm(start:start+width);

  %% Find steepest slope
  ROWsh = double(ROWsh);
  GRADown  = steep(ROWsh,7);                    % Measures steepness of slope
  GRADmin = min(GRADown);      % Finds minimum value of this array (steepest slope)
  POSown  = find(GRADown==GRADmin);                % Finds position of this point
  POSARRown(j) = POSown(1);
  val = [val;GRADmin/7];
%  ROWsh = uint8(ROWsh);

%% Plot position of steepest slope
%  p=1:length(ROWsh);
%  q=1:260;
%  for num = 1:260
%    CUT(num) = POSARRown(j);
%  end
%  plot(p,ROWsh,'-',CUT,q,'-');
%  axis([0 length(ROWsh)+2 0 260]);
end

SLOPE = smoothodd(val,5);
for k = 1:length(SLOPE)
  SLOPE(k) = 1/SLOPE(k);
end
SLOPE = abs(SLOPE);
SLOPE = SLOPE/max(SLOPE);
ave = mean(SLOPE(1:length(SLOPE)));
sd = std(SLOPE(1:length(SLOPE)));
for j = 1:length(SLOPE)
  if (SLOPE(j)<ave+0.5*sd)
    SLOPE(j) = ave+0.5*sd;
  end
end
SLOPE = SLOPE+(1-ave-0.5*sd);

figure;
```

```
plot(SLOPE);
ylabel('Slope');
%sd = std(SLOPE(1:length(SLOPE)));
%plot(1:length(SLOPE),SLOPE,'-',1:length(SLOPE),ave,'-');
%,1:length(SLOPE),ave-1*sd,'-');
%axis([0 length(SLOPE)+1 0 1]);
```

ROUTINE: steep

This routine finds the steepest slope in an array.

```
function y = steep(x,n);

for c = 1:length(x)-n
    y(c)=x(c+n)-x(c);  % Measures the difference in grayscale values between a point and
                       % another point distance n away
end
```

ROUTINE: smoothodd

This routine smoothes an array, and is the favoured method in this study. It only works for an odd number of entries in the array.

```
function Y = smoothodd(X,n)

mid = ceil(n/2);
fact = floor(n/2);
Y = [];
for k = mid:length(X)-fact;
  Y(k) = mean(X(k-fact:k+fact));
end
Y(1:fact) = Y(mid);
Y(length(X)-fact:length(X)) = Y(length(X)-mid);
```

ROUTINE: fndzer

This routine finds the first four positions where vector X changes sign (local maximum or minimum). This is used in examining the shape of the grayscale profile.

```
function zerpos = fndzer(X)

zerpos = [];
count = 0;
for c = 1:length(X)-1
  if (count<4)
    if (sign(X(c+1))==0)
      X(c+1)=(sign(X(c)))*0.1;
    end
    if ((sign(X(c))) ~= (sign(X(c+1))))
      zerpos = [zerpos;c];
      count = count + 1;
    end
```

```
  end
end
```

ROUTINE: areapl1

This routine plots a 3-dimensional view (a "mountain range" view) of the grayscale values in a matrix. This is particularly useful in visualising bone density around an implant. This routine uses MATLAB routines for detection of the implant edge.

```
%info = imfinfo('bl12quar.tif')
%X = imread('0meg2.tif');
%X = imadjust(Z,[0 0.75],[],1);
%Y = imread('0meg2ave.tif');
%J = histeq(X,255);
%subplot(1,2,1), imshow(X);
%mask1x = roicolor(X,240,254);
%mask2x = bwmorph(mask1x,'close');
%mask1x = bwmorph(mask2x,'bridge');
%mask2x = bwmorph(mask1x,'fill');
%mask1x = bwmorph(mask2x,'thin',3);
%mask2x = bwmorph(mask1x,'spur',3);
%mask1x = erode2(mask2x,5);
%clear mask2x;
%mask1y = roicolor(Y,240,254);
%mask2y = bwmorph(mask1y,'close');
%mask1y = bwmorph(mask2y,'bridge');
%mask2y = bwmorph(mask1y,'fill');
%mask1y = bwmorph(mask2y,'thin',3);
%mask2y = bwmorph(mask1y,'spur',3);
%mask1y = erode2(mask2y,5);
%clear mask2y;
%subplot(1,2,2), imshow(mask1x);
%zoom

%maskrotx = imrotate(mask1x,90);
%maskroty = imrotate(mask1y,90);
%XROT = imrotate(X,90);
%YROT = imrotate(Y,90);
clear ix jx iy jy;
[ix,jx] = find(maskrotx==1);
%[iy,jy] = find(maskroty==1);

%% Extract region-of-interest
Px = [];
for c = 1:200
  [ix] = [ix-1];
  v = [impixel(XROT,jx,ix)]';
  Px = [Px;v(1,:)];
end
%Py = [];
```

```
%for c = 1:100
%   [iy] = [iy+1];
%   v = [impixel(YROT,jy,iy)]';
%   Py = [Py;v(1,:)];
%end

%% Filter (average) image
h = fspecial('average',3);
P2x = uint8(round(filter2(h,Px,'same')));
%P2y = uint8(round(filter2(h,Py,'same')));

%% Plot 3-D surfaces (normal and "averaged")
%for c = 1:2
surf(Px);
  shading('flat');
  axis ij;
%   axis equal;
  set(gca,'Position',[0.1 0.1 0.8 0.85]);
%   set(gca,'DataAspectRatio',[1 1 1]);
%   axis([0 300 0 400 0 260]);
%% Zooming in routine below
%   set(gca,'CameraViewAngle',5);
%   colormap(map);  view(60,30);
%   colorbar;
  pause;

surf(P2x);
  shading('flat');
  axis ij;
%   axis equal;
  set(gca,'Position',[0.1 0.1 0.8 0.85]);
%   set(gca,'DataAspectRatio',[1 1 1]);
%   axis([0 300 0 400 0 260]);
%% Zooming in routine below
%   set(gca,'CameraViewAngle',5);
  % Rotating routine below
  %rotate(180)
%   colormap(map);
  view(60,30);
%   colorbar;
  pause;
%end
```

ROUTINE: areapl2

This routine plots a 3-dimensional view (a "mountain range" view) of the grayscale values in a matrix. This is particularly useful in visualising bone density around an implant. This routine uses custom-written routines for the detection of the implant edge.

```
%clear all;
```

```
cd c:\warren\xrays\armoed;
IM = imread('ar75por1.tif');
cd c:\matlab\bin;
X = double(IM);
%Z = imadjust(X,[0 0.5],[],0.7);
[r,c] = size(X);
J = image(X);
set(J,'CDataMapping','scaled');
h = get(J,'CData');

%% Find the edge of the implant
Z = [];
for j = 1:r
  ROW = h(j,:);
  ROWsm = smooth(ROW,3);
  GRADgrad = gradient(ROWsm);
  %% Find end of implant => label 'start'
  IMPL = find(ROWsm==255);
  start1 = IMPL(length(IMPL));
  start2 = find(round(GRADgrad(start1:length(ROWsm)))~=0);
  start = start1 + start2(1);
  POSAR(j) = start;   clear start1 start2;
end
%% Smooth POSAR
POSARsm = round(smooth(POSAR,3));

%% Show shape of edge
%Z = zeros(r,c);
%for j = 1:length(POSARsm)
%   Z(j,POSARsm(j)) = 1;
%end
%subplot(1,2,1), imagesc(X,[0 255]); colormap(gray);
%subplot(1,2,2), imshow(Z);
%imzoom on;

%% Extract grayscale values of area
width = 100;
h2 = [];
for j=1:r
  h2=[h2;h(j,POSARsm(j):POSARsm(j)+width)];
end

%% Filter (average) image
fil = fspecial('average',3);
Pfil = uint8(round(filter2(fil,P,'same')));

%% Plot 3-D surface
  surf(X);
  shading('flat');
```

```
  axis ij;
  axis equal;
  set(gca,'Position',[0.1 0.1 0.8 0.85]);
%  set(gca,'DataAspectRatio',[1 1 1]);
%  axis([0 300 0 400 0 280]);
%% Zooming in routine below
%  set(gca,'CameraViewAngle',5);
%  colormap(map);
  view(60,30);
  %  colorbar;

pause;
  surf(Pfil);
  shading('flat');
  axis ij;
%  axis equal;
  set(gca,'Position',[0.1 0.1 0.8 0.85]);
%  set(gca,'DataAspectRatio',[1 1 1]);
%  axis([0 300 0 400 0 280]);
%% Zooming in routine below
%  set(gca,'CameraViewAngle',5);
%  colormap(map);
  view(60,30);
%  colorbar;
```

```
function Y = convert(X);

x=[45.0 200];
y=[0.768 2.4923];
for j = 1:length(X)
  Y(j) = interp1(x,y,X(j));
end
```

```
function OUT = erode2(IN,num)
IN = ~IN;
for count = 1:num
  f = inline('sum(x(:))==7');
  lut = makelut(f,3);
  RIDGE = applylut(IN,lut);
 IN = uint8(double(IN) + double(RIDGE));
%  IN = double(IN) + double(RIDGE);
  [m,n] = size(IN);
  for i = 1:m
    for j = 1:n
      if IN(i,j)==2
        IN(i,j)=1;
      end
    end
  end
```

```
end
OUT = ~IN;
clear lut i j IN f RIDGE count m n;
```

ROUTINE: radluc

This routine correlates the profiles of the grayscale plots with several model profiles (both radiolucent and bony ingrowth), and in this way determines whether radiolucency or bony ingrowth appear to have occurred.

```
clear all;
cd c:\warren\xrays\powell;
PIC = double(imread('po75por2.tif')); %IMAGE being tested
cd c:\matlab\bin;
imagesc(X,[0 255]); colormap(gray);
%Z = imadjust(X,[0 0.5],[],0.7);
[r,c] = size(PIC);
%J = image(PIC);
%set(J,'CDataMapping','scaled');
%h = get(J,'CData');

% Establish profiles of radiolucent and bone ingrowth
load SHAPERLLOW;% Radiolucent shape
clear X Y Z ans SHAPERL1 SHAPERLGOOD SHAPEBONE1 SHAPEBONE2 SAMPLE;
plot(SHAPERLLOW); ylabel('SHAPERLLOW');
axis([0 length(SHAPERLLOW)+5 0 270]);
pause;
load SHAPERLGOOD;        % Radiolucent shape
clear ROW ROWsm X Y Z j c r ans SHAPERL1 SHAPEBONE1 SHAPEBONE2 SAMPLE;
plot(SHAPERLGOOD); ylabel('SHAPERLGOOD');
axis([0 length(SHAPERLGOOD)+5 0 270]);
pause;
load SHAPERL1;           % Radiolucent shape
clear X ans SAMPLE;
plot(SHAPERL1); ylabel('SHAPERL1');
axis([0 length(SHAPERL1)+5 0 270]);
pause;
load SHAPERL2;           % Radiolucent shape
clear X c j r ROW ROWsm SAMPLE;
plot(SHAPERL2); ylabel('SHAPERL2');
axis([0 length(SHAPERL2)+5 0 270]);
pause;
load SHAPERL4;           % Radiolucent shape
clear X ans SAMPLE;
plot(SHAPERL4); ylabel('SHAPERL4');
axis([0 length(SHAPERL4)+5 0 270]);
pause;
load SHAPEBONE1; % Bone shape
clear Y Z ans SAMPLE;
plot(SHAPEBONE1); ylabel('SHAPEBONE1');
```

```
axis([0 length(SHAPEBONE1)+5 0 270]);
pause;
load SHAPEBONE2;  % Bone shape
clear Y Z ans SAMPLE;
plot(SHAPEBONE2); ylabel('SHAPEBONE2');
axis([0 length(SHAPEBONE2)+5 0 270]);
pause;

% Clear variables
clear GRADgrad GRADown ROW steep j zer start SHAPEUNSURE RESUNSURE ans;

RATIO = [];
RESRL1 = [];
RESRL2 = [];
RESRL4 = [];
RESRLGOOD = [];
RESRLLOW = [];
%RESFLAT = [];
RESBONE1 = [];
RESBONE2 = [];
HIPOS = [];
LOPOS = [];
Iminarr = [];
RATIOmax = [];
for j = 5:5:r
  plot(PIC(j-4,:)); pause
  plot(PIC(j-3,:)); pause
  plot(PIC(j-2,:)); pause
  plot(PIC(j-1,:)); pause
  plot(PIC(j,:)); pause
  ROW = (PIC(j-4,:)+PIC(j-3,:)+PIC(j-2,:)+PIC(j-1,:)+PIC(j,:))/5;
  plot(ROW);zoom
  pause

  ROW = h(j,:);
  ROWsm = smooth(ROW,5);
        GRADgrad = gradient(ROWsm);
%       GRADown  = steep(ROWsm,12);

  %% Find end of implant => label 'start'
  IMPL = find(ROWsm==255);
  start1 = IMPL(length(IMPL));
  start2 = find(round(GRADgrad(start1:length(ROWsm)))~=0);
  start = start1 + start2(1);
  clear start1 start2 IMPL;

  subplot(4,2,1),
  plot(ROWsm(start:start+100));
  ylabel('Intensity');
```

```
  axis([0 102 0 260]);
  subplot(4,2,2), plot(SHAPERL1);
  ylabel('RL1');
  axis([0 100 0 260]);
  subplot(4,2,3), plot(SHAPERL2);
  ylabel('RL2');
  axis([0 100 0 260]);
  subplot(4,2,4), plot(SHAPERL4);
  ylabel('RL4');
  axis([0 100 0 260]);
  subplot(4,2,5), plot(SHAPERLGOOD);
  ylabel('RLGOOD');
  axis([0 100 0 260]);
  subplot(4,2,6), plot(SHAPERLLOW);
  ylabel('RLLOW');
  axis([0 100 0 260]);
  subplot(4,2,7), plot(SHAPEFLAT);
  ylabel('FLAT');
  axis([0 100 0 260]);
  subplot(4,2,7), plot(SHAPEBONE1);
  ylabel('BONE1');
  axis([0 100 0 260]);
  subplot(4,2,8), plot(SHAPEBONE2);
  ylabel('BONE2');
  axis([0 100 0 260]);
  imzoom on;

% Find first and second zeros after 'start' - these are local minima and maxima
%   zer = fndzer(GRADgrad(start:start+100));
%   Iminpos = zer(1);
%   Imaxpos = zer(2);
%   Imin = ROWsm(Iminpos+start-1);
%   Imax = ROWsm(Imaxpos+start-1);

% Calculate correlation coefficients for each shape
RESRL1 = [RESRL1;(corr2(smooth(PIC(j,start:start+20),3),SHAPERL1(1:18)))];
        RESRL1(round(j/20)+1)
RESRL2 = [RESRL2;(corr2(smooth(PIC(j,start:start+14),3),SHAPERL2(1:12)))];
        RESRL2(round(j/20)+1)
RESRL4 = [RESRL4;(corr2(smooth(PIC(j,start:start+26),3),SHAPERL4(1:24)))];
        RESRL4(round(j/20)+1)
RESRLGOOD=[RESRLGOOD;(corr2(smooth(PIC(j;start:start+100),3),SHAPERLGOOD))];
        RESRLGOOD(round(j/20)+1)
RESRLLOW = [RESRLLOW;(corr2(smooth(PIC(j,start:start+100),3),SHAPERLLOW))];
        RESRLLOW(round(j/20)+1)
RESFLAT = [RESFLAT;(corr2(smooth(PIC(j,start:start+100),3),SHAPEFLAT))-0.03];
        RESFLAT(round(j/20)+1)
RESBONE1 = [RESBONE1;(corr2(smooth(PIC(j,start:start+100),3),SHAPEBONE1))-0.05];
        RESBONE1(round(j/20)+1)
```

```
RESBONE2 = [RESBONE2;(corr2(smooth(PIC(j,start:start+100),3),SHAPEBONE2))-0.05];
        RESBONE2(round(j/20)+1)
clear TEMP HIGHPOS LOWPOS;
TEMP=[RESRL1(round(j/20)+1);RESRL2(round(j/20)+1);RESRLGOOD(round(j/20)+1);...
    .    RESFLAT(round(j/20)+1);RESBONE1(round(j/20)+1);RESBONE2(round(j/20)+1)];
  HI = max(TEMP);
  LO = min(TEMP);
  HIPOS = [HIPOS;find(TEMP==HI)];
  LOPOS = [LOPOS;find(TEMP==LO)];

%% Calculate ratios of max to min values
%  if ((Imaxpos-Iminpos)~=0)
%     RATIO = [RATIO;((Imax-Imin)/(Imaxpos-Iminpos))];
%     RATIOmax = [RATIOmax;((Imaxpos-Iminpos)/Imaxpos)];
%  end
%  Iminarr = [Iminarr;Iminpos];
%  (Imax-Imin)
%  (Imaxpos-Iminpos)
%  (Imax-Imin)/(Imaxpos-Iminpos)
%  (Imaxpos-Iminpos)/Imaxpos
%  if ((Imax-Imin)>10)&(Imaxpos-Iminpos)<10)
%  pause

end
%plot(smooth(RATIO,3)); pause;

%% Check for outlying points => set these to 0
%for j = 10:10:1440  %rw
%  if (Iminarr(j/10) > (mean(Iminarr)+std(Iminarr)))
%     RATIO(j/10) = 0;
%  end
%end
%figure; plot(smooth(RATIO,3));

%figure;
%subplot(5,1,1), plot(RESRLGOOD);
%ylabel('RLGOOD');
%subplot(5,1,2), plot(RESRL1);
%ylabel('RL1');
%subplot(5,1,3), plot(RESFLAT);
%ylabel('FLAT');
%subplot(5,1,4), plot(RESBONE1);
%ylabel('BONE1');
%subplot(5,1,5), plot(RESBONE2);
%ylabel('BONE2');

%% Threshold for radiolucency:     1 = definitely radiolucent
%                                  0.5 = unsure
%                                  0   = definitely not radiolucent
```

```
RATIO2 = smooth(RATIO,3);
RATIOmax2 = smooth(RATIOmax,3);
TRUFAL = [];
for j = 1:length(RATIO2)
  if (RATIO2(j)>=1) & (RATIOmax2(j)>=0.17)
    TRUFAL(j) = [1];
  elseif (RATIO2(j)>=1) & (RATIOmax2(j)<=0.17)
    TRUFAL(j) = [0.5];
  elseif (RATIO2(j)<1) & (RATIOmax2(j)>=0.17)
    TRUFAL(j) = [0.5];
  else TRUFAL(j) = [0];
  end
end
figure;
plot(TRUFAL);axis([0 length(TRUFAL)+2 -0.2 1.2]);
```

```
function rotate(deg)

[az,el] = view;
set(gca,'CameraViewAngleMode','manual');
ang = 0:deg/10:deg;
for i = 1:length(ang)
  view([az+ang(i) el]);
  drawnow
end
```

ROUTINE: trab

This routine assesses trabecular bone pattern (described in Appendix C). It correlates model patterns (in known directions) with those of images.

```
clear all;
cd c:\warren\xrays-old\powell\;
IMBIG = imread('pobone1.tif');
S = imread('pobone1.tif');
cd c:\matlab\bin\;
%Z = imadjust(IM,[0 0.5],[],1);
[r,c] = size(IMBIG);
xmax = fix(c/256)*256;
ymax = fix(r/256)*256;
IM = IMBIG(1:256,1:xmax);
SAMPLE = S(1:256,1:256);
clear S IMBIG;

%subplot(2,1,1), imshow(IM);
%subplot(2,1,2), imshow(SAMPLE);
%pause;

%% Correlate TRANSLATING images and plot results
T = [];
```

```
for dist = 1:10:xmax-256
  T=[T;corr2(IM(1:256,dist:dist+255),SAMPLE)];
end
figure; plot(T);
ylabel('Correlation: Translation (%)');
axis([0 length(T) -0.2 0.8]);
xlabel('Translated distance (x10 Pixels)');
%pause;

%% Correlate ROTATING images and plot results
%R = [];
%step = 10;
%for theta = 0:step:360
%  Srot = imrotate(SAMPLE,theta,'crop');
%  R = [R;corr2(IM(1:256,1:256),Srot)];
%end
%figure;
%axes('XTickLabelMode','manual');
%axes('XTickMode','manual');
%axes('XLimMode','manual');
%plot(R)
%hold on;
%axes('XLim',[0 360],'XTick',[0 30 60 90 120 150 180 210 240 270 300 330 360]);
%axes('XTick',[0 30 60 90 120 150 180 210 240 270 300 330 360]);
%axes('XTickLabels',[0 30 60 90 120 150 180 210 240 270 300 330 360]);
%hold on;
%plot(R);
%axes('YLim',[-0.2 1.01]);
%axes('XTick',[0 30 60 90 120 150 180 210 240 270 300 330 360]);
%axes('XTickLabels',[0 30 60 90 120 150 180 210 240 270 300 330 360]);
%ylabel('Correlation: Rotation (%)');
%axis([0 length(R) -0.2 0.9]);
%xlabel('Angle of Rotation (Degrees x10)');
%TOP = find(R==max(R))-1;

%% Correlate both TRANSLATING and ROTATING images
%step = 10;
%for xpos = 0:256:xmax-255
%  xpos+1
%  R = [];
%  for theta = 0:step:180
%    Srot = imrotate(SAMPLE,theta,'crop');
%    R = [R;corr2(IM(1:256,xpos+1:xpos+1+255),Srot)];
%  end
%  figure; plot(R);
%  ylabel('Correlation: Rotation');
%  TOP = find(R==max(R))
%  pause
%end
```

APPENDIX B

Questionnaire

Below is the questionnaire that was filled in by the patients participating in the study. The questionnaire is designed to assess the activity levels of the patients.

Where required, please place a cross (X) clearly in the relevant box.

1) Date of birth: _____

2) Present weight (kg): _____

3) If you have lost or gained weight since the hip replacement operation, please specify approximately how much: _____

4) Please describe your overall health - how you typically feel during daily activities:

very well	well	average	uncomfortable	unwell

5) What is your occupation/career? Please describe your activities (e.g. sitting, walking) during a typical day:

_____

_____

_____

6) Which term best describes your activity levels in general?

very active	active	average	inactive	sedentary

7) Approximately how many days was it between the time of the operation and:-
   a) the time that you began to place weight on the leg? _____
   b) the time that you began walking comfortably again? _____

8) How much of your typical day consists of walking or standing?

< 0.5 hr	0.5 - 1 hr	1 - 1.5 hrs	1.5 - 2 hrs	> 2 hrs

9) Do you make use of a walking aid, such as a walking stick? _____
If yes, how often do you use it? _____
_____

10) Do you participate in any of the following sports? If yes, how often?

	Yes	No	very occasionally	monthly	fortnightly	weekly	daily
Swimming							
Cycling							
Athletics							
Golf							
Soccer							
Rugby							
Hiking							
Squash							
Bowls							
Cricket							
Running							
Tennis							
Weights							
Climbing							
Tab tennis							
Canoeing							
Volleyball							

Other (specify type and regularity): _____
_____
_____

11) Do you experience any pain from the replaced hip joint?

often painful	mild/occasional pain	pain-free

12) If you have experienced any other problems (e.g. shortening of leg), or have any other comments, please indicate them:

_____
_____
_____

APPENDIX C

Detection of trabecular bone pattern

The assessment of the trabecular pattern of the bone was undertaken with a complementary objective. It was not expected that this would contribute greatly to the primary aim of this work, that of assessing the accuracy of the numerical model. Thus, the advances that were made are only the beginnings of what proved to be a very challenging task. However, it is clearly something that could ultimately prove useful if made more robust.

Two approaches were taken in assessing the trabecular pattern of the bone. Both methods used MATLAB routines to correlate a sample image (with a uni-directional trabecular pattern) with specific parts of a larger image. The MATLAB correlation routine required that the regions being compared be exactly the same size. The first approach was to "move" the sample image through the larger image, each time correlating the sample image with that portion of the larger image. This was done while moving the sample image both horizontally and vertically through the image. This is here referred to as translation of the sample image. The second approach was to correlate the sample image with a particular portion in the original image, and then rotate the image, each time calculating the correlation coefficient. The plotting of these values produced peaks where trabecular bone pattern was similar to the sample, and troughs where dissimilar. In this way, the general direction of trabecular bone pattern could be assessed.

The first task was to acquire a sample image of a suitable size. The use of several sample images of various intensities and trabecular spacings would also be useful, but wasn't investigated in this study. It was decided that this image would be 256x256 pixels in size, as this was a reasonable "block" size to work with, and one that contained sufficient trabecular pattern to make comparison meaningful. The image contained bone patterns that were strictly uni-directional (i.e. the trabecular walls were generally parallel and ran only in one direction). This was an obvious requirement in establishing precise trabecular directions. An example of this sample image is shown in Figure C.1.

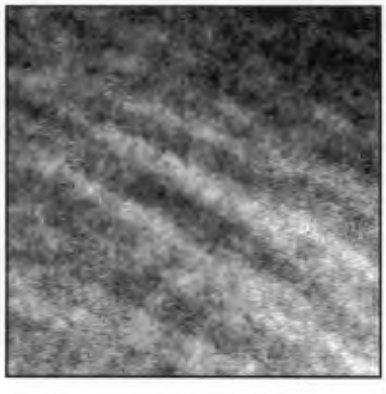

Figure C.1 Example of sample image used to assess trabecular bone pattern

Correlation during translation of the sample image

The first approach was to compare the sample image with sections (of the same size) of the larger image being examined. The method was to begin by correlating the sample image with

the upper left-hand corner (256x256 pixels) of the larger image. The sample image was then "moved" - correlated with the next position, a certain number of pixels (in this case 10) to the right. This was continued, each time recording the correlation coefficients in an array, until the border of the image was encountered. When plotted, this array produced peaks in regions of high correlation, and troughs where correlation was low. In this example, the trabeculae were generally slanted at a slight angle (see Figure C.1). This had the result that the translational correlation produced peaks and troughs as the trabeculae moved in and out of phase with the larger image. The result is shown in Figure C.2.

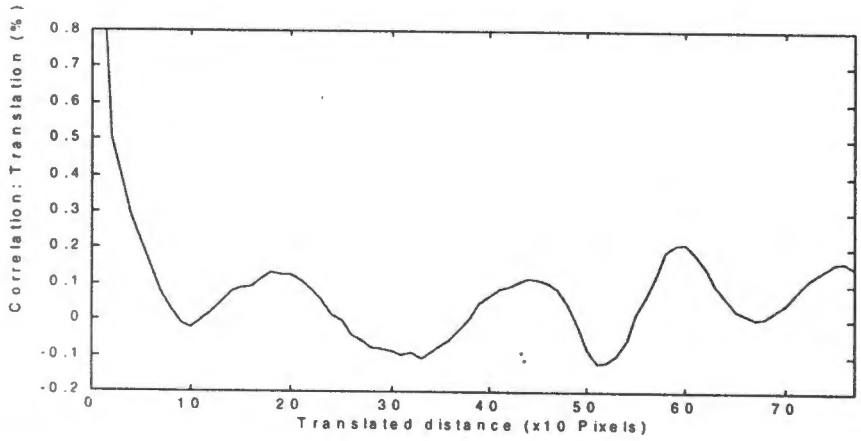

Figure C.2 Example of correlation during translation of the sample image

Although the correlation is relatively low even in regions where the trabeculae coincide (approximately 0.15), it is the shape of the curve that is of interest. Passing the sample image through an image and getting results like the one above is a clear indication of trabecular bone pattern being recognised. There is difficulty in extracting quantitative data from the above graph, as the correlation is low. Furthermore, the effectiveness of this procedure may vary somewhat depending on the brightness and quality of the image being tested. Also of interest is the fact that the graph shows negative correlation when out of phase. In this example, the sample image was taken out of the larger image, and hence the correlation is relatively high in certain positions.

Correlation during rotation of the sample image

The second approach was to position the sample image in a particular position in the original image, and then to rotate the image, each time recording the correlation coefficient in an array. The plotting of the values in these arrays produced peaks where trabecular bone pattern was similar to the sample, and troughs where dissimilar. An example (where the sample image comes from the larger image) is shown in Figure C.3.

The obvious feature of this graph is the spike that occurs at 180°. This is where the sample image is upside-down, and the trabeculae lie approximately in the original direction. Again the magnitude of the spike is relatively small (0.15), but the spike (relative to the rest of the graph) is a clear indication of matching trabecular pattern. It should be noted that because one image is rotated on itself, perfect correlation of 1.00 is found at 0° and 360°.

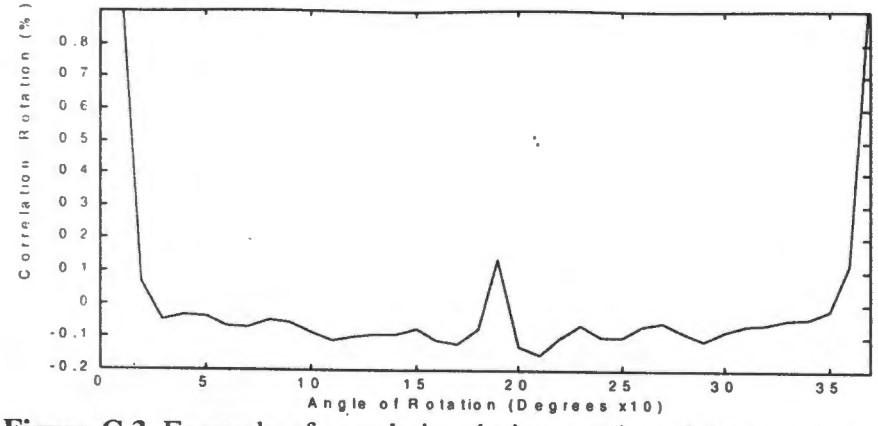

Figure C.3 Example of correlation during rotation of the sample image

Possibility of correlation during translation and rotation of the sample image

Correlating the sample image with the larger image while both translating and rotating the sample image is clearly the best method. This means the following: the correlation begins at the top, left-hand corner of the larger image, with the sample image in the normal, upright position. Then, before translating the image across the larger one, the image is rotated through 360° (or perhaps 180°). This will result in the best correlation (i.e. the trabecular bone pattern) being found for the first position. Then the sample image is translated across the larger image (e.g. by 10 pixels) to the next position, and the image again rotated, thus finding the best correlation in that position. This process is continued until the sample image has been moved through the entire image, each time finding the correlation while rotating the image.

There are two problems with this method. The most significant problem is that a procedure such as this requires a great deal of time to run. The execution of only the rotational correlation required a few minutes. The translational method across only one row of one image required a similar amount of time. The running of these two routines simultaneously, and through a significantly large image would require a substantial period of time, probably as long as 20 minutes. This would become a problem if this method were being used to extract information in a clinical setting, or more importantly, if this analysis is only a part of a greater overall analysis. The second problem is the fact that quantifying the data is not an easy task. In particular, the threshold to distinguish whether or not trabecular pattern has been recognised must be chosen very carefully. This may vary depending on the lightness/darkness and quality of the X-ray being tested. Due to these problems, this approach was not given a great deal of attention in this study.

APPENDIX D

Example of DEXA results

k = 1.225 d0 GROOTE SCHUUR HOSPITAL

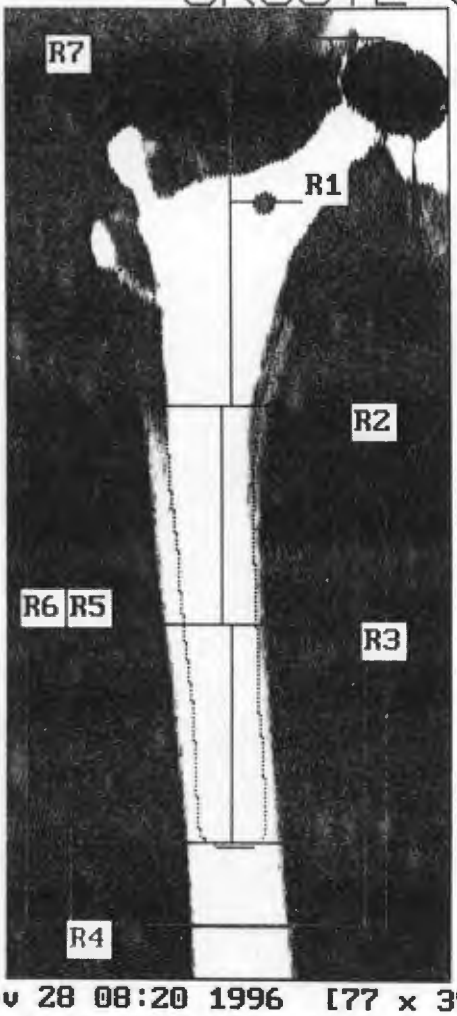

·Nov 28 08:20 1996 [77 x 391]

N11269607 Tue Nov 26 09:20 1996
Name:
Comment:
I.D.:
S.S.#:
ZIPCode:
Scan Code:
BirthDate:
Physician:
Image not for diagnostic use

C.F.	1.006	1.058	1.000
Region	Area (cm2)	BMC (grams)	BMD (gms/cm2)
GLOBAL	27.28	33.27	1.219
R1	2.29	1.98	0.862
R2	2.60	2.88	1.108
R3	3.06	4.12	1.347
R4	5.55	9.11	1.640
R5	3.60	4.97	1.381
R6	4.11	5.59	1.359
R7	6.16	4.92	0.799
NETAVG	26.89	32.89	1.223

HOLOGIC

REFERENCES

Berdie, D.R. & Anderson, J.F., Questionnaires: design and use, The Scarecrow Press, Metuchen, N.J., 1974

Bobyn, J.D., Pilliar, R.M., Cameron, H.U. & Weatherly, G.C., The optimum pore size for the fixation of porous-surfaced metal implants by the ingrowth of bone, *Clinical Orthopaedics and Related Research,* **150**, pp. 263 - 270, 1980

Bobyn, J.D., Cameron, H.U., Abdulla, D., Pilliar, R.M. & Weatherly, G.C., Biologic fixation and bone modelling with an unconstrained canine total knee prosthesis, *Clinical Orthopaedics and Related Research,* **166**, pp. 301 - 312, 1982

Bobyn, J.D. & Wilson, G.J., Effect of pore size on the peel strength of attachment of fibrous tissue to porous-surfaced implants, *Journal of Biomedical Materials Research,* **16**, pp. 571 - 584, 1982

Bobyn, J.D., Glassman, A.H., Goto, H., Krygier, J.J., Miller, J.E. & Brooks, C.E., The effect of stem stiffness on femoral bone resorption after canine porous-coated total hip arthroplasty, *Clinical Orthopaedics and Related Research*, **261**, pp. 196 - 213, 1990

Bobyn, J.D., Mortimer, E.S., Glassman, A.H., Engh, C.A., Miller, J.E. & Brooks, C.E., Producing and avoiding stress shielding: laboratory and clinical observations of noncemented total hip arthroplasty, *Clinical Orthopaedics and Related Research*, **274**, pp. 79 - 96, 1992

Bourne, G.H. (editor), The biochemistry and physiology of bone, Academic Press Inc., New York, 1956

Breckon, A., An investigation of the morphological and mechanical properties of cancellous bone in rheumatoid arthritis and osteoarthritis of the hip, MSc Thesis Project, Department of Biomedical Engineering, University of Cape Town, 1993

Cameron, H.U., Pilliar, R.M. & Macnab, I., The effect of movement on the bonding of porous metal to bone, *Journal of Biomedical Materials Research*, **7**, pp. 301 - 311, 1973

Cameron, H.U., Pilliar, R.M. & Macnab, I., The rate of bone ingrowth into porous metal, *Journal of Biomedical Materials Research*, **10**, pp. 295 - 302, 1976

Carter, D.R. & Hayes, W.C., The compressive behaviour of bone as a two-phase porous structure, *Journal of Bone and Joint Surgery*, **59 A**, pp. 954 - 962, 1977

Carter, D.R. & Spengler, D.M., Mechanical properties and composition of cortical bone, *Clinical Orthopaedics and Related Research*, **135**, pp. 192 - 217, 1978

Carter, D.R., Vasu, R. & Harris, W.H., Stress changes in the femoral head due to porous ingrowth surface replacement arthroplasty, *Journal of Biomechanics*, **17**, pp. 737 - 747, 1984

Chamay, A. & Tschantz, P., Mechanical influences in bone remodeling: Experimental research on Wolff's Law, *Journal of Biomechanics*, **5**, pp. 173 - 180, 1972

Coetzee, T., Drennans human osteology, Maskew Miller Ltd., Third edition, 1981

Collier, J.P., Bauer, T.W., Bloebaum, R.D., Bobyn, J.D., Cook, S.D., Galante, J.O., Harris, W.H., Head, W.C., Jasty, M.J., Mayor, M.B., Sumner, D.R. & Whiteside, L.A., Results of implant retrieval from post-mortem specimens in patients with well-functioning long-term total hip replacements, *Clinical Orthopaedics and Related Research*, **274**, pp. 97 - 112, 1992

Cook, S.D., Thomas, K.A. & Haddad, R.J., Histological analysis of retrieved human porous-coated total joint components, *Clinical Orthopaedics and Related Research*, **234**, 1988

Coventry, M. B., Lessons learned in 30 years of total hip arthroplasty, *Clinical Orthopaedics and Related Research*, **274**, pp. 22 - 29, 1992

Dalstra, M., Huiskes, R. & van Erning, L., Development and validation of a three-dimensional finite element model of the pelvic bone, *Journal of Biomechanical Engineering*, **117(3)**, pp. 272 - 278, 1995

Ducheyne, P., The fixation of permanent implants: a functional assessment, Functional behaviour of orthopedic biomaterials, Vol II: Applications, Edited by Ducheyne, P & Hastings, G.W., CRC Press, 1984

Engh, C.A., Bobyn, J.D. & Glassman, A.H., Porous coated hip replacement: the factors governing bone ingrowth, stress shielding, and clinical results, *Journal of Bone and Joint Surgery*, **69 B**, pp. 45 - 55, 1987

Engh, C.A. & Bobyn, J.D., The influence of stem size and extent of porous coating on femoral bone resorption after primary cementless hip arthroplasty, *Clinical Orthopaedics and Related Research*, **231**, pp. 7 - 28, 1988

Foddy, W., Constructing questions for interviews and questionnaires: theory and practice in social research, Cambridge University Press, 1993

Galante, J., Rostoker, W., Lueck, R. & Ray, R.D., Sintered fiber metal composites as a basis for attachment of implants to bone, *Journal of Bone and Joint Surgery*, **53 A**, pp. 101 - 114, 1971

Gibson, L.J., The mechanical behaviour of cancellous bone, *Journal of Biomechanics*, **18**, pp. 317 - 328, 1985

Griss, P., Assessment of clinical status of total joint replacement, Functional behaviour of orthopedic biomaterials, Vol II: Applications, Edited by Ducheyne, P & Hastings, G.W, CRC Press, 1984

Harris, W.H., The first 32 years of total hip arthroplasty: one surgeon's perspective, *Clinical Orthopaedics and Related Research*, **274**, pp. 6 - 11, 1991

Hollister, S.Y., Guldberg, R.E., Kuelske, C.L. & Mosier, S.M., Relative effects of wound healing and mechanical stimulus on early bone adaptation to porous coated implants, Second World Congress of Biomechanics, Vol II, pp. 242, 1994

Hori, R.Y. & Lewis, J.L., Mechanical properties of the fibrous tissue found at the bone-cement interface following total joint replacement, *Journal of Biomedical Materials Research*, **16**, pp. 911 - 927, 1982

Huiskes, R. & Chao, E.Y.S., Finite Element methods in orthopaedic biomechanics: the first decade, *Journal of Biomechanics*, **16**, pp. 385 - 409, 1983

Huiskes, R., Janssen, J.D. & Slooff, T.J., A detailed comparison of experimental and theoretical stress-analyses of a human femur, *Mechanical properties of bone*, Edited by Cowin, S.C., AMD **45**, pp. 211 - 234, 1981

Huiskes, R., Weinans, H. & Van Rietbergen, B., The relationship between stress shielding and bone resorption around total hip stems and the effects of flexible materials, *Clinical Orthopaedics and Related Research*, **274**, pp. 124 - 134, 1992

Manaster, B.J., Total Hip Arthroplasty: Radiographic Evaluation, *Radiographics*, **16**, pp. 645 - 660, 1996

Markolf, K.L., Amstutz, H.C. & Hirschowitz, D.L., The effect of calcar contact on femoral components micro-movement: a mechanical study, *Journal of Bone and Joint Surgery*, **62 B**, pp. 1315 - 1323, 1980

Morscher, E.W. & Dick, W., Cementless fixation of 'isoelastic' hip endoprostheses manufactured from plastic materials, *Clinical Orthopaedics and Related Research*, **176**, pp. 77 - 76, 1983

Müller, M.E., Lessons of 30 years of total hip arthroplasty, *Clinical Orthopaedics and Related Research*, **274**, pp. 12 - 21, 1992

Nilles, J.L., Coletti, J.R. & Wilson, C., Biomechanical evaluation of bone-porous material interfaces, *Journal of Biomedical Materials Research*, **7**, pp. 231 - 251, 1973

Oppenheim, A.N., Questionnaire design and attitude measurement, Published by Heinemann Educational Books Ltd., London, 1966

Park, Joon B., Orthopedic prosthesis fixation, The Biomedical Engineering Handbook, Edited by Bronzino, CRC Press, 1995

Park, S.H., Llinas, A., & Goel, V.K., Hard tissue replacements, The Biomedical Engineering Handbook, Edited by Bronzino, CRC Press, 1995

Pedersen, D.R., Brown, T.D. & Brand, R.A., Interstitial bone stress distributions accompanying ingrowth of a screen-like prosthesis anchorage layer, *Journal of Biomechanics*, **24**, pp. 1131 - 1142, 1991

Pilliar, R.M., Lee, J.M. & Maniatopoulos, C., Observations of the effect of movement on bone ingrowth into porous-surfaced implants, *Clinical Orthopaedics and Related Research*, **208**, pp. 109 - 113, 1986

Rohlmann, A., Mössner, U. & Bergmann, G., Finite-element-analysis and experimental investigation in a femur with hip endoprosthesis, *Journal of Biomechanics*, **16(9)**, pp. 727 - 742, 1983

Sadegh, A.M., Luo, G.M. & Cowin, S.C., Bone ingrowth: an application of the boundary element method to bone remodelling at the implant interface, *Journal of Biomechanics*, **26**, pp. 167 - 182, 1993

Salant, P. & Dillman, D.A., How to conduct your own survey, John Wiley and sons, 1994

Seeley, R.R., Stephens, T.D. & Tate, P., Anatomy and Physiology, Second edition, Mosby-Year Book Inc., 1992

Social and Community Planning Research, Questionnaire Design Manual: Technical manual no. 5, London, 1972

Spector, M., Current concepts of bone ingrowth and remodeling, *Non-cemented total hip arthroplasty*, Fitzgerald,R. (ed.), pp. 69 - 85, Raven Press, New York, 1988

Sumner, D.R. & Galante, J.O., Determinants of stress shielding: design versus materials versus interface, *Clinical Orthopaedics and Related Research*, **274**, pp. 202 - 212, 1992

Starke, G.R., Numerical simulation of implant-bone interaction following cementless joint replacement, PhD Thesis Project, Department of Mechanical Engineering, University of Cape Town, 1996

Vaughan, J., The physiology of bone, Third edition, Oxford University Press, New York, 1981

Valliappan, S., Svensson, N.L. & Wood, R.D., Three dimensional stress analysis of the human femur, *Comput. Biol. Med.*, 7, pp. 253 - 264, 1977

Verdonschot, N.J.J., Huiskes, R. & Freeman, M.A.R., Pre-clinical testing of hip prosthetic designs: a comparison of finite element calculations and laboratory tests, *Proceedings of the Institution of Mechanical Engineers*, Part H: Journal of engineering in medicine, **207(3)**, pp. 149 - 154, 1993

Weinans, H., Huiskes, R. & Grootenboer, H.J., Trends of mechanical consequences and modeling of a fibrous membrane around femoral hip prostheses, *Journal of Biomechanics*, **23**, pp. 991 - 1000, 1990

Weinans, H., Huiskes, R., van Rietbergen, B., Sumner, D.R., Turner, T.M. & Galante, J.O., Adaptive bone remodelling around bonded noncemented total hip arthroplasty: A comparison between animal experiments and computer simulation, *Journal of Orthopaedic Research*, **11(4)**, pp. 500 -513, 1993

Whalen, R.T., Carter, D.R. & Steele, C.R., Influence of physical activity on the regulation of bone density, *Journal of Biomechanics*, **21** (10), pp. 825 - 837, 1988

Whiteside, L.A., Amador, D. & Russel, K., The effects of the collar on total hip femoral component subsidence, *Clinical Orthopaedics and Related Research*, **231**, pp. 120 - 126, 1988